REPORT NO.
UC SESM 73-2

STRUCTURES AND MATERIALS RESEARCH
DEPARTMENT OF CIVIL ENGINEERING

COMPUTATIONAL PROCEDURE FOR INELASTIC FINITE ELEMENT ANALYSIS

by
HUNG-MING CHI
and
GRAHAM H. POWELL

JANUARY 1973

STRUCTURAL ENGINEERING LABORATORY
UNIVERSITY OF CALIFORNIA
BERKELEY CALIFORNIA

COMPUTATIONAL PROCEDURE FOR INELASTIC FINITE ELEMENT ANALYSIS

by

Hung-Ming Chi
Graduate Student

and

Graham H. Powell
Associate Professor of Civil Engineering

Division of Structural Engineering
and Structural Mechanics
Department of Civil Engineering
University of California, Berkeley

January 1973

ACKNOWLEDGEMENTS

The authors wish to thank Professors F. Baron and B. N. Parlett, who served on the dissertation committee for the thesis on which this report is based, and Mrs. Shirley Edwards who typed the manuscript.

Computer time was provided by the University of California Computer Center.

TABLE OF CONTENTS

1. INTRODUCTION

Since its first presentation in the early 1950's, the finite element method has emerged as one of the most powerful and versatile tools in the field of structural mechanics. The method, which was original developed for linear elastic systems, has proven also to provide one of the most effective numerical formulations for the analysis of nonlinear structures.

Two different types of nonlinearity may occur in structures, namely geometric nonlinearity, resulting from large displacements, and material nonlinearity, resulting from yield of the material or other nonlinearities in the stress-strain relationship. The application of the finite element method to nonlinear problems has been extensively studied during the past decade, and substantial advances have been made. Nevertheless, a great deal more work remains to be carried out before analysis of nonlinear structures can be carried out on a routine basis. The need for progress in the solution of problems with material nonlinearity is particularily important because of the many problems of this type which occur in engineering practice. The research described here is concerned only with the effects of material nonlinearity. The aim of the research has been to explore computational procedures, to determine which procedures are likely to be most efficient and most accurate, and to provide detailed documentation of the computational sequence. No new theoretical principles are established.

Recent investigations of elasto-plastic behavior in finite element analysis are numerous (26-53), and a variety of

solution procedures to account for plasticity have been proposed. These procedures are reviewed in Chapter 2, and a composite precedure suitable for general purpose use is then presented.

Chapters 3 and 4 consider what is identified as the "linearization" problem. The flow theory of plasticity is reviewed in Chapter 3, and incremental stress-strain relationships are derived. Applications are considered for elastic perfectly plastic material, general isotropic hardening, linear kinematic hardening, and a "parallel material" procedure which is equivalent to a particular type of nonlinear kinematic hardening. The application of the incremental stress-strain relationships in the formulation of the tangent stiffness matrix for an axisymmetric solid is considered in Chapter 4. A quadrilateral isoparametric element is considered, including a formulation in which additional incompatible modes of deformation are introduced to improve the bending characteristics.

Chapter 5 considers the "state determination" problem, in which, for a given displacement increment, the state of stress and strain at all points in the structure is determined. In addition, the unbalanced load on the structure, which is a measure of the accuracy of the solution, is determined. The logic of a computer program to apply the proposed solution procedure is described in Chapter 6. The results of analyses of an extensive series of example structures are presented in Chapter 7, and conclusions on the relative efficiency of several alternative computational procedures are drawn.

2. REVIEW OF SOLUTION PROCEDURES

2.1 SCOPE OF INVESTIGATION

2.1.1 Type of Nonlinearity

Figure 2.1 shows, in diagrammatic form, the type of nonlinear load-displacement relationship considered. It is important to recognize that this figure portrays the relationship correctly only for a structure with a single degree of freedom. For a structure with many degrees of freedom, the relationship is a complex one in a multidimensional space. Nevertheless, this type of diagram is convenient for illustrating concepts, provided its limitations are kept in mind. In this chapter, some general concepts are discussed, with reference to this type of diagram. The actual computational procedures for multidimensional systems are considered in subsequent chapters.

Nonlinearity of the type indicated in Fig. 2.1 could result from large displacement effects as well as material nonlinearity, and much of the discussion in this chapter applies regardless of the source of the nonlinearity. However, only material nonlinearity effects are considered for the remainder of this study. The procedures considered are applicable to arbitrary loading paths, including unloading and load reversal. However, unstable configurations are not considered, and the tangent stiffness relationship is assumed always to be positive definite.

2.1.2 Solution Procedure

The only method of structural analysis considered here is the direct stiffness method. The nonlinear problem is solved in a series of linear steps, by either step-by-step or iteration techniques. The equilibrium equations within any linear step are solved by Gauss elimination.

Alternative procedures might be used to solve the nonlinear analysis problem, particularly procedures involving a search in displacement space for the configuration having minimum potential energy (56, 57). However, such procedures have not been considered in this study.

2.2 STEP BY STEP METHODS

2.2.1 Simple Step by Step Procedure

Step by step methods are based on the assumption that if the loading is subdivided into several small increments, then the behavior is linear within any increment. That is, the nonlinear load-displacement relationship is approximated by a piecewise linear relationship. For analysis, a constant structure stiffness is assumed within any increment, and the stiffness will generally change between increments.

In the simplest procedure, the structure stiffness used within any increment is the tangent stiffness, K at the beginning of the increment, defined by

$$dR = K \cdot dr \qquad [2.1]$$

in which dR, dr = infinitesimal increments of load and displacement, respectively. The solution algorithm is then as follows

$$\Delta r_n = (K_n)^{-1} \cdot \Delta R_n \qquad [2.2]$$

$$r_n = r_{n-1} + \Delta r_n \quad ; \quad r_o = 0 \qquad [2.3]$$

in which ΔR_n and Δr_n are the load and displacement increments, respectively, for the nth increment, and in which $(K_n)^{-1}$ implies, for a multidimensional problem, solution of the equilibrium equations by Gauss elimination, not actual inversion of the stiffness matrix. The equations in this chapter will be written for a one-dimensional problem, as illustrated in Fig. 2.1, but in principle are applicable also to multidimensional problems.

This procedure has been widely used in elasto-plastic analysis (31,37,42,51). Mathematically it is equivalent to a crude Euler-Cauchy method. Its truncation error is proportional to the size of the load increment, and errors are likely to be accumulated over several steps, so that the solution diverges from the true load-displacement relationship, as indicated in Fig. 2.2.

The tangent stiffness, K_n, at the beginning of the nth load increment depends on the current state of stress and strain. The problem of determining the tangent stiffness for any given state will be termed the linearization problem. The computational procedures for the solution of this problem are considered in detail in Chapters 3 and 4. After the displacement incrememt, Δr,

has been found, it is necessary to compute the changes in stress and strain, and hence obtain the new state. This will be termed the state determination problem. A simplified discussion of the solution procedure for this problem is presented in the following section. Details of the computational technique for multi-dimensional problems are considered in Chapter 5.

2.2.2 State Determination Problem

The state determination problem is solved in two stages, as illustrated diagrammatically in Figs. 2.3a and 2.3b, with an optional third stage, as illustrated in Fig. 2.3c.

The first stage is based on the kinematic relationship between increments of displacement and strain. Given the displacement increment, Δr, the strain increment, $\Delta \epsilon$, is found, as indicated in Fig. 2.3a. The geometrical relationship between Δr and $\Delta \epsilon$ will be typically, although not necessarily, linear.

The second stage is based on the stress-strain relationship for the material. Given the strain increment, $\Delta \epsilon$, the stress increment, $\Delta \sigma$, is found, as indicated in Fig. 2.3b. The relationship between $\Delta \epsilon$ and $\Delta \sigma$ will generally be nonlinear.

A new state of stress and strain has therefore been found, and the step by step proceduce illustrated in Fig. 2.2 can therefore continue. As indicated in this figure, however, there will generally be an error at the end of any load increment, resulting from the fact that true behavior within an increment is not linear. A convenient measure of this error is the extent to which equilibrium is violated. The third stage of the state determination procedure serves to calculate magnitude of the error.

For any state of stress, σ, there will be a unique value of the external load required to satisfy the equations of equilibrium. This load will be termed the "internal resisting load", R^I, to distinguish it from the external applied load, R. The magnitude of R^I can be found by considering the equilibrium relationship between stresses and loads, as illustrated in Fig. 2.3c. This relationship will typically, although not necessarily, be linear. At the end of any load increment the magnitude of the error in equilibrium is given by

$$R^U = R - R^I \qquad [2.4]$$

in which R^U = unbalanced load.

2.2.3 Step by Step Procedure with Equilibrium Correction

The accuracy of the simple step by step procedure can easily be improved by calculating the unbalanced load at the end of each linear step and adding this load to the following load increment as illustrated in Fig. 2.4. The algorithm is

$$\Delta r_n = (K_n)^{-1} \cdot (\Delta R_n + R^u_{n-1}) \quad ; \; R^u_o = 0 \qquad [2.5]$$

$$r_n = r_{n-1} + \Delta r_n \quad ; \; r_o = 0 \qquad [2.6]$$

2.2.4 Step by Step Procedures with Adaptable Step Size

A disadvantage of step by step procedures with predetermined load increments is that the error originating within any increment varies with the degree of nonlinearity of the

behavior, as indicated in Fig. 2.4. Improved accuracy can be obtained by automatically subdividing any load increment into smaller parts if the departure from the true behavior during the increment exceeds a specified amount.

Ideally, the permissible departure might be specified in terms of a maximum permissible unbalanced load. The computational procedure would then involve computation of the unbalanced load assuming application of the full load increment, followed by scaling down of the computed displacement increment if the equilibrium unbalance is excessive. A new state and new tangent stiffness would then be defined, and the procedure repeated until the entire load increment had been applied. A typical loading path might be as indicated in Fig. 2.5.

In practice, direct limitation of the unbalanced loads may be difficult. This is because the relationship between displacement increment and unbalanced load is generally nonlinear, and hence there may be a difficulty in selecting appropriate scaling factors for reduction of the computed displacements. In the analysis of elasto-plastic structures, this is most likely to occur when materials have well defined yield stresses with sudden changes of elastic modulus, as in elastic perfectly plastic behavior. A similar result can be achieved in such cases by specifying limits on the amount by which the stress computed assuming linear behavior may exceed the actual yield stress. This is illustrated for a simple yielding material in Fig. 2.6. Computational procedures for the more general case are described in Chapter 6.

2.2.5 Higher Order Step by Step Procedures

The accuracy of step by step procedures can also be improved by estimating the chord stiffness within each load increment, rather than by using the tangent stiffness at the beginning of the increment (30,34,39). A variety of procedures is possible, some having a formal mathematical basis and others based more on intuitive reasoning. Techniques of this type are not included within the general computational procedure proposed in this report, and hence will not be considered further. Nevertheless, they comprise an important and powerful class of procedures which should not be ignored.

2.3 ITERATION METHODS

2.3.1 General

In many cases it may not be necessary or desirable to determine the load-displacement relationship by step by step methods. Rather, the analyst may wish to apply the load in a single increment, and obtain only a single point in the load-displacement space. In such cases, the nonlinear problem may be solved by iteration. Iteration procedures may also be of value in combination with step by step techniques, to obtain a more accurate result by eliminating the equilibrium unbalance at the end of each step.

Iteration procedures are reviewed in the following sections for loads applied in single increments. Combinations of iteration and step by step techniques are also considered.

2.3.2 Constant Stiffness Iteration

A commonly used iteration procedure is illustrated diagrammatically in Fig. 2.7. This is commonly referred to as the "initial stress" procedure (50), but will be termed here "constant stiffness" iteration.

The procedure involves an initial formulation of the stiffness, K_0, for the unstressed structure, and its triangularization by an appropriate reduction technique. The iteration sequence then consists of the successive solution of a series of equilibrium equations according to the algorithm

$$\Delta r_n = (K_0)^{-1} \cdot (R - R^I_{n-1}) \qquad [2.7]$$

$$r_n = r_{n-1} + \Delta r_n \quad ; \quad r_0 = 0 \qquad [2.8]$$

in which Δr_n is the displacement increment computed in step n, R is the total applied external load, and R^I_n is the internal resisting load at the end of step n.

As before, the quantity

$$R^U_n = R - R^I_n \qquad [2.9]$$

is the unbalanced load on the structure at the end of step n, which is a measure of the extent to which equilibrium is violated, and hence of the convergence of the iteration procedure. The applied external load, R, is always either known explicitly or easily determined. For the cases considered in this report, this

load is assumed to be constant, but in the general case it could be variable. For example, variable loading occurs in the case of fluid pressures acting on structures which undergo significant changes of shape.

For a linear elastic structure, the stress, σ_n, and hence the internal resisting load, R_n^I, are uniquely defined for any given displacement, r_n. For inelastic structures, however, the stresses are not uniquely defined in terms of displacement, because the behavior is generally path dependent. This problem is considered in detail later, and for the time being it will be assumed that the stresses can be uniquely determined in all cases.

It may be noted that the internal resisting load in the initial undisplaced configuration, R_o^I, need not necessarily be zero, because temperature change and similar effects may induce initial stresses.

2.3.3 Constant Strain and Constant Stress Procedures

The state determination procedure shown in Fig. 2.3 may be identified as a "constant strain" procedure (29). The significance of this term is illustrated in Fig. 2.8a. By contrast an alternative "constant stress" procedure is illustrated in Fig. 2.8b. These terms lead, in turn, to concepts of "initial stress" and "initial strain".

In the solution of the state determination problem according to the sequence shown in Fig. 2.3, the strain increment is considered to be defined in terms of the computed displacement increment, and the corresponding stress increment is then found. The internal resisting load, R^I, and the unbalanced load, R^U,

can then be determined, and the iteration can proceed. However, an alternative procedure may be used to calculate R^u, which has given rise to the term "initial stress".

If large displacement effects are ignored, the only source of nonlinearity is the nonlinear material stress-strain relationship. In the constant stiffness iteration procedure, the stiffness K_o is obtained assuming the elastic modulus E_o shown in Fig. 2.8a. It follows, in any iteration step, that if the stress increment were equal to

$$\Delta \sigma_n^L = E_o \cdot \Delta \epsilon_n \qquad [2.10]$$

in which $\Delta \sigma_n^L$ = "linear" stress increment, then the unbalanced load would be zero. This is simply because the conditions of linearity assumed in the linearization phase would actually be satisfied, and hence the linear solution would be exact. In fact, however, the stress increment is $\Delta \sigma_n$, as defined previously. An "unbalanced stress", σ_n^u, may therefore be identified, where

$$\begin{aligned} \sigma_n^u &= (\sigma_{n-1} + \Delta \sigma_n^L) - (\sigma_{n-1} + \Delta \sigma_n) \\ &= \Delta \sigma_n^L - \Delta \sigma_n \\ &= E_o \Delta \epsilon_n - \Delta \sigma_n \end{aligned} \qquad [2.11]$$

The stress σ_n^u may be identified as an "initial" stress, leading to an equilibrium unbalance which must be eliminated by iteration. Such a stress can be regarded as similar to a stress produced by restraint of thermal expansion. The unbalanced load, R_n^u, can

then be obtained as the reverse of the loading which would be in equilibrium with σ_n^u .

The magnitude of R_n^u obtained in this way will be identical to that obtained by Eq. 2.4. However, the procedure based on unbalanced stress is less direct than that based on Eq. 2.4, and is conceptually more complex. The procedure described previously for obtaining R_n^u is therefore to be preferred.

A slightly different approach is to treat the equilibrium unbalance as originating with an initial strain, ϵ_n^u , such that

$$\sigma_n^u = E_o \cdot \epsilon_n^u \qquad [2.12]$$

Again there is a similarity with thermal stress analysis, the initial strain being numerically equal to the unrestrained temperature strain. In the solution of inelastic problems by iteration, ϵ_n^u is as shown in Fig. 2.8a.

Intuitively, the constant stiffness iteration process might be expected to converge slowly. Some means of over-relaxation might therefore be sought to speed convergence. The "constant stress" procedure illustrated in Fig. 2.8b is essentially an over-relaxation procedure, in which the initial strain is assumed to be $\bar{\epsilon}_n^u$ rather than ϵ_n^u . The reasoning behind the use of this initial strain is that for a simple one-dimensional system in which the load-displacement and stress-strain relationships have identical form, convergence is obtained in the second iteration step. The iterative sequence for such a case is illustrated in Fig. 2.9.

In certain cases, this procedure has led to improved convergence (45). In many cases, however, the procedure fails to converge. An obvious example of such a situation occurs for an elastic perfectly plastic material. Clearly, if a linear stress, σ_n^L, is computed which exceeds the yield stress of the material, then the initial strain, $\bar{\epsilon}_n^u$, is infinite, and the procedure will not converge.

Because it is applicable only in certain cases, the constant stress procedure has not been considered further in the studies reported here, and the constant strain procedure has been used exclusively. Also, no attempts have been made to explore other over-relaxation schemes, although it is recognized that such schemes might greatly improve the convergence of the constant stiffness iteration process.

2.3.4 Newton-Raphson Iteration

The constant stiffness iteration procedure retains the triangularized form of the stiffness matrix in the initial configuration, and uses this to solve each new set of equations. More rapid convergence would be expected if a new stiffness were computed at the end of each step, and used in the following step, as indicated in Fig. 2.10. The iteration sequence is then

$$\Delta r_n = (K_{n-1})^{-1} \cdot (R - R^I_{n-1}) \qquad [2.13]$$

$$r_n = r_{n-1} + \Delta r_n \quad ; \quad r_0 = 0 \qquad [2.14]$$

in which K_n is the tangent stiffness matrix for the configuration defined by r_n . This is Newton-Raphson iteration.

This procedure can be expected to converge more rapidly than constant stiffness iteration, but at the cost of additional computational effort for each iteration, because a new stiffness matrix must be reformed and re-triangularized. A major purpose of the research described in this report has been to assess the relative computational efficiency of the constant stiffness and Newton-Raphson procedures.

2.3.5 Mixed Iteration Procedures

Newton-Raphson iteration is likely to require fewer iteration cycles to converge, whereas constant stiffness iteration requires less computational effort for each cycle. The most efficient computational procedure might therefore be one in which the stiffness is reformed for some steps of the iteration, but kept constant for others. Two possible schemes are illustrated in Fig. 2.11.

In Fig. 2.11a, the stiffness is kept constant for a predetermined number of iteration cycles (in this case three), and is then changed. In Fig. 2.11b the stiffness is reformed at each step until the unbalanced load is reduced below a predetermined value, and is then kept constant for the remaining steps. This second procedure would appear to be preferable, because the stiffness is automatically reformed when the degree of nonlinearity is large, at which time recalculation of the stiffness is desirable,

yet the stiffness is maintained constant if the degree of non-linearity is small, at which time little is to be gained by recalculating the stiffness.

A variety of other mixed procedures are possible. Procedures of the type illustrated in Fig. 2.11b are incorporated into the general purpose solution procedure proposed here.

2.3.6 Combined Step by Step and Iteration Methods

Iteration can easily be applied within any load increment of a step by step procedure in order to reduce the unbalanced load to an acceptable value before applying the next increment. Combinations of step by step and iteration procedures can therefore be applied, and may be desirable in many cases.

2.4 OVERSHOOT AND REVERSAL TOLERANCES

2.4.1 Overshoot Tolerance

The use of an overshoot tolerance to prevent the solution in any linear step from departing too far from the true solution was considered for step by step methods in Section 2.2.4. A similar procedure is applicable to iterative methods, and could be used to help speed convergence. The technique is simple to apply, involving merely scaling the computed displacement increments by an appropriate factor, and calculating the strain and stress increments for these reduced displacements. The iteration algorithm then proceeds as before, with no change. The way in which a Newton-Raphson iteration procedure might be modified by the use of an overshoot tolerance is indicated in

Fig. 2.12. For simple one-dimensional behavior of the type illustrated, the convergence is not improved. However, the situation in a multi-dimensional case is more complex.

The use of overshoot tolerances have the further advantage that the strain path followed during loading is constrained to follow the "true" path more closely than if unlimited overshoot were permitted. Because the behavior of inelastic structures is path dependent, more accurate results might therefore be obtained.

2.4.2 Reversal Tolerance

A major difficulty with load reversal on inelastic structures is that the tangent modulus of a yielded material will generally have two values, namely that corresponding to continued yielding and that corresponding to unloading. For a step by step solution, the structure tangent stiffness obtained assuming continued yielding may therefore be a poor approximation to the actual tangent stiffness if unloading occurs, and hence the computed behavior within a load increment may depart substantially from the true behavior. For an iterative solution, the unbalanced load obtained through the use of an inaccurate tangent stiffness may be so large that convergence may be difficult to obtain.

The technique proposed here to avoid problems during reversal of stress or load is in two parts. Firstly, for each new loading case the analyst is required to specify whether the entire structure is expected to continue loading or to unload back into the elastic range. In most cases the expected behavior will be simple to determine. Secondly, in order to account for

(a) those cases where reversal of strain occurs even when the load is increasing and (b) those cases with complex loading paths in which it may not be clear whether or not the entire structure will unload, the analyst is also required to specify a stress reversal tolerance. This tolerance is similar in concept to the overshoot tolerance, and is used to prevent the linearized solution from departing too far from the true load-displacement relationship.

Use of the reversal tolerance is illustrated in Fig. 2.13. For this case, let the structure tangent stiffness be calculated on the assumption of continued loading. If strain reversal occurs the stress increment, $\Delta\sigma$, must be computed by following the unloading part of the stress-strain relationship. Hence, if the strain increment is large, the "linear" stress increment, $\Delta\sigma^{L}$ which would be based on the yielded tangent modulus for this case, may be grossly different from the true increment, $\Delta\sigma$, which is based on the unloading modulus. The unbalanced stress, σ^{u} , may therefore be excessive.

The magnitude of σ^{u} can be controlled by requiring that if unloading occurs, $\Delta\sigma$ may not exceed a specified magnitude, defined in terms of a predetermined unloading tolerance. If $\Delta\sigma$ exceeds the permissible value, then the computed displacements and strains are simply reduced by an appropriate scaling factor, α , as indicated in Fig. 2.13. The computation then continues as for cases in which an overshoot tolerance is imposed. The technique is applicable both to iterative and step by step procedures.

2.5 MEASURE OF CONVERGENCE

The unbalanced load, R^u, is a convenient measure of the error at any stage of an analysis. For structures with more than one degree of freedom, however, this unbalanced load is a vector, and not a single quantity. In this case, several different measure of the magnitude of the vector might be selected. The measure used here is the magnitude of the numerically largest term (the maximum norm), which is the largest unbalanced load for any degree of freedom of the structure. Other possible measures include the root mean square value of the terms of the vector (Euclidean norm) and the sum of the absolute values of the terms (absolute norm).

2.6 PROPOSED SOLUTION STRATEGY

Within a single computer program, it is possible to permit the user to select any one of a wide variety of solution strategies simply by specifying the magnitudes of three convergence tolerances. These tolerances are as follows:

(1) Final convergence tolerance, t_3. If the largest unbalanced load is less than this value, the solution for the current loading has converged with sufficient accuracy, and the next loading is considered.

(2) Constant stiffness tolerance, t_2. If the largest unbalanced load is less than this tolerance, the stiffness matrix is not reformed for the next iteration step, but the solution iterates with the same stiffness as in the current step. If this tolerance is equal to or less than t_3, a new stiffness will be formed at each step, corresponding to Newton-Raphson iteration.

If this tolerance is moderately small, the solution will iterate with a varying stiffness until this initial tolerance is reached, and will then iterate with constant stiffness. This is the mixed iteration procedure described in Section 2.3.5. If this tolerance is very large, the iteration will be with constant stiffness throughout.

(3) Step by step convergence tolerance, t_1 . This tolerance is used when a loading is applied in a number of equal increments. At the end of any increment, if (a) the largest unbalanced load is less than this tolerance and (b) this is not the last increment, then the next increment is added. If this tolerance is equal to or less than t_3 , the solution will iterate to final convergence within each increment. If this tolerance is moderately large, the solution will not iterate if the largest unbalanced load is less than the tolerance, but will iterate if the unbalanced load exceeds the tolerance. The iteration will not proceed to final convergence, but only until the largest unbalanced load is reduced below t_1 . However, the solution will automatically iterate to final convergence within the last load increment. If this tolerance is very large the solution will proceed immediately to the next load increment, as in a step by step solution with equilibrium correction, and will iterate to final convergence only within the last increment.

If the magnitude of these three tolerances are classified as "small", "moderate" and "large", a total of 13 different solution procedures can be identified. These procedures are summarized in Table 2.1 and are illustrated in Fig. 2.14.

All of these procedures can be further modified by use of an overshoot tolerance, as indicated for Newton-Raphson iteration in Fig. 2.12.

With this range of solution strategies, it should be possible for an experienced user to select an efficient procedure for virtually any type of problem. An example of the relative efficiencies obtained by different procedures is presented in Chapter 7.

TABLE 2.1 SOLUTION PROCEDURES OBTAINED BY VARYING TOLERANCE VALUES

Method Number	No. of Load Increments	Convergence Tolerances			Remark
		t_1	t_2	t_3	
1	1	arbitrary	small	small	Newton-Raphson Iteration
2	1	arbitrary	large	small	Constant Stiffness Iteration
3	1	arbitrary	moderate	small	Mixed Iteration of Methods 1 and 2
4	>1	large	large	large	Step by Step with simple equilibrium correction
5	>1	large	small	small	Step by Step, Newton-Raphson Iteration at last increment
6	>1	large	large	small	Step by Step, Constant Stiffness Iteration at last increment
7	>1	large	moderate	small	Step by Step, Mixed Iteration at last increment
8	>1	small	small	small	Step by Step, Newton-Raphson Iteration within each increment
9	>1	small	large	small	Step by Step, Constant Stiffness Iteration within each increment
10	>1	small	moderate	small	Step by Step, Mixed Iteration within each increment
11	>1	moderate	small	small	Iterate with Newton-Raphson Iteration } to coarse convergence tolerance, t_1, in all except last step. Iterate to final convergence tolerance, t_3 in last step
12	>1	moderate	large	small	Iterate with Constant Stiffness Iteration
13	>1	moderate	moderate	small	Iterate with Mixed Iteration

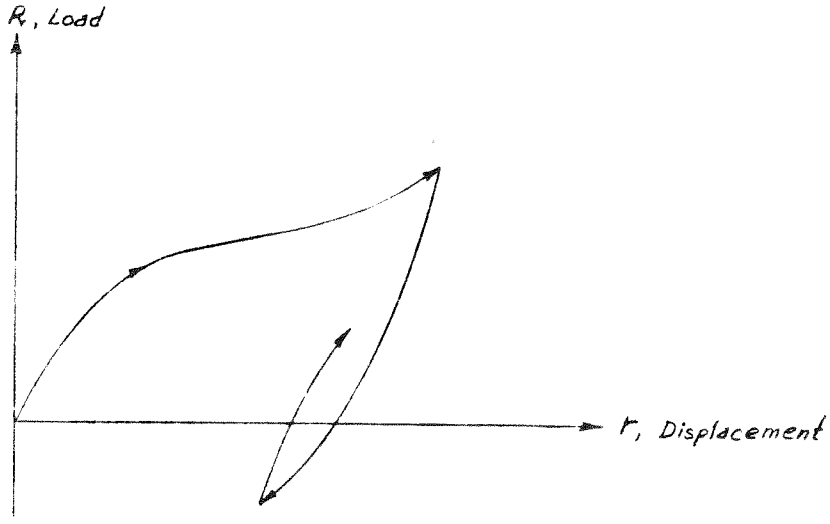

FIG 2.1 TYPE OF LOAD-DISPLACEMENT RELATIONSHIP CONSIDERED

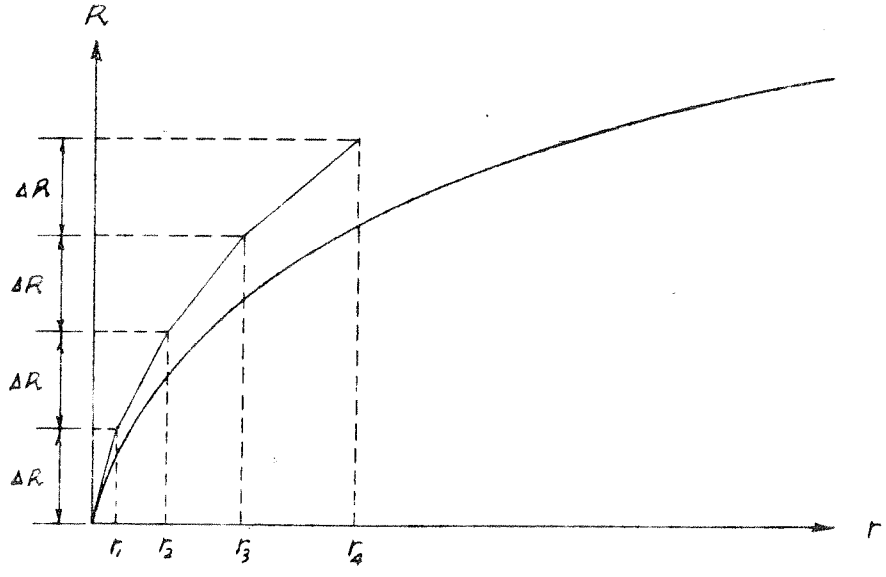

FIG 2.2 STEP BY STEP WITH TANGENT STIFFNESS

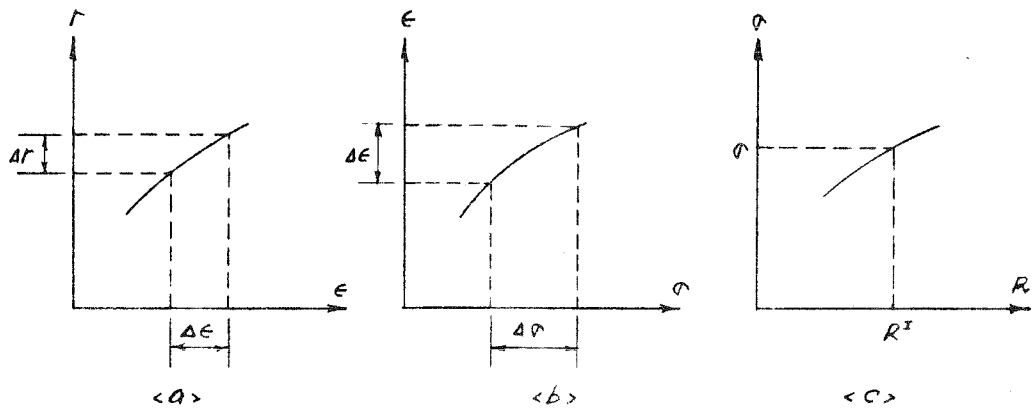

FIG 2.3 STATE DETERMINATION PROBLEM

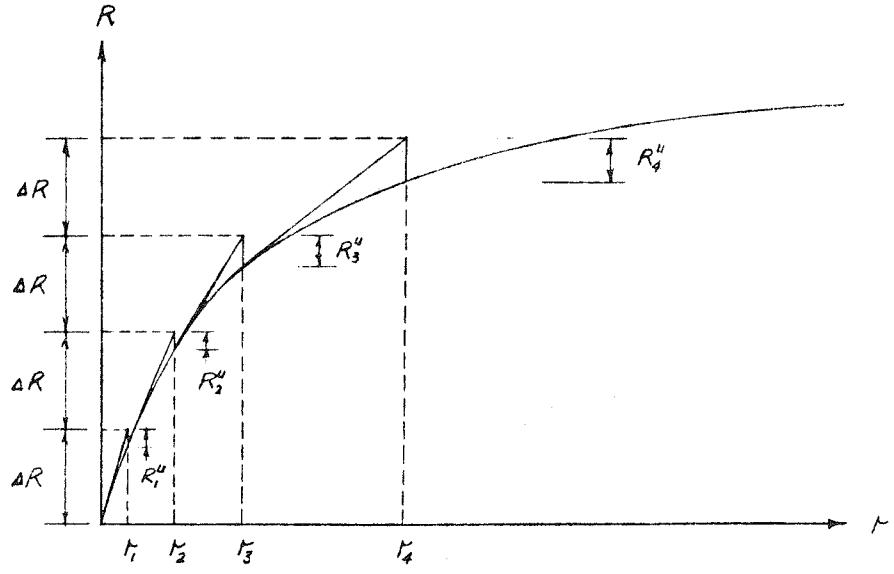

FIG 2.4 STEP BY STEP WITH EQUILIBRIUM CORRECTION

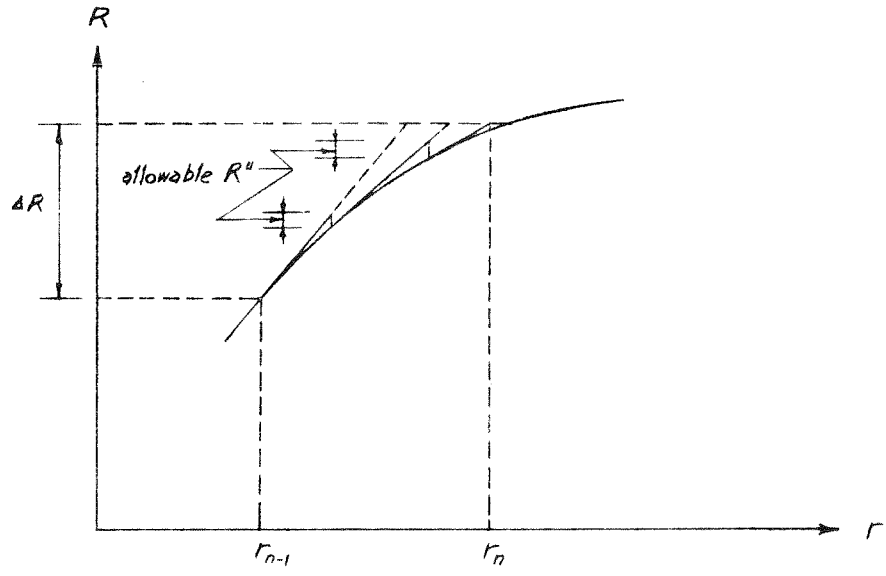

FIG 2.5 AUTOMATIC INCREMENT SUBDIVISION

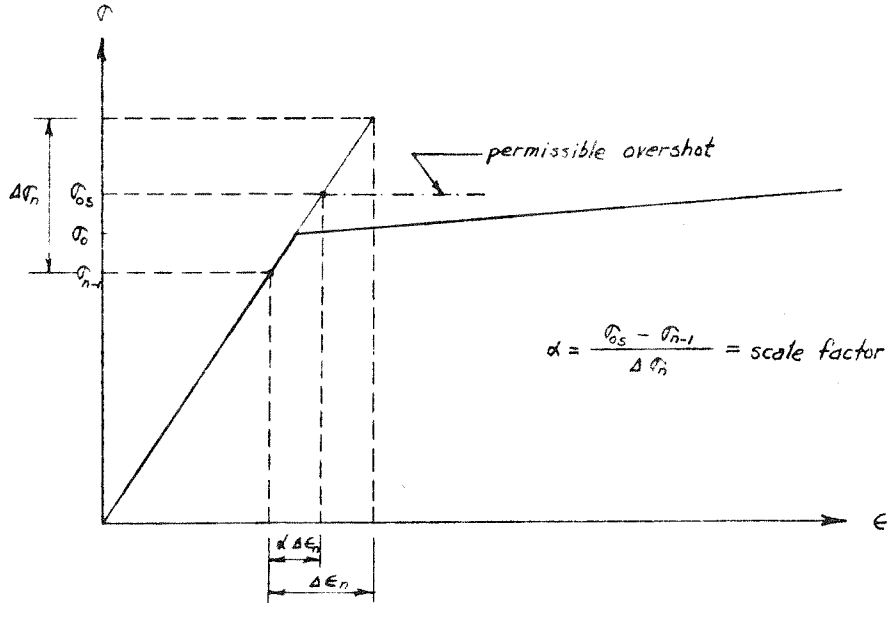

FIG 2.6 CORRECTION FOR OVERSHOOT

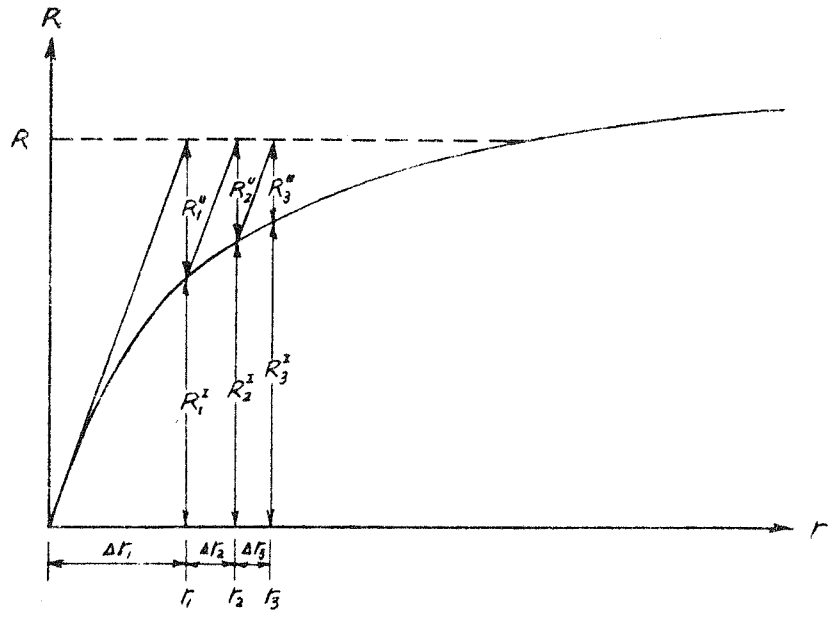

FIG 2.7 CONSTANT STIFFNESS ITERATION

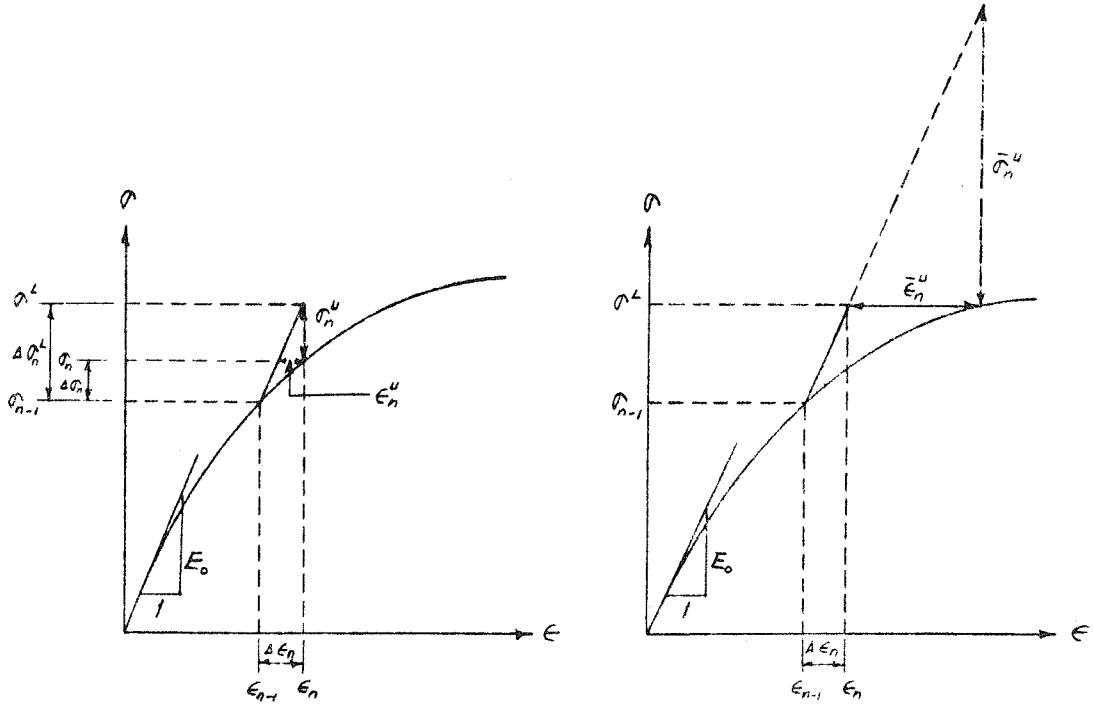

(a) Constant Strain (b) Constant Stress

FIG 2.8 CONSTANT STRAIN AND CONSTANT STRESS PROCEDURES

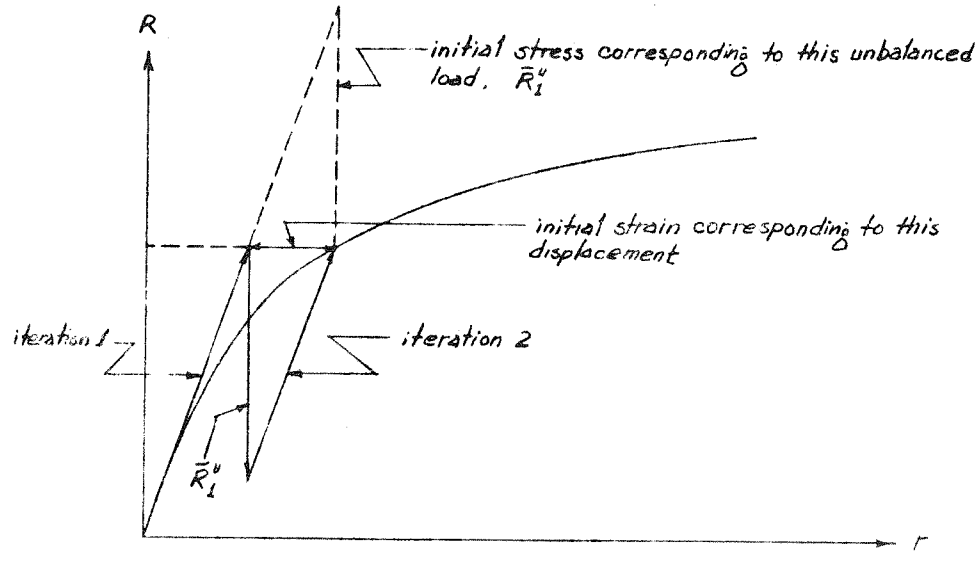

FIG 2.9 OVER RELAXATION FOR SIMPLE SYSTEM BASED ON CONSTANT STRESS PROCEDURE

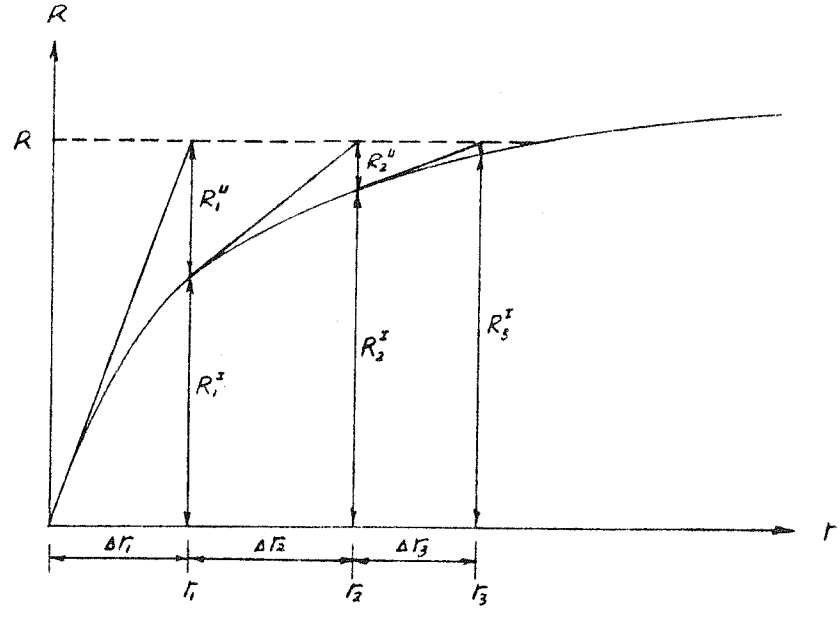

FIG 2.10 NEWTON-RAPHSON ITERATION

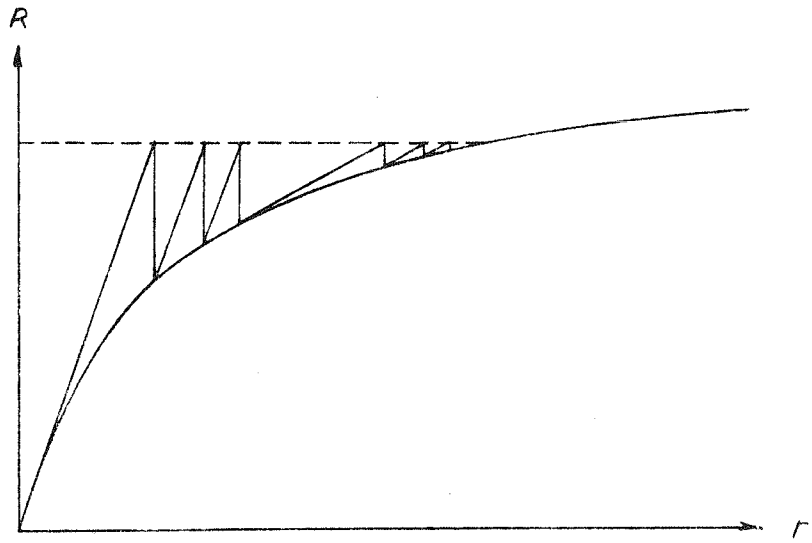

<a>

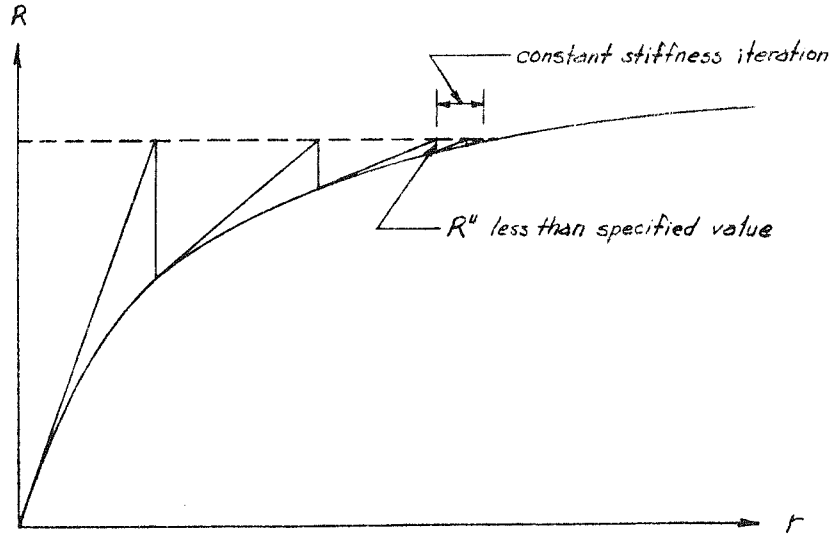

<b>

FIG 2.11 MIXED ITERATION PROCEDURES

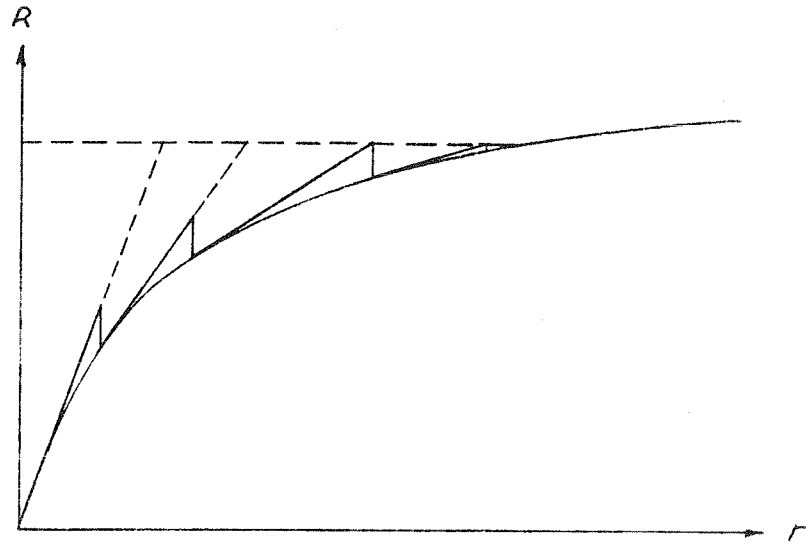

FIG 2.12 NEWTON-RAPHSON ITERATION WITH OVERSHOOT LIMIT

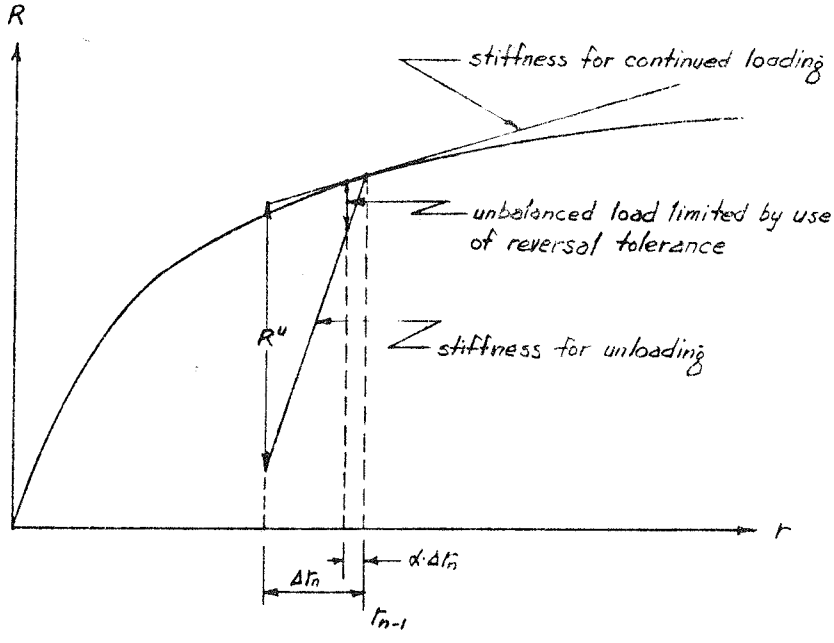

FIG 2.13 CONTROL OF UNBALANCED LOAD WITH REVERSAL TOLERANCE

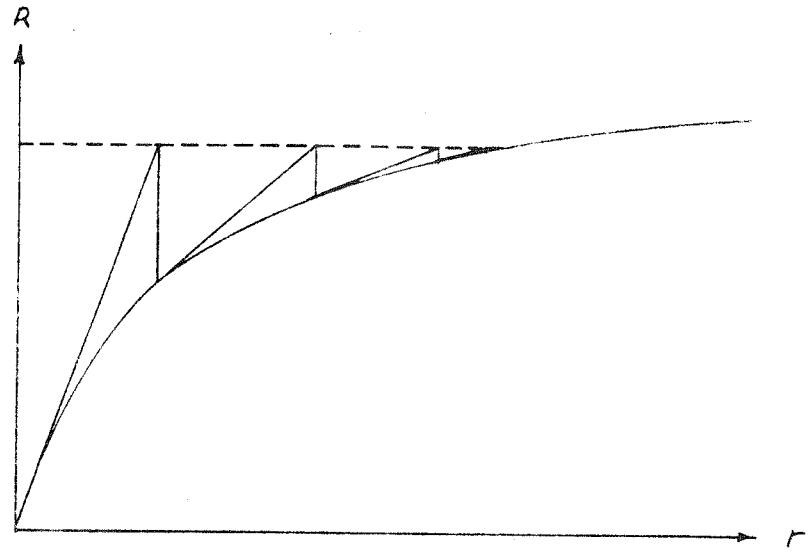

FIG 2.14 <a> METHOD 1

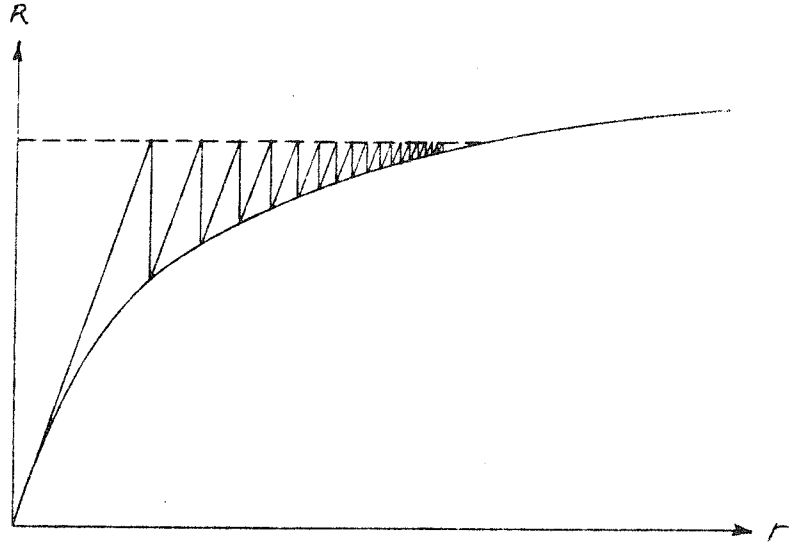

FIG 2.14 <b> METHOD 2

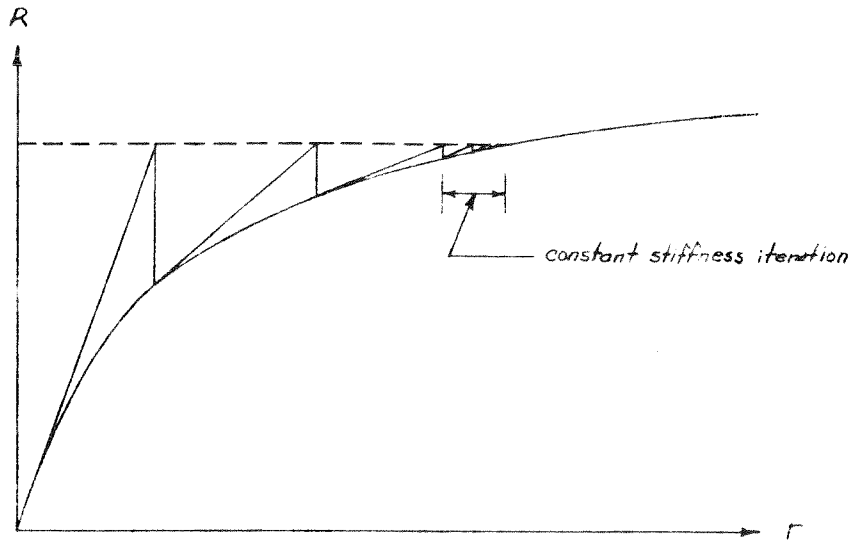

FIG 2.14 <c> METHOD 3

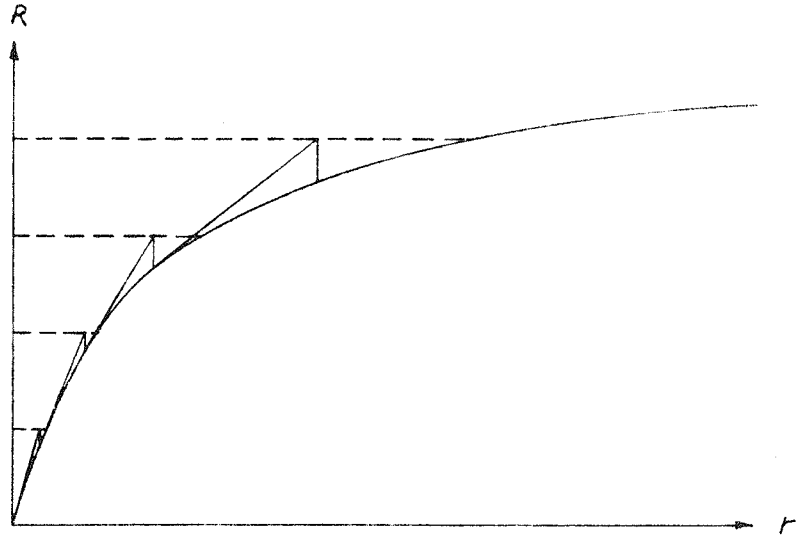

FIG 2.14 <d> METHOD 4

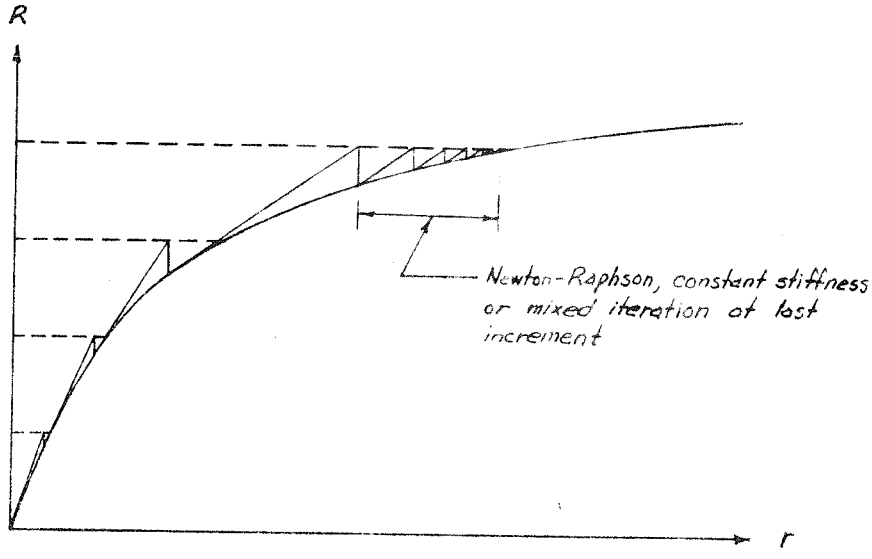

FIG 2.14 <e> METHODS 5, 6, 7

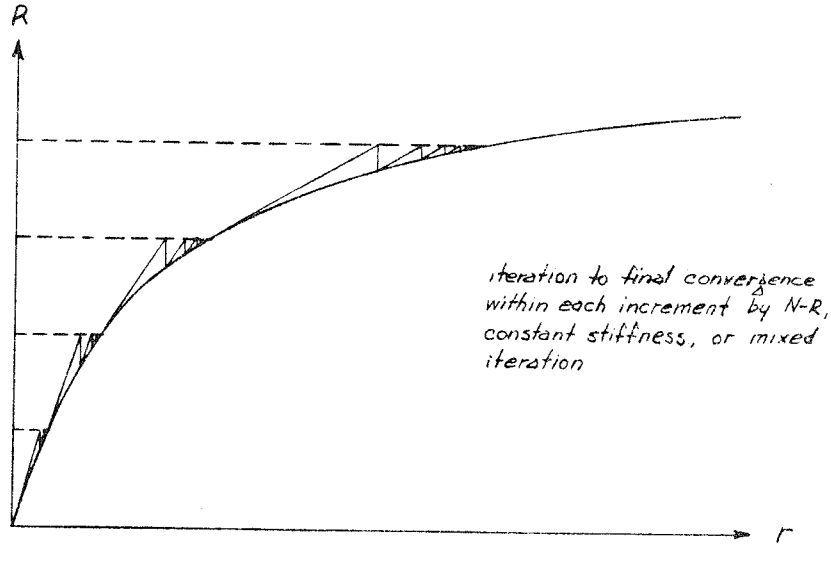

FIG 2.14 <f> METHODS 8, 9, 10

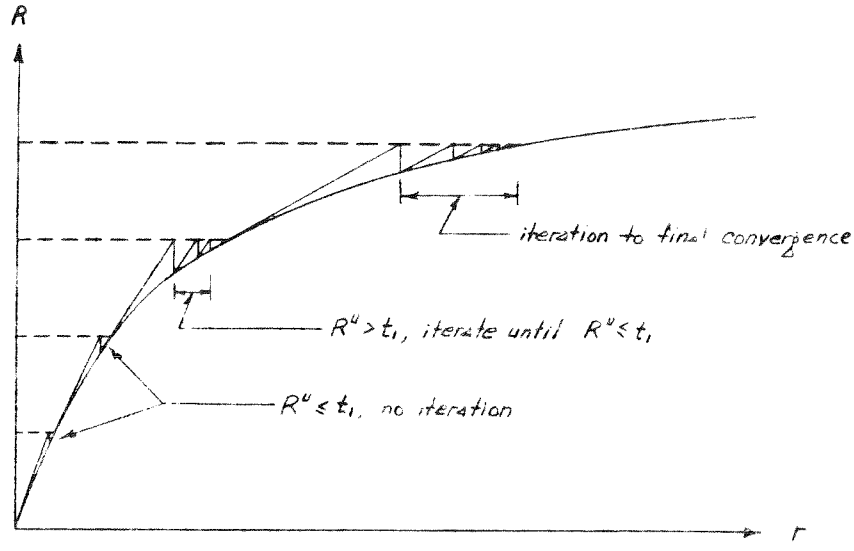

FIG 2.14 <$\frac{3}{8}$> METHODS 11, 12, 13

3. ELASTO-PLASTIC STRESS-STRAIN RELATIONSHIP

3.1 GENERAL

All solution procedures of the type considered herein involve successive solutions of a number of linearization and state determination problems. In order to deal with these two problems in elasto-plastic analysis, it is necessary to derive an incremental elasto-plastic stress-strain relationship. A number of assumptions and principles which are needed to formulate this relationship are reviewed in this chapter. More complete details and discussions may be found in the classical works of Hill (3), Nadai (5), Prager (8), Naghdi (19), etc.

The application of the incremental stress-strain relationship in the determination of the structure tangent stiffness and the solution of the state determination problem are considered in Chapters 4 and 5, respectively.

3.2 GENERAL FORM

It is assumed that there exists a scalar yield function, or loading function, which defines the boundary between the elastic and plastic ranges. The function is assumed to depend on the state of stress and the strain history, and may be written as

$$f(\underline{\sigma}, \underline{\epsilon}^p) = 0 \qquad [3.1]$$

where $\underline{\sigma}$ is the stress vector, $\underline{\epsilon}^p$ is the plastic strain vector, and the presence of $\underline{\epsilon}^p$ implies dependence on the history of strain as well as total strain. The function must define a closed

surface in stress space. For elastic states of stress $f<0$; for plastic states $f=0$; and no meaning is associated with $f>0$.

The function f must remain zero when going from one plastic state to another. Hence

$$df = \left(\frac{\partial f}{\partial \underline{\sigma}}\right)^T \cdot d\underline{\sigma} + \left(\frac{\partial f}{\partial \underline{\epsilon}^p}\right)^T \cdot d\underline{\epsilon}^p = 0 \qquad [3.2]$$

It is assumed that any increment, $d\underline{\epsilon}$, of total strain may be decomposed into an elastic component, $d\underline{\epsilon}^e$, and a plastic component, $d\underline{\epsilon}^p$. That is

$$d\underline{\epsilon} = d\underline{\epsilon}^e + d\underline{\epsilon}^p \qquad [3.3]$$

The increments of stress are assumed to be related to the elastic strain increments by the original elastic stress-strain relationship. That is

$$d\underline{\sigma} = \underline{C}^e \cdot d\underline{\epsilon}^e \qquad [3.4]$$

where $\underline{C}^e$ is the material elasticity matrix.

It also follows from Drucker's postulate (7) that the normality rule will apply. This rule states that the incremental plastic strain vector is always normal to the yield surface. That is

$$d\underline{\epsilon}^p = \lambda \cdot \left(\frac{\partial f}{\partial \underline{\sigma}}\right) \qquad [3.5]$$

where λ is an arbitrary constant and $(\partial f/\partial \underline{\sigma})$ defines the outward normal to the yield surface. Substitution of equations [3.4] and [3.5] into equation [3.2] gives

$$
\begin{aligned}
0 &= \left(\frac{\partial f}{\partial \underline{\sigma}}\right)^T \cdot \left[\underline{C}^e \cdot (d\underline{\epsilon} - d\underline{\epsilon}^p)\right] + \left(\frac{\partial f}{\partial \underline{\epsilon}^p}\right)^T \cdot d\underline{\epsilon}^p \\
&= \left(\frac{\partial f}{\partial \underline{\sigma}}\right)^T \cdot \underline{C}^e \cdot d\underline{\epsilon} - \left[\left(\frac{\partial f}{\partial \underline{\sigma}}\right)^T \underline{C}^e - \left(\frac{\partial f}{\partial \underline{\epsilon}^p}\right)^T\right] \cdot d\underline{\epsilon}^p \qquad [3.6] \\
&= \left(\frac{\partial f}{\partial \underline{\sigma}}\right)^T \cdot \underline{C}^e \cdot d\underline{\epsilon} - \left[\left(\frac{\partial f}{\partial \underline{\sigma}}\right)^T \cdot \underline{C}^e - \left(\frac{\partial f}{\partial \underline{\epsilon}^p}\right)^T\right] \cdot \lambda \cdot \left(\frac{\partial f}{\partial \underline{\sigma}}\right)
\end{aligned}
$$

or

$$
\lambda = \frac{\left(\frac{\partial f}{\partial \underline{\sigma}}\right)^T \cdot \underline{C}^e \cdot d\underline{\epsilon}}{\left[\left(\frac{\partial f}{\partial \underline{\sigma}}\right)^T \underline{C}^e \left(\frac{\partial f}{\partial \underline{\sigma}}\right) - \left(\frac{\partial f}{\partial \underline{\epsilon}^p}\right)^T \left(\frac{\partial f}{\partial \underline{\sigma}}\right)\right]} \qquad [3.7]
$$

The increment of elastic strain may now be expressed as

$$
\begin{aligned}
d\underline{\epsilon}^e &= d\underline{\epsilon} - d\underline{\epsilon}^p \\
&= d\underline{\epsilon} - \frac{\left(\frac{\partial f}{\partial \underline{\sigma}}\right)\left(\frac{\partial f}{\partial \underline{\sigma}}\right)^T \cdot \underline{C}^e \cdot d\underline{\epsilon}}{\left[\left(\frac{\partial f}{\partial \underline{\sigma}}\right)^T \underline{C}^e \left(\frac{\partial f}{\partial \underline{\sigma}}\right) - \left(\frac{\partial f}{\partial \underline{\epsilon}^p}\right)^T \left(\frac{\partial f}{\partial \underline{\sigma}}\right)\right]} \qquad [3.8]
\end{aligned}
$$

If both sides of Eq. [3.8] are premultiplied by $\underline{C}^e$, then

$$
\underline{C}^e \cdot d\underline{\epsilon}^e = \left\{\underline{C}^e - \frac{\underline{C}^e \cdot \left(\frac{\partial f}{\partial \underline{\sigma}}\right)\left(\frac{\partial f}{\partial \underline{\sigma}}\right)^T \cdot \underline{C}^e}{\left[\left(\frac{\partial f}{\partial \underline{\sigma}}\right)^T \underline{C}^e \left(\frac{\partial f}{\partial \underline{\sigma}}\right) - \left(\frac{\partial f}{\partial \underline{\epsilon}^p}\right)^T \left(\frac{\partial f}{\partial \underline{\sigma}}\right)\right]}\right\} \cdot d\underline{\epsilon}
$$

or

$$
d\underline{\sigma} = \underline{C}^{ep} \cdot d\underline{\epsilon} \qquad [3.9]
$$

in which

$$
\underline{C}^{ep} = \underline{C}^e - \frac{\underline{C}^e \cdot \left(\frac{\partial f}{\partial \underline{\sigma}}\right)\left(\frac{\partial f}{\partial \underline{\sigma}}\right)^T \cdot \underline{C}^e}{\left[\left(\frac{\partial f}{\partial \underline{\sigma}}\right)^T \underline{C}^e \left(\frac{\partial f}{\partial \underline{\sigma}}\right) - \left(\frac{\partial f}{\partial \underline{\epsilon}^p}\right)^T \left(\frac{\partial f}{\partial \underline{\sigma}}\right)\right]} \qquad [3.10]
$$

This is the incremental stress-strain relationship for elasto-plastic materials.

3.3 ELASTIC PERFECTLY PLASTIC MATERIAL

For an elastic perfectly plastic material, the yield function is a function of the stress, $\underline{\sigma}$, only and not of the strain, $\underline{\epsilon}^p$, so that $\frac{\partial f}{\partial \underline{\epsilon}^p} = \underline{0}$, and Eq. [3.10] becomes

$$\underline{C}^{ep} = \underline{C}^{e} - \frac{\underline{C}^{e}\left(\frac{\partial f}{\partial \underline{\sigma}}\right)\left(\frac{\partial f}{\partial \underline{\sigma}}\right)^{T}\cdot\underline{C}^{e}}{\left(\frac{\partial f}{\partial \underline{\sigma}}\right)^{T}\underline{C}^{e}\left(\frac{\partial f}{\partial \underline{\sigma}}\right)} \qquad [3.11]$$

Evaluation of $\underline{C}^{ep}$ requires an explicit expression for the yield function. The two most popular expressions for the yield function are those based on the von Mises and Tresca yield criteria. For the von Mises criterion

$$f = \left\{\frac{1}{2}\left[(\sigma_x-\sigma_y)^2+(\sigma_y-\sigma_z)^2+(\sigma_z-\sigma_x)^2+6(\tau_{xy}^2+\tau_{yz}^2+\tau_{zx}^2)\right]\right\}^{1/2} - \sigma_0 = 0 \qquad [3.12]$$

and for the Tresca criterion

$$f = [\sigma_{max.} - \sigma_{min.}] - \sigma_0 = 0 \qquad [3.13]$$

in which σ_0 is the yield stress in pure tension

When the von Mises criterion is used, the elasto-plastic material matrix, $\underline{C}^{ep}$, for an elastic perfectly plastic material can be expressed in closed form as

$$\underline{C}^{ep} = \frac{E}{1+\nu}\begin{bmatrix} \frac{1-\nu}{1-2\nu} - \frac{\sigma_x'^2}{S} & & & & & \\ \frac{\nu}{1-2\nu} - \frac{\sigma_x'\sigma_y'}{S} & \frac{1-\nu}{1-2\nu} - \frac{\sigma_y'^2}{S} & & & & \\ \frac{\nu}{1-2\nu} - \frac{\sigma_x'\sigma_z'}{S} & \frac{\nu}{1-2\nu} - \frac{\sigma_y'\sigma_z'}{S} & \frac{1-\nu}{1-2\nu} - \frac{\sigma_z'^2}{S} & \text{Sym.} & & \\ -\frac{\sigma_x'\tau_{xy}'}{S} & -\frac{\sigma_y'\tau_{xy}'}{S} & -\frac{\sigma_z'\tau_{xy}'}{S} & \frac{1}{2} - \frac{\tau_{xy}'^2}{S} & & \\ -\frac{\sigma_x'\tau_{yz}'}{S} & -\frac{\sigma_y'\tau_{yz}'}{S} & -\frac{\sigma_z'\tau_{yz}'}{S} & -\frac{\tau_{xy}'\tau_{zx}'}{S} & \frac{1}{2} - \frac{\tau_{yz}'^2}{S} & \\ -\frac{\sigma_x'\tau_{zx}'}{S} & -\frac{\sigma_y'\tau_{zx}'}{S} & -\frac{\sigma_z'\tau_{zx}'}{S} & -\frac{\tau_{xy}'\tau_{yz}'}{S} & -\frac{\tau_{yz}'\tau_{zx}'}{S} & \frac{1}{2} - \frac{\tau_{zx}'^2}{S} \end{bmatrix} \qquad [3.14]$$

in which

$$\sigma_x' = \sigma_{11}' \;, \quad \tau_{xy}' = \sigma_{12}' \;, \quad \text{etc.}$$

$$\sigma_{ij}' = \text{stress deviators} = \sigma_{ij} - \frac{1}{3}\delta_{ij}\sigma_{kk}$$

$$S = \frac{2}{3}\bar{\sigma}^2 \;, \quad \text{and} \quad \bar{\sigma} = \text{effective stress} = \left(\frac{3}{2}\sigma_{ij}'\sigma_{ij}'\right)^{1/2}$$

This expression was first given by Yamada et al (43,48)

For the Tresca criterion, the yield surface is discontinuous and is defined by six functions. Within a region defined by any one of these functions (a "regular" point), Eq. [3.11] still applies. However, at the junction of two surfaces (a "singular" point), it is necessary to satisfy the normality rule for both surfaces simultaneously. Koiter (9) has shown that if the two adjacent surfaces described by $f_i = 0$ and $f_j = 0$ act independently, the total plastic deformation can be written as the sum of contributions from f_i and f_j, each obeying Eq. [3.6] with f_i or f_j replacing f. That is

$$d\underline{\epsilon}^p = \lambda_i\left(\frac{\partial f_i}{\partial \underline{\sigma}}\right) + \lambda_j\left(\frac{\partial f_j}{\partial \underline{\sigma}}\right) \qquad [3.15]$$

Koiter has further shown that the constants λ_i and λ_j may be determined from the surfaces $f_i = 0$, and $f_j = 0$ in a manner similar to that of λ in Eq. [3.7]. It follows that

$$\lambda_i = \left[\left(\frac{\partial f_i}{\partial \underline{\sigma}}\right)^T \underline{C}^e \, d\underline{\epsilon}\right] \Big/ \left[\left(\frac{\partial f_i}{\partial \underline{\sigma}}\right)^T \underline{C}^e \left(\frac{\partial f_i}{\partial \underline{\sigma}}\right)\right] \qquad [3.16]$$

$$\lambda_j = \left[\left(\frac{\partial f_j}{\partial \underline{\sigma}}\right)^T \underline{C}^e \, d\underline{\epsilon}\right] \Big/ \left[\left(\frac{\partial f_j}{\partial \underline{\sigma}}\right)^T \underline{C}^e \left(\frac{\partial f_j}{\partial \underline{\sigma}}\right)\right] \qquad [3.17]$$

and hence

$$\underline{C}^{ep} = \underline{C}^e - \left[\frac{\underline{C}^e \left(\frac{\partial f_i}{\partial \underline{\sigma}}\right)\left(\frac{\partial f_i}{\partial \underline{\sigma}}\right)^T \underline{C}^e}{\left(\frac{\partial f_i}{\partial \underline{\sigma}}\right)^T \underline{C}^e \left(\frac{\partial f_i}{\partial \underline{\sigma}}\right)} + \frac{\underline{C}^e \left(\frac{\partial f_j}{\partial \underline{\sigma}}\right)\left(\frac{\partial f_j}{\partial \underline{\sigma}}\right)^T \underline{C}^e}{\left(\frac{\partial f_j}{\partial \underline{\sigma}}\right)^T \underline{C}^e \left(\frac{\partial f_j}{\partial \underline{\sigma}}\right)}\right] \qquad [3.18]$$

3.4 STRAIN HARDENING THEORIES

3.4.1 Hardening Rules

It is known that during plastic deformation the yield surface is continuously changing in size and shape. Several procedures to account for this effect have been suggested. These include the isotropic hardening theory of Taylor and Quinney (1), the slip theory of Batdorf and Budiansky (10), the piecewise linear hardening theory of Hodge (13), the kinematic hardening theory of Prager (11), and Ziegler's modification of this theory (18).

Projections of a Tresca yield surface on the π -plane (the plane $\sigma_1 + \sigma_2 + \sigma_3 = 0$) are shown, in Fig. 3.1. Isotropic hardening, as illustrated in Fig. 3.1a, assumes a uniform expansion of the yield surface during plastic deformation. It does not account for Bauschinger's effect, which has been

observed in many experimental studies. Consequently, despite its mathematical simplicity, the use of this theory is questionable in all situations except those involving only monotonically increasing stress.

The slip theory, as illustrated in Fig. 3.1b, predicts the formation of a corner on the yield surface during plastic flow. The stress-strain relationship becomes complex, which is a serious obstacle in analytical procedures. Furthermore, the Bauschinger effect is not taken into account.

The independent piecewise hardening theory, as illustrated in Fig. 3.1c, assumes that only one facet of the yield surface is caused to move by plastic deformation. An extension of this concept, which takes Bauschinger's effect into account, assumes interdependent piecewise linear hardening as illustrated in Fig. 3.1d. This theory assumes that all facets of the yield surface change in some inter-related manner during plastic flow. These theories are limited to piecewise linear yield surfaces, and their mathematical complexity is a handicap in applications.

The kinematic hardening theory assumes that the yield surface translates as a rigid body in stress space, maintaining its size, shape and orientation during plastic deformation. The primary aim of this theory is to provide a means of accounting for the Bauschinger effect. It predicts a Bauschinger effect for completely reversed loading conditions such that the range of elastic stress remains unchanged. The theory proposed by Prager, as illustrated in Fig. 3.1e, predicts that the yield

surface moves in a direction normal to itself at the instantaneous stress state. However, it has been claimed that inconsistencies arise when this theory is applied in various subspaces of stress (14,16,18). In order to remove these inconsistencies, Ziegler (16,18) suggested a modification, as illustrated in Fig. 3.1f. This modification assumes that the yield surface translates in the direction of the vector from the center of the surface to the instantaneous stress state. Both theories are coincident when the von Mises yield criterion is employed (19).

In the following sections, expressions for the matrix $\underline{C}^{ep}$ are derived for two simple cases, namely isotropic strain hardening and linear kinematic strain hardening.

3.4.2 Isotropic Hardening

The form of the yield function for isotropic hardening can be expressed as

$$f(\underline{\sigma}, \underline{\varepsilon}^p) = f^*(\underline{\sigma}) - \kappa(\underline{\varepsilon}^p) = 0 \qquad [3.19]$$

where f^* is a function of stress alone, and the parameter κ depends on the plastic strain history. There are two procedures to express the parameter, κ . In the first, κ is given in terms of the plastic work, W^p , as

$$\kappa = \kappa\left(\int dW^p\right) \qquad [3.20]$$

in which

$$dW^P = \underline{\sigma}^T \cdot d\underline{\epsilon}^P = \bar{\sigma} \cdot d\bar{\epsilon}^P$$

$$\bar{\sigma} = \text{effective stress} = \left(\frac{3}{2}\underline{\sigma}'^T \cdot \underline{\sigma}'\right)^{1/2}$$

$$d\bar{\epsilon}^P = \text{effective plastic strain} = \left(\frac{2}{3} d\underline{\epsilon}^{P^T} \cdot d\underline{\epsilon}^P\right)^{1/2}$$

In the second, K is expressed in terms of the effective plastic strain, as

$$K = K\left(\int d\bar{\epsilon}^P\right) \qquad [3.21]$$

Bland (12) has shown that these two procedures are equivalent.

For the von Mises criterion, Eq. [3.19] may be written as

$$f(\underline{\sigma}, \underline{\epsilon}^P) = \left(\frac{3}{2}\underline{\sigma}'^T \cdot \underline{\sigma}'\right)^{1/2} - \bar{\sigma}(\underline{\epsilon}^P) = 0 \qquad [3.22]$$

From Equations [3.20], [3.21] and [3.22], the quantities required to construct the elasto-plastic material property matrix, $\underline{C}^{ep}$, can be found. Thus

$$\frac{\partial f}{\partial \underline{\sigma}} = \frac{3}{2} \cdot \frac{1}{\bar{\sigma}} \cdot \underline{\sigma}' \qquad [3.23]$$

$$\frac{\partial f}{\partial \underline{\epsilon}^P} = -\frac{\partial \bar{\sigma}}{\partial \underline{\epsilon}^P} = -\frac{\partial \bar{\sigma}}{\partial \bar{\epsilon}^P} \cdot \frac{\partial \bar{\epsilon}^P}{\partial W^P} \cdot \frac{\partial W^P}{\partial \underline{\epsilon}^P}$$

$$= -\frac{\partial \bar{\sigma}}{\partial \bar{\epsilon}^P} \cdot \frac{1}{\bar{\sigma}} \cdot \underline{\sigma} \qquad [3.24]$$

Substitution of Equations [3.23] and [3.24] into Equation [3.10] gives

$$\underline{C}^{ep} = \underline{C}^{e} - \frac{\underline{C}^{e}\left(\frac{\partial f}{\partial \underline{\sigma}}\right)\left(\frac{\partial f}{\partial \underline{\sigma}}\right)^{T}\underline{C}^{e}}{\left[\left(\frac{\partial f}{\partial \underline{\sigma}}\right)^{T}\underline{C}^{e}\left(\frac{\partial f}{\partial \underline{\sigma}}\right) + H'\right]} \qquad [3.25]$$

where $H' = \frac{\partial \bar{\sigma}}{\partial \bar{\epsilon}^{p}}$ can be determined provided the relationship between $\bar{\sigma}$ and $\bar{\epsilon}^{p}$ is defined. Typically, the data from a uniaxial tension test will be known. The incremental stress-strain relationship may be written as

$$d\sigma = E_T \cdot d\epsilon = E_T \cdot \left(\frac{d\sigma}{E_o} + d\epsilon^{p}\right)$$

so that

$$\frac{1}{\frac{d\sigma}{d\epsilon^{p}}} = \frac{1}{\frac{d\bar{\sigma}}{d\bar{\epsilon}^{p}}} = \frac{1}{H'} = \frac{1}{E_T} - \frac{1}{E_o} \qquad [3.26]$$

in which E_T is the tangent modulus.

3.4.3 Kinematic Hardening

The yield function for kinematic hardening may be expressed as

$$f(\underline{\sigma}, \underline{\epsilon}^{p}) = f^{*}(\underline{\sigma} - \underline{\alpha}) - k = 0 \qquad [3.27]$$

where $\underline{\alpha}$ is a stress vector defining the translation of the yield surface. Shield and Ziegler (16) have defined $\underline{\alpha}$ by

$$d\underline{\alpha} = g(\underline{\sigma}, \underline{\epsilon}^{p}) \cdot d\underline{\epsilon}^{p} \qquad [3.28]$$

in which g is a hardening parameter. This parameter is constant if simple linear hardening is assumed, so that

$$d\underline{\alpha} = g \cdot d\underline{\epsilon}^p \qquad [3.29]$$

and

$$\underline{\alpha} = g \cdot \underline{\epsilon}^p \qquad [3.30]$$

The constant g in this case is the slope of the relationship between deviator stress and plastic strain. If the data from a uniaxial tension test is used, it follows that

$$g = \frac{d\sigma'}{d\epsilon^p} = \frac{\frac{2}{3}d\sigma}{d\epsilon^p} = \frac{2}{3} \cdot \frac{d\sigma}{d\epsilon^p} = \frac{2}{3}H' \qquad [3.31]$$

in which H' is as defined for Eq. [3.26].

It may be noted that K in Eq. [3.27] is constant, rather than variable as it is in Eq. [3.19] for isotropic hardening. The information on plastic deformation history is therefore contained within the vector $\underline{\alpha}$.

If the von Mises criterion is adopted, the yield function becomes

$$f(\underline{\sigma}, \underline{\epsilon}^p) = \left[\frac{3}{2}(\underline{\sigma}'-\underline{\alpha})^T(\underline{\sigma}'-\underline{\alpha})\right]^{1/2} - \sigma_o = 0 \qquad [3.32]$$

in which σ_o is the uniaxial yield stress.

From Eqs. [3.30] and [3.32]

$$\frac{\partial f}{\partial \underline{\sigma}} = \frac{3}{2} \cdot \frac{1}{\sigma_o} \cdot (\underline{\sigma}' - \underline{\alpha}) \qquad [3.33]$$

$$\frac{\partial f}{\partial \underline{\epsilon}^p} = -\frac{3}{2} \cdot \frac{1}{\sigma_o} \cdot g \cdot (\underline{\sigma}' - \underline{\alpha}) \qquad [3.34]$$

The elasto-plastic material property matrix is therefore given by

$$\underline{C}^{ep} = \underline{C}^e - \frac{\underline{C}^e \left(\frac{\partial f}{\partial \underline{\sigma}}\right)\left(\frac{\partial f}{\partial \underline{\sigma}}\right)^T \underline{C}^e}{\left[\left(\frac{\partial f}{\partial \underline{\sigma}}\right)^T \underline{C}^e \left(\frac{\partial f}{\partial \underline{\sigma}}\right) + \frac{g}{4} \cdot \frac{1}{\sigma_o^2} \cdot g \cdot (\underline{\sigma}' - \underline{\alpha})^T (\underline{\sigma}' - \underline{\alpha})\right]} \qquad [3.35]$$

It can be shown that $\frac{g}{4} \cdot \frac{1}{\sigma_o^2} \cdot g \cdot (\underline{\sigma}' - \underline{\alpha})^T (\underline{\sigma}' - \underline{\alpha}) = H'$ so that Eq. 3.35 is identical to Eq. 3.25.

3.5 PARALLEL MATERIAL PROCEDURE FOR STRAIN HARDENING

3.5.1 Concept

The foregoing kinematic hardening theory assumes a bilinear stress-strain relationship, and is theoretically consistent for this type of relationship only. For more complex stress-strain relationship, there exists no well established procedure for the specification of the hardening parameter, g . An approximate approach has been suggested by Isakson et al (36), but it has been recognized that this approach may lead to inaccurate representation of the hardening behavior under some circumstances. A simple kinematic hardening model which is applicable to a wide range of stress-strain relationships is considered in this section. The concept is not original, having been previously applied to elements under both uniaxial stress (6,22,58) and biaxial stress (59).

The material is assumed to be composed of several component materials, acting in parallel and subjected to identical total strains. The materials are all elastic perfectly plastic, but each has a different yield stress and elastic modulus.

The concept is illustrated for a simple one-dimensional case in Fig. 3.2. As shown in Fig. 3.4, a Bauschinger effect with a constant elastic stress range is automatically obtained with this type of model. Fig. 3.3 shows how complex stress-strain relationships can be obtained by combining several elastic perfectly plastic relationships in parallel.

For multi-dimensional stress the principle is exactly the same. The elasto-plastic material property matrix for each component material is as developed in Section 3.3. The matrix for the resultant material is obtained by simple addition of the matrices for the component materials, and it is not necessary to postulate a strain hardening law. As shown in Chapter 7, the resultant material appears to behave in the same way as Prager's kinematic hardening model with the von Mises criterion, although an investigation to explore this in detail has not been possible within the current study.

This model has the advantage of mathematical and conceptual simplicity. Computationally, it is necessary to keep track of the status of each component material, and to ensure that the strains in all component materials are identical. In most cases no computational difficulties are introduced. However, a particular problem which may arise in the plane stress problems should be recogized, as considered in the following section.

3.5.2 Relationships for Plane Stress

In a plane stress problem,

$$\sigma_z = 0 \qquad [3.36]$$

where the z direction is normal to the stress plane. It is important to note that this equation must be satisfied for the resultant material, and not necessarily for each component material. That is, the sum of the σ_z stresses on all component materials must be zero, but the stress on any individual component may be nonzero. At the same time, the strain ϵ_z must be the same in all components.

For simplicity, it is assumed here that the shear stresses τ_{yz} and τ_{zx} are zero in each component material although this assumption is not essential. It follows that, the constitutive relationship for the ith component can be written as

$$\begin{Bmatrix} d\sigma_x \\ d\sigma_y \\ d\tau_{xy} \\ d\sigma_z \end{Bmatrix}_i = \begin{bmatrix} C_{11} & C_{12} & C_{13} & C_{14} \\ C_{21} & C_{22} & C_{23} & C_{24} \\ C_{31} & C_{32} & C_{33} & C_{34} \\ C_{41} & C_{42} & C_{43} & C_{44} \end{bmatrix}_i \begin{Bmatrix} d\epsilon_x \\ d\epsilon_y \\ d\gamma_{xy} \\ d\epsilon_z \end{Bmatrix}_i \qquad [3.37]$$

Because the strains $d\epsilon_x$, $d\epsilon_y$, $d\epsilon_z$ and $d\gamma_{xy}$ are identical for all components, and

$$\begin{Bmatrix} d\sigma_x \\ d\sigma_y \\ d\tau_{xy} \\ d\sigma_z \end{Bmatrix} = \sum_{i=1}^{n} \begin{Bmatrix} d\sigma_x \\ d\sigma_y \\ d\tau_{xy} \\ d\sigma_z \end{Bmatrix}_i \quad ; \quad n = \text{number of components}$$

the constitutive relationship for the resultant material is simply

$$\begin{Bmatrix} d\sigma_x \\ d\sigma_y \\ d\tau_{xy} \\ d\sigma_z \end{Bmatrix} = \sum_{i=1}^{n} \begin{bmatrix} C_{11} & C_{12} & C_{13} & C_{14} \\ C_{21} & C_{22} & C_{23} & C_{24} \\ C_{31} & C_{32} & C_{33} & C_{34} \\ C_{41} & C_{42} & C_{43} & C_{44} \end{bmatrix}_i \begin{Bmatrix} d\epsilon_x \\ d\epsilon_y \\ d\gamma_{xy} \\ d\epsilon_z \end{Bmatrix} \qquad [3.38]$$

$$= \begin{bmatrix} D_{11} & D_{12} & D_{13} & D_{14} \\ D_{21} & D_{22} & D_{23} & D_{24} \\ D_{31} & D_{32} & D_{33} & D_{34} \\ D_{41} & D_{42} & D_{43} & D_{44} \end{bmatrix} \begin{Bmatrix} d\epsilon_x \\ d\epsilon_y \\ d\gamma_{xy} \\ d\epsilon_z \end{Bmatrix}$$

or

$$\begin{Bmatrix} d\sigma_x \\ d\sigma_y \\ d\tau_{xy} \end{Bmatrix} = \begin{bmatrix} D_{11} & D_{12} & D_{13} \\ D_{21} & D_{22} & D_{23} \\ D_{31} & D_{32} & D_{33} \end{bmatrix} \begin{Bmatrix} d\epsilon_x \\ d\epsilon_y \\ d\gamma_{xy} \end{Bmatrix} + \begin{Bmatrix} D_{14} \\ D_{24} \\ D_{34} \end{Bmatrix} \cdot d\epsilon_z \qquad [3.39]$$

Hence

$$d\sigma_z = 0 = D_{41} \cdot d\epsilon_x + D_{42} \cdot d\epsilon_y + D_{43} \cdot d\gamma_{xy} + D_{44} \cdot d\epsilon_z \qquad [3.40]$$

which yields

$$d\epsilon_z = -\frac{D_{41}}{D_{44}} \cdot d\epsilon_x - \frac{D_{42}}{D_{44}} \cdot d\epsilon_y - \frac{D_{43}}{D_{44}} \cdot d\gamma_{xy} \qquad [3.41]$$

Substitution of Eq. [3.41] into Eq. [3.37] yields the stress-strain relationship for plane stress for the ith component material as

$$\begin{Bmatrix} d\sigma_x \\ d\sigma_y \\ d\tau_{xy} \\ d\sigma_z \end{Bmatrix}_i = \begin{bmatrix} C_{11}-C_{14}\frac{D_{41}}{D_{44}} & C_{12}-C_{14}\frac{D_{42}}{D_{44}} & C_{13}-C_{14}\frac{D_{43}}{D_{44}} \\ C_{21}-C_{24}\frac{D_{41}}{D_{44}} & C_{22}-C_{24}\frac{D_{42}}{D_{44}} & C_{23}-C_{24}\frac{D_{43}}{D_{44}} \\ C_{31}-C_{34}\frac{D_{41}}{D_{44}} & C_{32}-C_{34}\frac{D_{42}}{D_{44}} & C_{33}-C_{34}\frac{D_{43}}{D_{44}} \\ C_{41}-C_{44}\frac{D_{41}}{D_{44}} & C_{42}-C_{44}\frac{D_{42}}{D_{44}} & C_{43}-C_{44}\frac{D_{43}}{D_{44}} \end{bmatrix}_i \cdot \begin{Bmatrix} d\epsilon_x \\ d\epsilon_y \\ d\gamma_{xy} \end{Bmatrix} \qquad [3.42]$$

Although Eq. [3.40] should strictly be used in plane stress analyses, it is probably sufficiently accurate in most cases to assume that $d\sigma_z$ is zero in each component material, and hence to obtain the plane stress-strain relationship for the resultant material by adding the component plane stress-strain relationships. It may also be justifiable to evaluate finite element stiffness matrix for each component material, and to obtain a resultant stiffness by addition at the element level, rather than at the material level. It might further be possible to obtain different hardening behavior by combining in parallel materials with simple isotropic or kinematic hardening rules, rather than only elastic perfectly plastic materials.

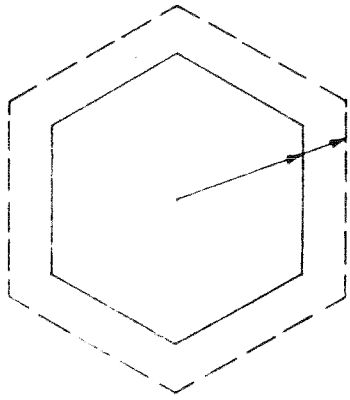

<a> Isotropic Hardening Theory

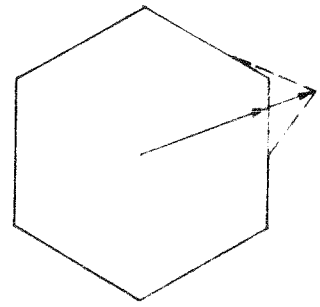

<b> Slip Theory

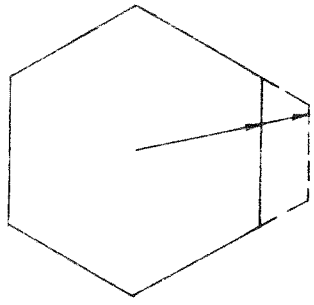

<c> Independently Piecewise Linear Hardening Theory

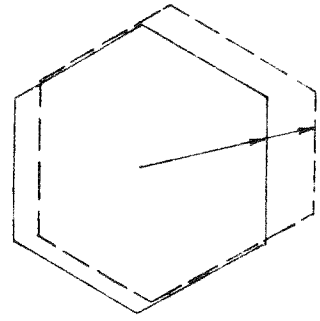

<d> Inter-related Piecewise Linear Hardening Theory

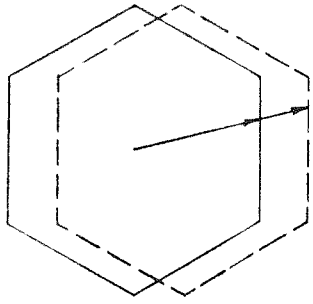

<e> Kinematic Hardening Theory (Prager's)

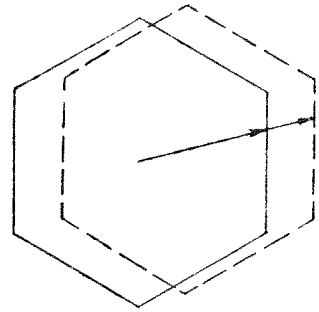

<f> Ziegler's Modification of Kinematic Hardening Theory

FIG 3-1 VARIOUS HARDENING RULES (DASH LINE) FOR TRESCA'S INITIAL YIELD CRITERION (SOLID LINE)

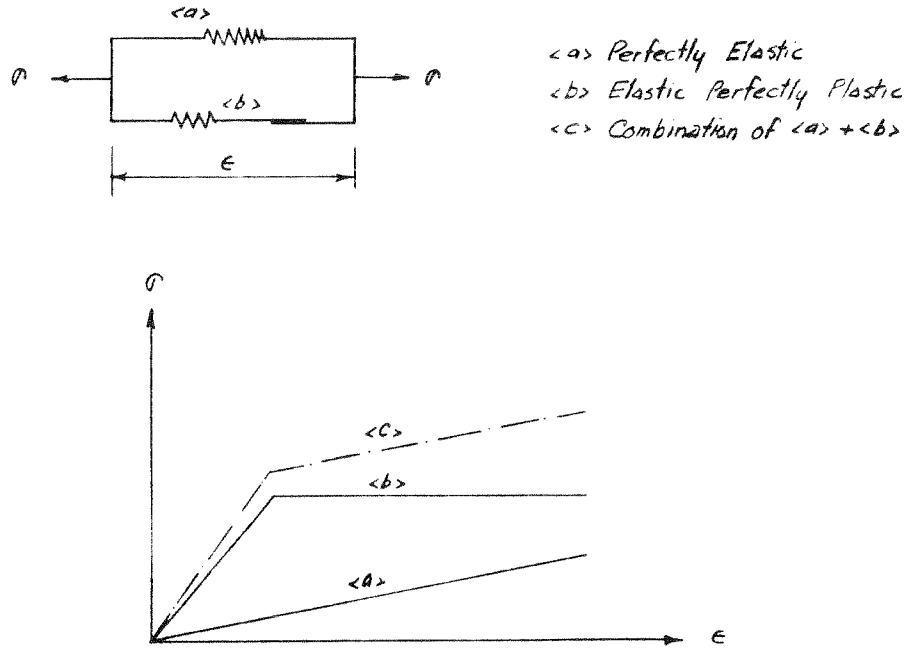

FIG 3-2 PARALLEL MATERIAL MODEL FOR STRAIN HARDENING MATERIALS

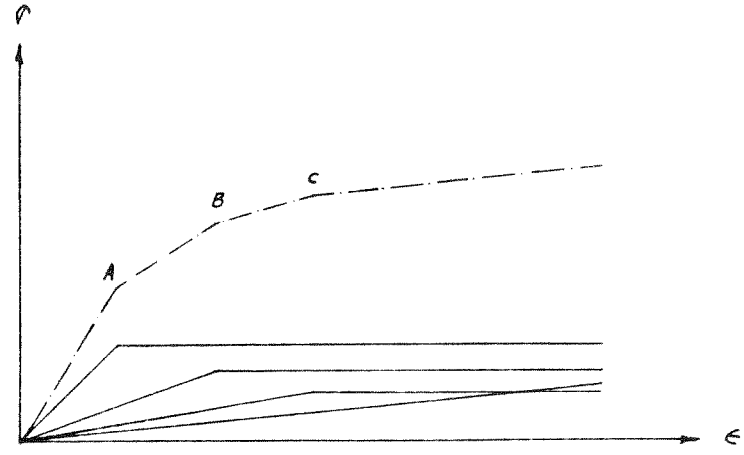

FIG 3-3 NONLINEAR STRAIN HARDENING REPRESENTED BY SEVERAL COMPONENT MATERIALS

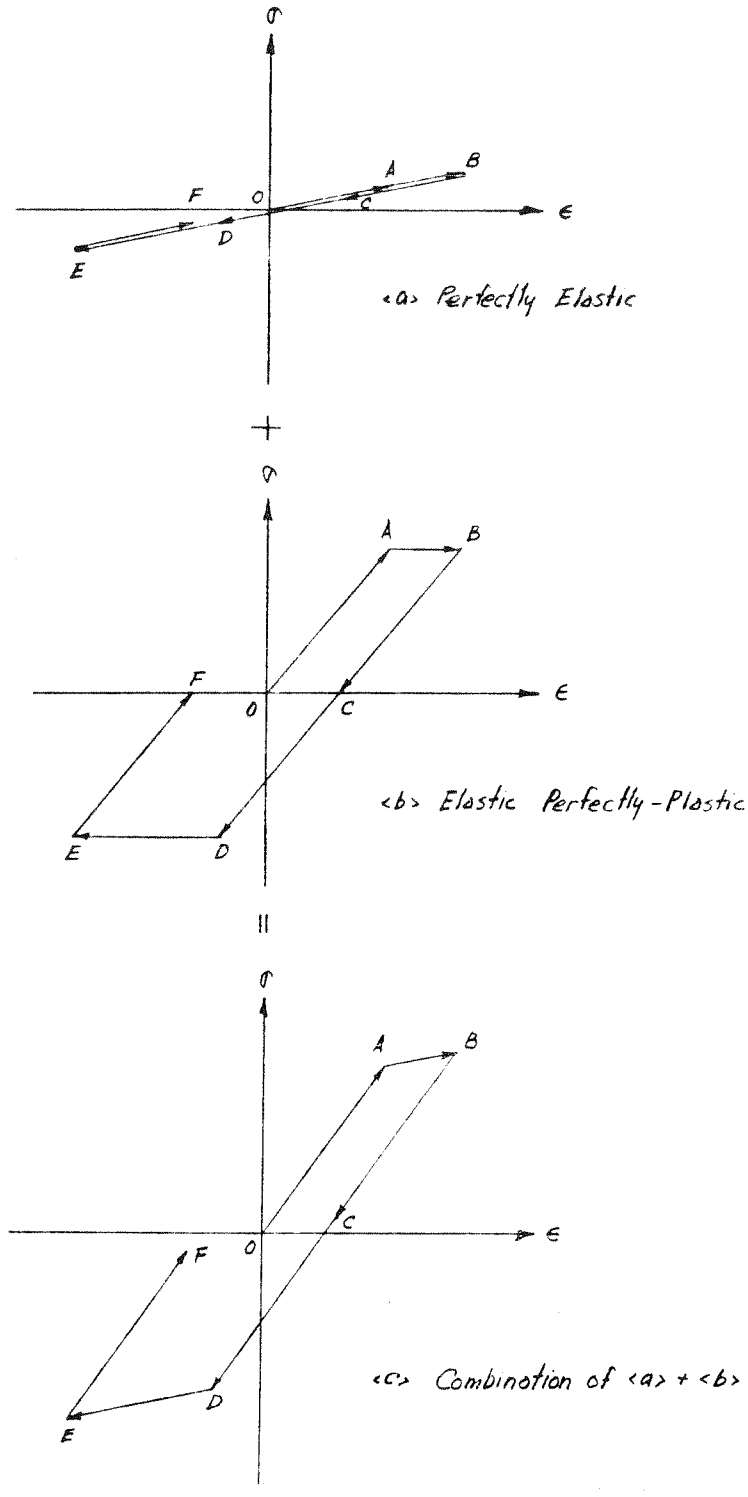

FIG 3-4 BAUSCHINGER EFFECT EXHIBITED BY THE PARALLEL MATERIAL MODEL

4. FINITE ELEMENT STIFFNESS

4.1 COMPATIBLE ISOPARAMETRIC QUADRILATERAL (Q4)

Quadrilateral plane and axisymmetric elements of Zienkiewicz-Irons isoparametric type (40,49) have been used in this study. These elements have been extensively applied for elastic analyses, and some applications in inelastic analyses have also been reported (51,52,53). The element stiffness formulation is well known, but is repeated here for completeness.

For an axisymmetric solid element, the geometry and displacement fields are defined in a polar coordinate system, r, z, θ, by

$$r = \sum_{i=1}^{4} h_i r_i$$
$$z = \sum_{i=1}^{4} h_i z_i \qquad [4.1]$$

and

$$u_r = \sum_{i=1}^{4} h_i u_{r_i}$$
$$u_z = \sum_{i=1}^{4} h_i u_{z_i} \qquad [4.2]$$

in which the interpolation functions are defined by

$$h_1 = \frac{1}{4}(1-s)(1-t)$$
$$h_2 = \frac{1}{4}(1+s)(1-t)$$
$$h_3 = \frac{1}{4}(1+s)(1+t)$$
$$h_4 = \frac{1}{4}(1-s)(1+t) \qquad [4.3]$$

and in which s-t is a natural coordinate system (Fig. 4.1) such that s and t vary from -1 to +1. The coordinates r_i , z_i and displacements u_{r_i} , u_{z_i} are the coordinates and displacements at the nodal points. The relationships derived in Chapter 3 for x, y, z coordinates apply directly in the polar coordinate system.

Evaluation of the strains from the displacements requires the inverse of the chain rule for differentiation, as follows:

$$\begin{Bmatrix} \frac{\partial}{\partial r} \\ \\ \frac{\partial}{\partial z} \end{Bmatrix} = \frac{1}{J} \begin{bmatrix} \frac{\partial z}{\partial t} & -\frac{\partial z}{\partial s} \\ \\ -\frac{\partial r}{\partial t} & \frac{\partial r}{\partial s} \end{bmatrix} \begin{Bmatrix} \frac{\partial}{\partial s} \\ \\ \frac{\partial}{\partial t} \end{Bmatrix} \qquad [4.4]$$

where the Jacobian, J, is defined by

$$J(s,t) = \frac{\partial r}{\partial s}\frac{\partial z}{\partial t} - \frac{\partial r}{\partial t}\frac{\partial z}{\partial s} \qquad [4.5]$$

For axisymmetric deformation the strains are related to the displacements by

$$\begin{Bmatrix} \epsilon_r \\ \epsilon_z \\ \epsilon_\theta \\ \gamma_{rz} \end{Bmatrix} = \begin{bmatrix} \frac{\partial}{\partial r} & 0 \\ 0 & \frac{\partial}{\partial z} \\ \frac{1}{r} & 0 \\ \frac{\partial}{\partial z} & \frac{\partial}{\partial r} \end{bmatrix} \begin{Bmatrix} u_r \\ u_z \end{Bmatrix} \qquad [4.6]$$

Substitution of Eqs. [4.1], [4.2] and [4.3] into Eq. [4.6] and use of Eq. [4.4] yields the relationship between strain and nodal displacement as

$$\underline{\epsilon} = \underline{B}(s,t) \cdot \underline{U} \qquad [4.7]$$

in which the strain-displacement transformation matrix, $\underline{B}$, is a function of the natural coordinates s , t. For any given numerical values of s and t, the matrix $\underline{B}$ can be evaluated.

The finite element stiffness matrix, $\underline{k}$, is given by

$$\underline{k} = \int_V \underline{B}^T \cdot \underline{C} \cdot \underline{B} \cdot dv \qquad [4.8]$$

where $\underline{C}$ is the material property matrix, equal to $\underline{C}^e$ at unyielded material points and $\underline{C}^{ep}$ at yielded points. For the axisymmetric element

$$\begin{aligned} \underline{k} &= 2\pi \int_r \int_z \underline{B}^T \underline{C} \cdot \underline{B} \cdot r \, dr \cdot dz \\ &= 2\pi \int_{-1}^{+1} \int_{-1}^{+1} \underline{B}^T(s,t) \cdot \underline{C}(s,t) \cdot \underline{B}(s,t) \cdot r(s,t) \cdot J(s,t) \cdot ds \cdot dt \end{aligned} \qquad [4.9]$$

For elasto-plastic analyses, matrix $\underline{B}$ is constant at any point, whereas matrix $\underline{C}$ will change as the material yields.

4.2 INCOMPATIBLE ISOPARAMETRIC QUADRILATERAL (Q4I4)

The compatible isoparametric element has been shown to possess poor bending characteristics (54,55). In order to improve the bending behavior, the addition of a number of extra deformation modes was suggested by Wilson et al (54). The displacement functions for the incompatible modes are of the form

$$U_r = \sum_{i=1}^{4} h_i U_{r_i} + h_5 \alpha_1 + h_6 \alpha_2$$
$$U_z = \sum_{i=1}^{4} h_i U_{z_i} + h_5 \alpha_3 + h_6 \alpha_4 \qquad [4.10]$$

in which the additional functions h_5 and h_6 are given by

$$h_5 = (1 - s^2)$$
$$h_6 = (1 - t^2) \qquad [4.11]$$

The displacement amplitudes, α_1 through α_4, constitute additional degrees of displacement freedom. These degrees of freedom are not constrained to be identical in adjacent elements, but are permitted to take values which minimize the element strain energy. As a result, displacement compatibility at the element boundaries is not satisfied. However, the resulting element has good bending characteristies and appears to provide accurate results for a wide variety of problems.

With the additional degrees of freedom, the element stiffness matrix is of size 12 x 12. This may be partitioned into matrices associated with the eight nodal displacements and the four internal degrees of freedom as

$$\begin{Bmatrix} \underline{R}_c \\ \hline \underline{R}_i \end{Bmatrix} = \left[\begin{array}{c|c} \underline{k}_{cc} & \underline{k}_{ci} \\ \hline \underline{k}_{ic} & \underline{k}_{ii} \end{array}\right] \begin{Bmatrix} \underline{U} \\ \hline \underline{\alpha} \end{Bmatrix} \qquad [4.12]$$

or

$$\underline{R}_c = \underline{k}_{cc} \cdot \underline{U} + \underline{k}_{ci} \cdot \underline{\alpha} \qquad [4.13a]$$

$$\underline{R}_i = \underline{k}_{ic} \cdot \underline{U} + \underline{k}_{ii} \cdot \underline{\alpha} \qquad [4.13b]$$

For minimum element strain energy, $\underline{R}_i = \underline{0}$. Hence

$$\underline{\alpha} = - \underline{k}_{ii}^{-1} \cdot \underline{k}_{ic} \cdot \underline{U} \qquad [4.14]$$

Substitution of Eq. [4.14] into Eq. [4.13a] yields

$$\begin{aligned} \underline{R}_c &= [\, \underline{k}_{cc} - \underline{k}_{ci} \cdot \underline{k}_{ii}^{-1} \cdot \underline{k}_{ic} \,] \cdot \underline{U} \\ &= \underline{k}^{*} \cdot \underline{U} \end{aligned} \qquad [4.15]$$

Computationally, this is the well known static condensation procedure (60). The element stiffness after static condensation is of size 8 x 8.

To evaluate element strains, it is desirable to have the strain-displacement transformation matrix $\underline{B}$ in terms of nodal displacements only. A similar condensation procedure may be applied to this transformation as follows

$$\underline{\epsilon} = < \underline{B}_c \,\vdots\, \underline{B}_i > \cdot \left\{ \begin{array}{c} \underline{U} \\ \cdots \\ \underline{\alpha} \end{array} \right\} \qquad [4.16]$$

or

$$\begin{aligned} \underline{\epsilon} &= \underline{B}_c \, \underline{U} + \underline{B}_i \cdot \underline{\alpha} \\ &= [\, \underline{B}_c - \underline{B}_i \cdot \underline{k}_{ii}^{-1} \cdot \underline{k}_{ic} \,] \cdot \underline{U} \\ &= \underline{B}^{*} \cdot \underline{U} \end{aligned} \qquad [4.17]$$

It should be noted that the condensed transformation matrix $\underline{B}^{*}$ does not remain unchanged as the element yields, because the submatrices $\underline{k}_{ii}$ and $\underline{k}_{ic}$ may change. The influence of this is considered subsequently.

4.3 NUMERICAL INTEGRATION

The integration for Eq. [4.9] is conveniently performed by Gaussian quadrature integration. The integral is reduced to the form

$$\underline{k} = 2\pi \sum_{i=1}^{n} \sum_{j=1}^{m} H_i H_j \underline{B}^T(s_i, t_j)\, \underline{C}(s_i, t_j)\, \underline{B}(s_i, t_j)\, r(s_i, t_j)\, J(s_i, t_j) \quad [4.18]$$

in which s_i and t_j are the coordinates of the integration points and H_i and H_j are the corresponding weight factors.

The matrix products ($H_i H_j \underline{B}^T \underline{C}\, \underline{B}\, r\, J$) are formed at each integration point, and then summed to obtain the element stiffness matrix

A Gaussian quadrature formula of order n itegrates a polynomial f(x) of degree (2n - 1) exactly. Hence, a 2 x 2 Gaussian quadrature formula provides an exact integral for an elastic Q4 element of rectangular shape, whereas a 3 x 3 formula is required for the Q4I4 element.

It was shown by Willam (47) that the use of a 2 x 2 integration rule for an element similar to the Q4I4 element reduced the time to form the element stiffness by 40%, and yielded consistently more flexible results. Willam concluded that it is desirable to form the element stiffness with a 2 x 2 integration rule, in spite of the theoretical objections. This conclusion is applicable, however, only for an elastic element. For an inelastic element it is necessary not only to interpolate displacements and strains within the element, but also the material properties. A crude assumption might be that the material property matrix $\underline{C}$, is constant throughout an element, based, say, on the conditions at

the centroid. It is preferable, however, to account more accurately for the spread of plasticity through an element. A convenient procedure is to monitor the conditions at each integration point, and to use a different $\underline{C}$ at each point, based on the conditions at that point. This procedure has been used by Zienkiewicz (53), Bergan (51) and Larsen (52). If an n x m integration order is used, the spread of plasticity through the element can clearly be taken into account more accurately as n and m are increased. Thus, a 2 x 2 integration order might be suitable for the analysis of bulky solids with fairly fine element subdivisions. However, for the analysis of a shell with only a single element layer through the shell thickness, the number of integration points through the thickness should clearly be larger than 2. In the computer program used for the analyses in this report, provision has been made for the integration order, n x m, to be varied, with any values of n and m provided the product does not exceed 20.

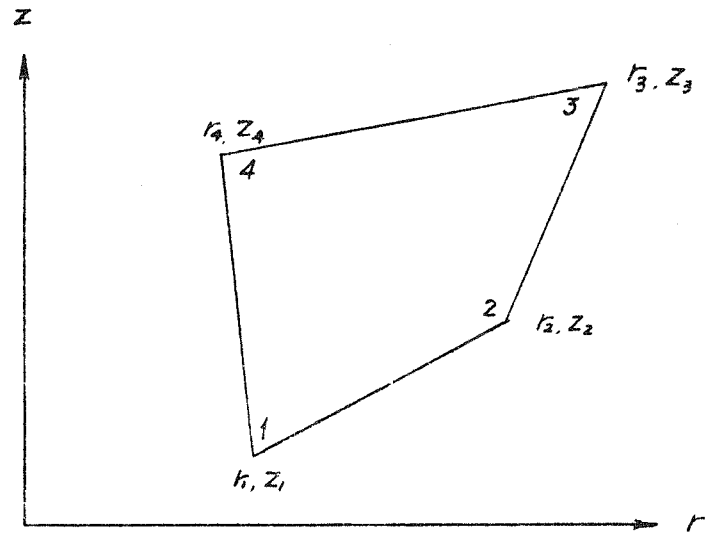

<a> Global System

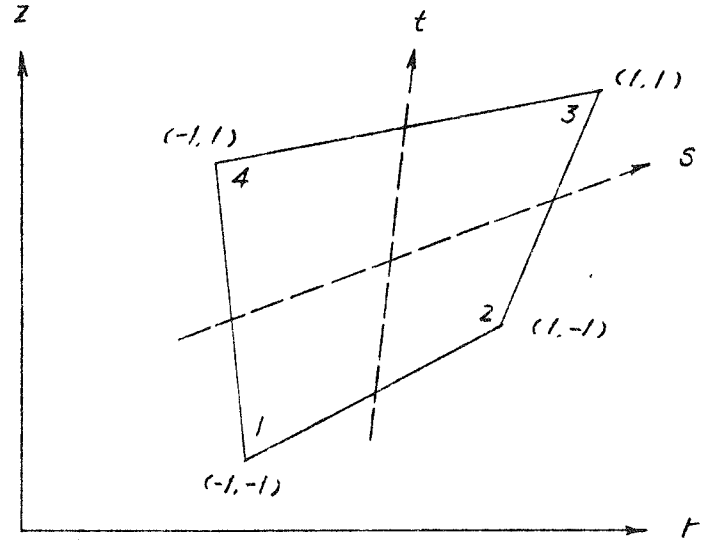

<b> Local System

FIG 4-1 COORDINATE SYSTEMS

5. STATE DETERMINATION

5.1 COMPUTATIONAL STEPS

The solution of the state determination problem can be expressed symbolically as

$$d\underline{r} \xrightarrow{\underline{B}} d\underline{\epsilon} \xrightarrow{\underline{C}} d\underline{\sigma} \xrightarrow{\underline{B}^T} \underline{R}^x \qquad [5.1]$$

the solution is carried out in three steps as follows:

(1) Determine the incremental strain vector at each integration point from the incremental displacement vector.

(2) Evaluate the incremental stress vector corresponding to the incremental strain vector at each integration point, and hence determine the new stress condition.

(3) From the total stress determine the internal resisting force for each element and the complete structure. Hence, determine the unbalanced nodal forces.

An shown subsequently, these three steps are not strictly independent for elements such as the Q4I4 element, which have incompatible modes. To simplify the discussion, the steps are first described for the Q4 element. The complications introduced for the Q4I4 element are then considered separately.

5.2 STRAIN CALCULATION

For any displacement increment, $\Delta \underline{r}$, the strain increment at a point (s,t) is determined by direct application of the strain-displacement transformation. That is

$$\Delta \underline{\epsilon}(s,t) = \underline{B}(s,t) \cdot \Delta \underline{r} \qquad [5.2]$$

5.3 STRESS CALCULATION

5.3.1 Cases to be Considered

Let the stress vector at any integration point at the beginning of an iteration step be $\underline{\sigma}_1$, which is known, and at the end of the step be $\underline{\sigma}_2$, which is to be found. Four cases must be considered, as follows:

(1) Elastic case: elastic at both $\underline{\sigma}_1$ and $\underline{\sigma}_2$.

(2) Transitional case: elastic at $\underline{\sigma}_1$, plastic at $\underline{\sigma}_2$.

(3) Plastic case: plastic at both $\underline{\sigma}_1$ and $\underline{\sigma}_2$.

(4) Unloading case: plastic at $\underline{\sigma}_1$, but unloading.

These cases are considered in turn in the following sections.

5.3.2 Elastic Case

For a strain increment $\Delta \underline{\epsilon}$, the corresponding elastic stress increment is easily obtained by using the elastic material property matrix, $\underline{C}^e$. That is

$$\Delta \underline{\sigma} = \underline{C}^e \cdot \Delta \underline{\epsilon} \qquad [5.3]$$

5.3.3 Transitional Case: von Mises Criterion

In this case, the material behaves elastically for a part of the step and plastically for the remainder. Because the behavior is path dependent, it is necessary to make an assumption about the loading path within the iteration step. The assumption which is made is that the strains vary proportionately within the step.

With this assumption, that part of the strain increment for which the material remains elastic is determined, together with the corresponding stress increase. That is, a ratio β is determined such that

$$\Delta \underline{\epsilon}^e = \beta \cdot \Delta \underline{\epsilon} \qquad [5.4]$$

and the stress point given by

$$\underline{\sigma}_y = \underline{\sigma}_i + \beta \cdot \underline{C}^e \Delta \underline{\epsilon} = \underline{\sigma}_i + \beta \cdot \Delta \underline{\sigma}^e \qquad [5.5]$$

lies on the yield surface. The remaining strain is then considered as for the plastic case.

The equation of the yield surface for the von Mises criterion can be written as

$$f = \left(\frac{3}{2} \hat{\underline{\sigma}}^T \hat{\underline{\sigma}}\right)^{1/2} - \sigma_o = 0 \qquad [5.6]$$

in which $\hat{\underline{\sigma}} = \underline{\sigma}' - \underline{\alpha}$

$\underline{\sigma}'$ = vector of deviatoric stresses

$\underline{\alpha}$ = stress vector representing translation of the yield surface during previous kinematic hardening.

σ_o = yield stress in uniaxial tension, modified to account for previous isotropic hardening.

The ratio β must satisfy the equation

$$\left[\frac{3}{2}\left(\hat{\underline{\sigma}}_1+\beta\cdot\Delta\hat{\underline{\sigma}}^{L}\right)^{T}\cdot\left(\hat{\underline{\sigma}}_1+\beta\cdot\Delta\hat{\underline{\sigma}}^{L}\right)\right]^{1/2}=\sigma_o \qquad [5.7]$$

in which $\Delta\hat{\underline{\sigma}}^{L}$ is the deviatoric stress vector corresponding to $\Delta\underline{\sigma}^{L}$. Hence

$$\left[\frac{3}{2}\Delta\hat{\underline{\sigma}}^{L^T}\cdot\Delta\hat{\underline{\sigma}}^{L}\right]\beta^2+\left[3\,\hat{\underline{\sigma}}_1^{T}\cdot\Delta\hat{\underline{\sigma}}^{L}\right]\beta+\left[\frac{3}{2}\hat{\underline{\sigma}}_1^{T}\cdot\hat{\underline{\sigma}}_1-\sigma_o^2\right]=0 \qquad [5.8]$$

Eq. [5.8] is quadratic in β . If

$A=\frac{3}{2}\Delta\hat{\underline{\sigma}}^{L^T}\cdot\Delta\hat{\underline{\sigma}}^{L}$ which must always be positive,

$B=3\,\hat{\underline{\sigma}}_1^{T}\cdot\Delta\hat{\underline{\sigma}}^{L}$ which must be positive for this case,

$C=\frac{3}{2}\hat{\underline{\sigma}}_1^{T}\cdot\hat{\underline{\sigma}}_1-\sigma_o^2$ which must be negative for this case,

then the roots are

$$\beta=\frac{-B\pm\sqrt{B^2-4AC}}{2A} \qquad [5.9]$$

Because β must be positive, it follows that the required root is

$$\beta=\frac{-B+\sqrt{B^2-4AC}}{2A} \qquad [5.10]$$

5.3.4 Transitional Case: Tresca Criterion

In six dimensional stress space, the Tresca yield surface is defined by six functions, or facets, which are quadratic functions of stress. In three dimensional principal stress space these facets are planar. In order to determine that proportion of the strain increment required to reach the yield surface, it is again necessary to solve a quadratic equation. In general, however,

one value of β must be found for each of the facets. The smallest positive value is then the one required, and the facet giving this value is the facet with which contact is first made.

Because the Tresca criterion is difficult to consider in computations, and because it appears to represent the behavior of actual materials less accurately than the von Mises criterion, its use has not been explored in detail in the current study. In particular, only an approximate solution of the state determination problem has been devised for this criterion.

For the transitional case, it is assumed that the loading path within any iteration step is such that (a) the strains (and hence the elastic stresses in six dimensional space) vary proportionately, as before, and in addition (b) that the principal stresses also vary proportionately. In fact, these two assumptions are inconsistent, because the relationship between the principal stresses and the stresses in six dimensional space is not a linear one. However, these assumptions permit substantial computational simplifications for both the transitional and plastic cases.

In principal stress space, the facets of the yield surface are defined by a set of linear functions

$$f_n = f_n^* - \sigma_o = 0$$

or

$$f_n^*(\underline{p}) = \sigma_o \qquad ; \quad n = 1, 2, 3, 4, 5, 6 \qquad [5.11]$$

in which $\underline{p}$ = vector of principal stresses. Alternatively, the functions may be expressed as

$$\phi_n(\underline{p}) = \frac{f_n^*(\underline{p})}{\sigma_o} = 1 \qquad [5.12]$$

The function ϕ_n for any facet therefore equals 1 on the facet, less than 1 inside, and more than 1 outside. For yielding on the m^{th} facet, the ratio β_m can be determined as

$$\beta_m = \frac{1 - \phi_m^P}{\phi_m^Q - \phi_m^P} \qquad [5.13]$$

in which ϕ^P and ϕ^Q are the function values at points P and Q, respectively in Fig. 5.1. The smallest positive value of β_m is the required value, β . It is then also assumed that

$$\Delta \underline{\epsilon}^e = \beta \cdot \Delta \underline{\epsilon} \qquad [5.14]$$

$$\underline{\sigma}_y = (\underline{\sigma}_i + \underline{C}^e \Delta \underline{\epsilon}^e) \cdot \gamma \qquad [5.15]$$

and

$$\Delta \underline{\epsilon}^{ep} = (1 - \beta) \cdot \Delta \underline{\epsilon} \qquad [5.16]$$

in which γ is a scale factor, approximately equal to 1, applied to place the new stress point exactly on the yield surface. The remaining strain, $\Delta \underline{\epsilon}^{ep}$, is considered as described for the plastic case.

5.3.5 Plastic Case: von Mises Criterion

As with the transitional case, it is assumed that the strains vary proportionately during any iteration step. During straining of the yielded material the flow rule should be satisfied at all times. Hence

$$d\underline{\sigma} = \underline{C}^{ep}(\underline{\sigma}, \underline{\epsilon}^p) \cdot d\underline{\epsilon}^{ep} \qquad [5.17]$$

and

$$\Delta \underline{\sigma} = \int_0^{\Delta \underline{\epsilon}^{ep}} \underline{C}^{ep}(\underline{\sigma}, \underline{\epsilon}^p) \cdot d\underline{\epsilon}^{ep} \qquad [5.18]$$

in which $\Delta \underline{\sigma}$ = stress increment

$\underline{C}^{ep}$ = elasto-plastic material property matrix, as derived in Chapter 3, which in general is a function of both stress and plastic strain

$\Delta \underline{\epsilon}^{ep}$ = elasto-plastic strain increment.

Because $\underline{C}^{ep}$ varies along the loading path, the integral of Eq. [5.18] can generally not be evaluated explicitly, and numerical methods must therefore be used. Euler's method and Runge-Kutta methods have been considered in the current study, although other procedures might also be applicable.

The integration problem is of the following form. Given the differential equation

$$dy = \dot{g}(x, y) \cdot dx \qquad [5.19]$$

and the initial value $y_0 = y(x_0)$, determine $y_1 = y(x_0 + \Delta x)$ for a given Δx .

The equations for Euler's method and for Runge-Kutta methods of second, third and fourth order are then as follows. Details may be found in many texts (23,24)

(1) Euler's method

$$y_1 = y_0 + \Delta x \cdot \dot{g}(x_0, y_0) \qquad [5.20]$$

(2) Second Order Runge-Kutta method.

$$y_1 = y_0 + \Delta x \cdot g\left(x_0 + \frac{1}{2}\Delta x,\ y_0 + \frac{1}{2}\Delta x \cdot g(x_0, y_0)\right) \qquad [5.21a]$$

or

$$y_1 = y_0 + \frac{1}{2}\Delta x \cdot \left[g(x_0, y_0) + g(x_0 + \Delta x,\ y_0 + \Delta x \cdot g(x_0, y_0))\right] \qquad [5.21b]$$

(3) Third Order Runge-Kutta method

$$y_1 = y_0 + \frac{1}{9}(2k_1 + 3k_2 + 4k_3) \qquad [5.22a]$$

$$k_1 = \Delta x \cdot g(x_0, y_0)$$
$$k_2 = \Delta x \cdot g\left(x_0 + \frac{1}{2}\Delta x,\ y_0 + \frac{1}{2}k_1\right)$$
$$k_3 = \Delta x \cdot g\left(x_0 + \frac{3}{4}\Delta x,\ y_0 + \frac{3}{4}k_2\right)$$

or

$$y_1 = y_0 + \frac{1}{6}(k_1 + 4k_2 + k_3) \qquad [5.22b]$$

$$k_1 = \Delta x \cdot g(x_0, y_0)$$
$$k_2 = \Delta x \cdot g\left(x_0 + \frac{1}{2}\Delta x,\ y_0 + \frac{1}{2}k_1\right)$$
$$k_3 = \Delta x \cdot g(x_0 + \Delta x,\ y_0 - k_1 + 2k_2)$$

(4) Fourth Order Runge-Kutta method

$$y_1 = y_0 + \frac{1}{6}(k_1 + 2k_2 + 2k_3 + k_4) \qquad [5.23]$$

$$k_1 = \Delta x \cdot g(x_0, y_0)$$
$$k_2 = \Delta x \cdot g\left(x_0 + \frac{1}{2}\Delta x,\ y_0 + \frac{1}{2}k_1\right)$$
$$k_3 = \Delta x \cdot g\left(x_0 + \frac{1}{2}\Delta x,\ y_0 + \frac{1}{2}k_2\right)$$
$$k_4 = \Delta x \cdot g(x_0 + \Delta x,\ y_0 + k_3)$$

All of these methods are simple to program for the computer. The number of evaluations of $g(x,y)$ increases from one for Euler's method to four for the fourth order Runge-Kutta method. For an elasto-plastic analysis, each evaluation requires

the computation of $\underline{C}^{ep}$ according to the equations of Chapter 3. The computational effort required is small. Hence, although a low order method may give sufficiently accurate results for most cases, it is recommended that the fourth order Runge-Kutta method be used. Accuracy can also be improved by dividing $\Delta\underline{\epsilon}$ into a number of increments, and applying the numerical method sequentially to each increment. In the analyses considered here, however, the integration has been carried out considering $\Delta\underline{\epsilon}$ as only a single increment.

A similar solution procedure to that considered here has been applied by other workers (38,50,51,52), although the nature of the procedure and its approximations have not been clearly explained. In all cases, the equivalent of Euler's method appears to have been used.

For the fourth order Runge-Kutta method, the procedure for the von Mises criterion is as follows. The procedures for the other methods are similar

(1) At the beginning of the step, or, for a transitional case, at the point of yield, evaluate

$$\Delta\underline{\sigma}_1 = \underline{C}^{ep}(\underline{\sigma}_1, \underline{\epsilon}_1^p) \cdot \Delta\underline{\epsilon}^{ep} \qquad [5.24]$$

and

$$\Delta\underline{\epsilon}_1^p = \Delta\underline{\epsilon}^{ep} - \underline{C}^{e^{-1}} \cdot \Delta\underline{\sigma}_1 \qquad [5.25]$$

(2) Compute $\Delta\underline{\sigma}_2 = \underline{C}^{ep}(\underline{\sigma}_1 + \frac{1}{2}\Delta\underline{\sigma}_1, \underline{\epsilon}_1^p + \frac{1}{2}\Delta\underline{\epsilon}_1^p) \cdot \Delta\underline{\epsilon}^{ep}$ [5.26]

and

$$\Delta\underline{\epsilon}_2^p = \Delta\underline{\epsilon}^{ep} - \underline{C}^{e^{-1}} \cdot \Delta\underline{\sigma}_2 \qquad [5.27]$$

(3) Evaluate

$$\Delta \underline{\sigma}_3 = \underline{C}^{ep}(\underline{\sigma}_1 + \tfrac{1}{2}\Delta \underline{\sigma}_2,\ \underline{\epsilon}_1^p + \tfrac{1}{2}\Delta \underline{\epsilon}_2^p) \cdot \Delta \underline{\epsilon}^{ep} \qquad [5.28]$$

and

$$\Delta \underline{\epsilon}_3^p = \Delta \underline{\epsilon}^{ep} - \underline{C}^{e-1} \cdot \Delta \underline{\sigma}_3 \qquad [5.29]$$

(4) Calculate

$$\Delta \underline{\sigma}_4 = \underline{C}^{ep}(\underline{\sigma}_1 + \Delta \underline{\sigma}_3,\ \underline{\epsilon}_1^p + \Delta \underline{\epsilon}_3^p) \cdot \Delta \epsilon^{ep} \qquad [5.30]$$

(5) Evaluate the final stress increment and plastic strain increment by

$$\Delta \underline{\sigma} = \frac{1}{6}[\Delta \underline{\sigma}_1 + 2 \cdot \Delta \underline{\sigma}_2 + 2 \cdot \Delta \underline{\sigma}_3 + \Delta \underline{\sigma}_4] \qquad [5.31]$$

and

$$\Delta \underline{\epsilon}^p = \Delta \underline{\epsilon}^{ep} - \underline{C}^{e-1} \cdot \Delta \underline{\sigma} \qquad [5.32]$$

(6) The final stresses and plastic strains are then

$$\underline{\sigma}_2 = \underline{\sigma}_1 + \Delta \underline{\sigma} \qquad [5.33]$$

$$\underline{\epsilon}_2^p = \underline{\epsilon}_1^p + \Delta \underline{\epsilon}^p \qquad [5.34]$$

(7) For strain hardening materials, update the hardening parameter. For isotropic hardening, the best procedure is probably to compute the effective stress corresponding to the stress state $\underline{\sigma}_2$, and to set the hardening parameter, $\bar{\sigma}(\underline{\epsilon}^p)$ in Eq. [3.22], equal to this effective stress. The new stress point therefore lies exactly on the yield surface.

For linear kinematic hardening, the change in the hardening parameter, $\Delta \underline{\alpha}$, can be obtained from Eq. [3.29], as

$$\Delta \underline{\alpha} = g \cdot \Delta \underline{\epsilon}^p \qquad [5.35]$$

However, the stress point may not lie exactly on the new yield surface. Hence, it is recommended that the stress vector, $\underline{\sigma}_2$, be scaled to place it on the yield surface. A similar modification will be needed for elastic perfectly plastic materials. In the numerical examples considered during this investigation, the stress points obtained by the fourth order Runge-Kutta procedure were always very close to the yield surface, and the scaling of the stresses required changes no larger than one percent.

It may be noted that is is not necessary to monitor the plastic strains or to modify the yield surface if an elastic perfectly plastic material (or the parallel material strain hardening model) is used. This is because $\underline{C}^{ep}$ is independent of $\underline{\epsilon}^p$, and $\underline{\epsilon}^p$ can always be found as

$$\underline{\epsilon}^p = \underline{\epsilon} - \underline{C}^{e-1} \underline{\sigma} \qquad [5.36]$$

5.3.6 Plastic Case: Tresca Criterion

Within any facet of the Tresca yield surface, the state determination procedure for the plastic case is similar in principle to that for the von Mises criterion, the only difference being in the equation of the yield surface. A problem arises, however, if the stress point moves from one facet to an adjacent facet, or to an "edge" between facets. Again, because the Tresca criterion is not of primary interest, it has not been explored in detail during the current study. Nevertheless, some analyses using the Tresca criterion have been carried out, and a simplified approximate solution to the problem of movement between facets has

been devised. This solution applies for elastic perfectly plastic materials only.

The solution is based on the assumption that the state determination problem can be solved in principal stress space. As with the solution for the transitional case, this involves the assumption that the strain variation within the step is such that the principal stresses vary proportionately. The procedure is as follows at any integration point.

(1) Determine the strain and stress increments assuming the material property matrix applying at the beginning of the interation step (or, for a transitional case, at the point of yield). The equations are

$$\Delta \underline{\epsilon}_n = \underline{B} \cdot \Delta \underline{r}_n \qquad [5.37]$$

$$\Delta \underline{\sigma}_n = \underline{C}_n^{ep} \cdot \Delta \underline{\epsilon}_n \qquad [5.38]$$

$$\underline{\sigma}_n = \underline{\sigma}_{n-1} + \Delta \underline{\sigma}_n \qquad [5.39]$$

(2) Calculate the principal stress vectors $\underline{p}_n$ and p_{n-1} for the stress states $\underline{\sigma}_n$ and $\underline{\sigma}_{n-1}$ respectively. The stress state $\underline{\sigma}_{n-1}$ will lie on facet i, as indicated by point P in Fig. 5.2.

(3) Evaluate the factors by which the stress increment, $\Delta \underline{p}_n$, must be scaled to move from facet i to each of the adjacent facets:

$$\beta_j = \frac{1 - \phi_j(\underline{p}_{n-1})}{\phi_j(\underline{p}_n) - \phi_j(\underline{p}_{n-1})} \quad ; \quad j = (i-1) \text{ or } (i+1) \qquad [5.40]$$

Only the positive value is required, and the facet which gives this value is the facet toward which the stress point moves. If $\beta_j \geq 1$, the stress point remains on the current facet, and the solution is complete for this iteration step.

(4) If $\beta_j < 1$, the stress point moves to facet j , shown as point Q in Fig. 5.2. The stress state at point R is

$$\underline{\sigma}_n = \underline{\sigma}_{n-1} + \beta_j \cdot \Delta \underline{\sigma}_n \qquad [5.41]$$

For simplicity, it is again assumed that the remaining strain for the iteration step can be obtained by scaling the strain using β_j . That is, the remaining strain is $(1-\beta_j)\cdot\Delta\underline{\epsilon}$. As noted previously, this assumption is not strictly correct.

The procedure can now be repeated from step 1 with a new material property matrix corresponding to the new facet. If the stress point moves into the new facet, the procedure is exactly as above. However, if the stress point moves back to the previous facet, this indicates that the final stress state is on the edge between facets. Hence $\underline{C}^{ep}$ is computed according to Eq. [3.18], and the final stress increment is obtained accordingly.

5.3.7 Unloading Case

For any given strain increment, $\Delta\underline{\epsilon}$, applied to a yielding material, a test for unloading can be obtained by considering what would happen if the material were elastic. Clearly, continued loading is indicated if the value of the yield function increases,

and unloading is indicated if this value decreases. That is, for unloading

$$\left(\frac{\partial f}{\partial \underline{\sigma}}\right)^T \cdot \Delta \underline{\sigma}^L < 0 \qquad [5.42]$$

in which

$$\Delta \underline{\sigma}^L = \underline{C}^e \cdot \Delta \underline{\epsilon} \qquad [5.43]$$

is the elastic stress increment which would correspond to the given strain increment. The derivative with respect to $\underline{\epsilon}^p$ is not considered in Eq. [5.42], because $\underline{\epsilon}^p$ is constant for an elastic material. Hence, for unloading,

$$\left(\frac{\partial f}{\partial \underline{\sigma}}\right)^T \cdot \underline{C}^e \cdot \Delta \underline{\epsilon} < 0 \qquad [5.44]$$

This criterion is simple to apply.

If unloading is indicated, the situation corresponds to either an elastic or a transitional case, and is treated accordingly. As noted in Section 2.4, however, it is inadvisable to permit large stress changes on unloading because the elasto-plastic material property and stiffness matrices used to compute the strain increment may be greatly different from the elastic matrices required during unloading. Changes such that the yield function is exceeded at some other point on the yield surface should particularly be avoided. To avoid this problem, a reversal tolerance should be specified. The procedure for applying this tolerance is considered in Section 6.2.

5.3.8 Path Independent Procedure

A major source of uncertainty in the application of iterative solution techniques to the analysis of inelastic structures is that the strain path followed during the analysis may differ substantially from that followed in the actual structure. Because the behavior of inelastic structures is path dependent, the state of stress and strain obtained by iteration may differ substantially from the "true" state.

With the solution strategy proposed, the effects of path dependence can best be minimized by applying the loading in a series of small increments, so that the "true" loading path is followed closely. In many cases, however, it may be desirable to apply the load in a single large increment, or in a small number of increments of moderate size. In such cases the problem of path dependence arises.

For the state determination problem as described in the preceeding sections, the stress and strain increments for any load increment are obtained by summing the increments from each iteration step. That is, for the n^{th} iteration step

$$\delta \underline{\epsilon}_n = \underline{B} \cdot \delta \underline{r}_n \qquad [5.45]$$

in which δ indicates the increment within the iteration step, and

$$\delta \underline{\sigma}_n = \underline{h}_n (\delta \underline{\epsilon}_n) \qquad [5.46]$$

in which the functional relationship, $\underline{h}_n$, between the stress and strain increments is that implied by the state determination procedures just considered. Then

$$\Delta \underline{\epsilon}_n = \Delta \underline{\epsilon}_{n-1} + \delta \underline{\epsilon}_n \quad ; \quad \Delta \underline{\epsilon}_0 = \underline{0} \qquad [5.47]$$

$$\Delta \underline{\sigma}_n = \Delta \underline{\sigma}_{n-1} + \delta \underline{\sigma}_n \quad ; \quad \Delta \underline{\sigma}_0 = \underline{0} \qquad [5.48]$$

in which Δ indicates the accumulated increments since the beginning of the iteration sequence for the load increment.

Because the loading path defined by the sequence of increments $\delta \underline{\epsilon}$ and $\delta \underline{\sigma}$ may differ substantially from the "true" loading path, errors may result. The procedure defined by Eqs. [5.45] through [5.48] will be termed a "path dependent" procedure.

The problem of path dependence might be overcome, at least partially, by adopting a state determination procedure which is path independent within any load increment. A procedure of this type is contrasted with the path dependent procedure for the transitional case in Figs. 5.3 and 5.4. The equations of the path independent procedure are as follows.

$$\delta \underline{\epsilon}_n = \underline{B} \cdot \Sigma \underline{r}_n \qquad [5.49]$$

$$\Delta \underline{\epsilon}_n = \Delta \underline{\epsilon}_{n-1} + \Sigma \underline{\epsilon}_n \qquad [5.50]$$

$$\Delta \underline{\sigma}_n = \underline{h}_n (\Delta \underline{\epsilon}_n) \qquad [5.51]$$

That is, instead of $\Delta \underline{\sigma}$ being determined by summing a number of increments, $\Sigma \underline{\sigma}$, it is calculated at each iteration step from the total accumulated strain for the load increment. Assuming

that the procedure converges, it would be expected that the final strain increment, and hence the final stress increment, would be independent of the displacement path defined by the displacements δr. That is, within the load increment, the effects of path dependence should be eliminated.

This procedure has been investigated, and compared with the path dependent procedure. The results of some analyses are presented in Chapter 7. An alternative means to reduce the influence of path dependence is through the use of an overshoot tolerance, as described in Sections 2.4 and 6.2.

5.4 RESISTING LOAD

After the new stresses, $\underline{\sigma}$, have been obtained, the internal resisting force for each element is determined by direct application of the relationship,

$$\underline{R}^I = \int_v \underline{B}^T \underline{\sigma} \, dV \qquad [5.52]$$

The resisting force for the complete structure can therefore be assembled, the unbalanced load can be determined, and a convergence check can be carried out.

5.5 COMPLICATIONS FOR ELEMENTS WITH INCOMPATIBLE MODES

For fully compatible elements, the three steps indicated in Eq. [5.1] for the state determination problem can be carried out independently. For elements with incompatible modes, however, the strain-displacement transformation matrix, $\underline{B}$, is conveniently condensed to the matrix $\underline{B}^*$, given by Eq. [4.17]. Because the

condensation operation depends on the element stiffness, and because the stiffness of an elasto-plastic element depends on the material stresses, it follows that $\underline{B}^*$ generally will not remain constant.

A numerically consistent solution can be obtained by recovering the amplitudes of the incompatible modes for each iteration step, and using the uncondensed strain-displacement transformation as defined by Eq. [4.16]. The internal resisting loads, $\underline{R}^I$, would then also include terms corresponding to the incompatible modes, which would have to be considered in the unbalanced load computation. While this procedure would be consistent, it has the disadvantage of being more complex computationally. Hence, in the computer program developed for this study, it has been assumed that the strain increments in any iteration step can be obtained from the equation

$$\Delta \underline{\epsilon} = \underline{B}_i^* \cdot \Delta \underline{r} \qquad [5.53]$$

in which $\Delta \underline{r}$ includes only the nodal displacements and not the amplitudes of the incompatible modes, and $\underline{B}_i^*$ is the condensed transformation matrix for the state at the beginning of the iteration step. Once $\Delta \underline{\epsilon}$ has been obtained, the stress calculation proceeds exactly as before. It then remains to calculate the internal resisting force, $\underline{R}^I$.

Strictly, the resisting force should be computed using the uncondensed strain-displacement transformation matrix. If this were done, the forces corresponding to the incompatible modes would not generally be zero, because of the incorrect assumption

that the condensed transformation matrix is constant throughout the iteration step. For simplicity, it has been decided to use a condensed transformation matrix, and hence to ignore any loads associated with the incompatible modes. It is believed that these loads will be small, and that they would not imply excessive constraints on the freedom of the element to adopt a minimum energy state of stress and strain. The element resisting forces have therefore been determined from

$$\underline{R}^{I} = \int_{v} \underline{B}^{*T} \underline{\sigma} \cdot dV \qquad [5.54]$$

in which $\underline{B}^{*}$ may be the condensed transformation matrix for any one of (a) the state at the beginning of the iteration step, (b) the state at the end of the step, or (c) a fully elastic state. The most rational choice might appear to be the transformation corresponding to the state at the end of the step, which is the state for which the internal resisting load is required. However, it can be argued that the resisting force might most consistently be determined by first unloading the structure an infinitesimal amount, to return it to an elastic condition without changing the stresses, and then determining the resisting force using the condensed transformation matrix for an elastic element. This procedure has the advantage that the condensed elastic transformation remains unchanged, whereas the elasto-plastic transformation changes progressively.

Examples showing the use of these different transformations are presented in Chapter 7.

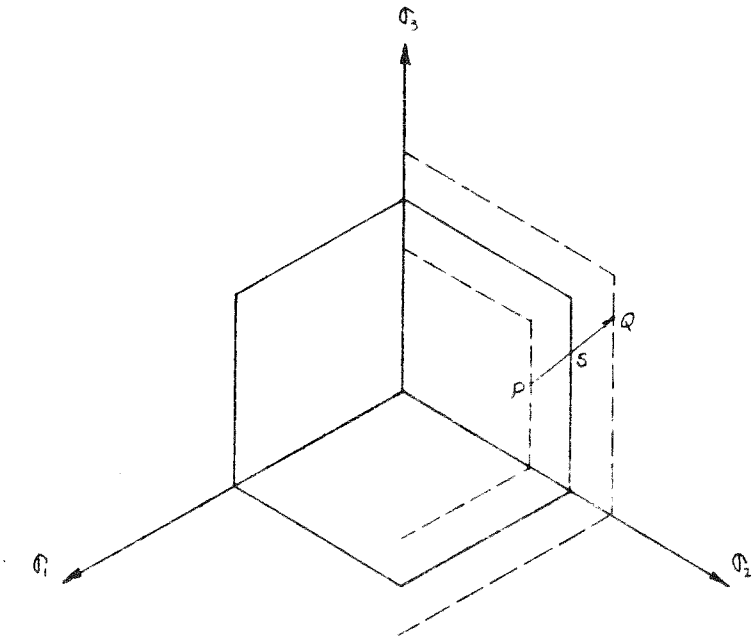

FIG 5-1 TRANSITIONAL CASE : TRESCA

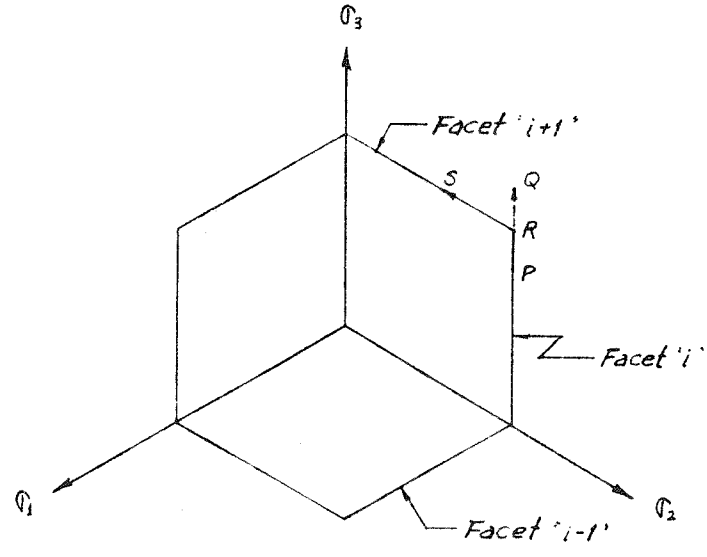

FIG. 5-2 PLASTIC CASE : TRESCA FOR $\beta < 1.0$

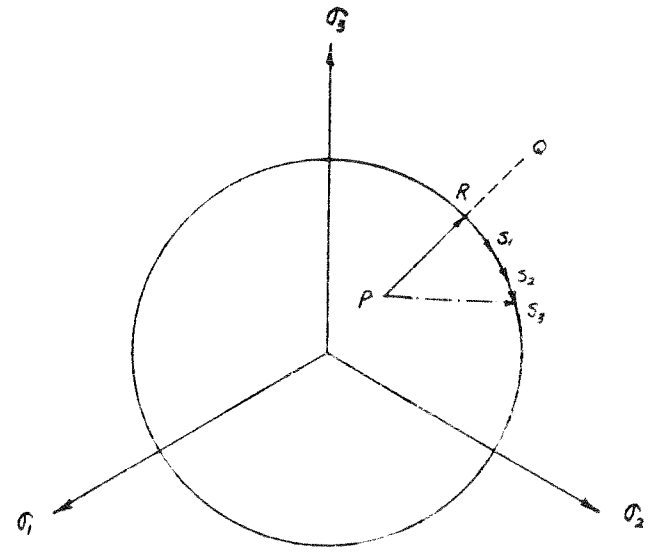

FIG 5-3 PATH DEPENDENT PROCEDURE

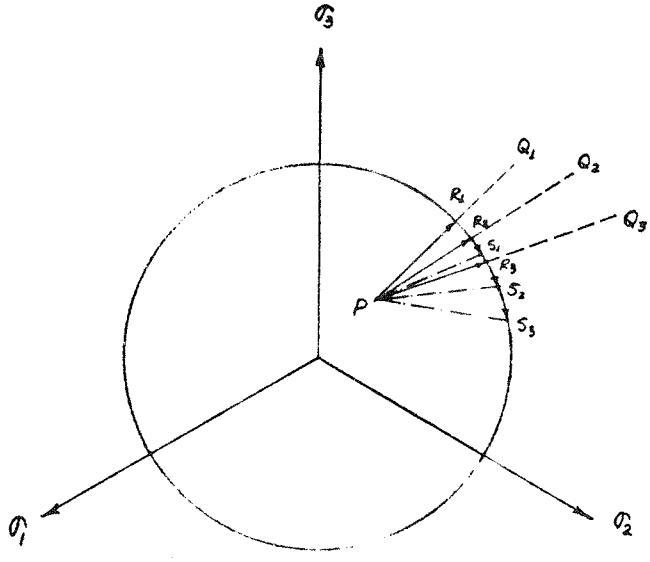

FIG 5-4 PATH INDEPENDENT PROCEDURE

6. COMPUTER PROGRAM LOGIC

6.1 GENERAL

The procedures described in previous chapters have been incorporated into a computer program for the analyses of plane and axisymmetric problems. Because the program is experimental, it has limited capabilities. In particular, only the "parallel material" strain hardening procedure has been considered. Nevertheless, the program is believed to be fairly efficient, and can be applied to a wide range of problems.

A simplified flow chart showing the computational modules is given in Fig. 6.1. Overall control of the execution is maintained by a main program, which calls the various computational modules in sequence. Most of these modules follow well known procedures, and need not be described in detail. However, the modules SCLDWN, ELOPLA, and CONVRG involve specialized logic. Hence, details of these modules are presented in the following sections.

6.2 COMPUTATIONAL MODULE "SCLDWN"

In many cases, the results obtained within any linear step may deviate substantially from the "exact" results. Excessive deviations could affect the accuracy of the final results or lead to convergence difficulties. By means of the module SCLDWN, provision has been made to control the magnitudes of these deviations.

Depending on the load increment and the nature of the problem, a stress point may lie outside the yield surface at the

end of any iteration step. For example, the stress state at the beginning of a step might be at point A in Figs. 6.2 and 6.3, and at the end of the step at point C. The distance of point C beyond the yield surface gives a measure of the departure of the linearized solution from the true solution, and may be excessive. In order to ensure that the solution stays close to the true path, the user may wish to limit the amount of overshoot by specifying an overshoot tolerance.

The yield function may be expressed as

$$\phi = \frac{f^*(\underline{\sigma})}{\sigma_o} \qquad [6.1]$$

in which $f^*(\underline{\sigma}) = (\frac{3}{2}\underline{\sigma}'^T\underline{\sigma}')^{1/2}$ for the von Mises criterion and $f^*(\underline{\sigma}) = (\sigma_i - \sigma_j)\ ;\ i,j=1,2,3\ ;\ i \neq j$ for the Tresca criterion The value of ϕ is equal to unity for stress states exactly on the yield surface. If the values of ϕ at stress states B and C are ϕ^B and ϕ^C respectively, and if state B is at the permissible overshoot limit, as shown in Figs. 6.2 and 6.3, then the value of ϕ^B is equal to the specified overshoot tolerance, t_o. That is

$$\phi^B = t_o \geq 1 \qquad [6.2]$$

If $\phi^C > \phi^B$, it implies that the amount of overshoot is excessive, and the increment must be scaled down. The scale factor, α, for the von Mises criterion, is determined by

$$\alpha = \frac{-B + \sqrt{B^2 - 4AC}}{2A} \qquad [6.3]$$

with

$$A = \frac{3}{2}\,\Delta\underline{\sigma}'^{T}\,\Delta\underline{\sigma}' \qquad \text{which is always positive}$$

$$B = 3\,\underline{\sigma}_1'^{T}\,\Delta\underline{\sigma}' \qquad \text{which is positive in this case}$$

$$C = \frac{3}{2}\,\underline{\sigma}_1'^{T}\,\underline{\sigma}_1' - (t_o\,\sigma_o)^2 \qquad \text{which is negative in this case}$$

in which $\Delta\underline{\sigma}'$ is the deviatoric stress vector associated with the computed stress increment $\Delta\underline{\sigma}$, and $\underline{\sigma}_1'$ is the deviatoric stress vector corresponding to the stress state at the beginning of the step.

For the Tresca criterion, the following equation is applied to all six facets to get six scale factors.

$$\alpha_i = \frac{t_o - \phi_i^A}{\phi_i^C - \phi_i^A} \qquad ; \quad i = 1, \cdots, 6 \qquad [6.4]$$

in which ϕ_i is defined by Eq. [5.12], and ϕ_i^C and ϕ_i^A are the values at states C and A, respectively. The smallest positive factor is the one required.

The reversal tolerance, t_r, is similar to the overshoot tolerance, t_o, except that it is applied in unloading situations, as shown in Fig. 6.4. The scale factor, α, is controlled by the reversal tolerance.

For the von Mises criterion, the scale factor α is determined from

$$\alpha = \frac{-B - \sqrt{B^2 - 4AC}}{2A} \qquad [6.5]$$

with

$A = \frac{3}{2} \Delta \underline{\sigma}'^{T} \cdot \Delta \underline{\sigma}'$ which is always positive

$B = 3\, \underline{\sigma}_1'^{T} \cdot \Delta \underline{\sigma}'$ which is negative in this case

$C = \frac{3}{2} \underline{\sigma}_1'^{T} \cdot \underline{\sigma}_1' - (t_r \sigma_0)^2$ which is positive in this case

For the Tresca criterion, Eq. [6.4] is applicable, except that the overshoot tolerance is replaced by the reversal tolerance. That is

$$\alpha_i = \frac{t_r - \phi_i^A}{\phi_i^c - \phi_i^A} \quad ; \quad i = 1, \cdots, 6 \qquad [6.6]$$

An algorithm to determine the scale factor is shown in Fig. 6.5. The steps are as follows for a typical integration point.

(1) The stress existing at the start of the iteration step, $\underline{\sigma}$, and the displacement increment $\Delta \underline{r}$ are known. The overshoot and reversal tolerances, t_o and t_r , are specified. The scale factor, FACTOR, is initialized to unity.

(2) Evaluate the strain increment from $\Delta \underline{\varepsilon} = \underline{B} \cdot \Delta \underline{r}$, and the stress increment from $\Delta \underline{\sigma} = \underline{C}_A \cdot \Delta \underline{\varepsilon}$ where $\underline{C}_A = \underline{C}$ at the beginning of the iteration step.

(3) Check the status at the beginning of the iteration step. If elastic go to step 8. Otherwise continue to the next step.

(4) Check for unloading using $\left[\left(\frac{\partial f}{\partial \underline{\sigma}} \right)^{T} \underline{C}^e \Delta \underline{\varepsilon} \right]$ as noted in Section 5.3.8. If the material unloads go to next step. Otherwise go to step 8

(5) For the unloading case, form the elastic material property matrix $\underline{C}^e$, and recalculate the stress increment from $\Delta\underline{\sigma} = \underline{C}^e \Delta\underline{\epsilon}$.

(6) For the specified reversal tolerance, t_r , evaluate the scale factor α , as described previously.

(7) Check if α is less than "FACTOR". If so, set FACTOR equal to α . By this procedure, the smallest scale factor is retained.

(8) With the specified overshoot tolerance, t_o , evaluate the scale factor, α , as described previously.

(9) Check if α is less than FACTOR. If so, set FACTOR equal to α . Again this serves to retain the smallest scale factor.

(10) Repeat steps (2) through (9) for all integration points in all elements, and hence get the final smallest value of FACTOR.

6.3 COMPUTATIONAL MODULE "ELOPLA"

The computational module "ELOPLA" is a subroutine for evaluation of the stress increment when the strain increment is given. The elastic,transitional and plastic cases are considered. The unloading case has already been converted to either an elastic or a transitional case in SCLDWN. The computational algorithms for the von Mises and Tresca criteria are outlined in Figs. 6.6 and 6.7. Details of the procedure have been described in Chapter 5, and need not repeated here.

6.4 COMPUTATIONAL MODULE "CONVRG"

The computational module "CONVRG" exercises control over the solution procedure. The procedure for any step is based on the values of the three convergence tolerances at the end of the previous step. The three tolerances are as follows:

(1) Final convergence tolerance, t_3 . If the largest unbalanced load is less than this value the solution for the current load increment has converged with sufficient accuracy, and the next load increment is considered.

(2) Constant stiffness tolerance, t_2 . If the largest unbalanced load is less than this tolerance the stiffness matrix is not reformed for the next iteration step, but the solution iterates with the same stiffness as in the current step.

(3) Step by step convergence tolerance, t_1 . The tolerance is used where a load increment is applied stepwise, in a number of equal subincrements. At the end of any subincrement, if (a) the largest unbalanced load is less than this tolerance and (b) this is not the last subincrement, then the next subincrement is added.

The sequence in which the tolerances are checked is shown as a flow diagram in Fig. 6.8.

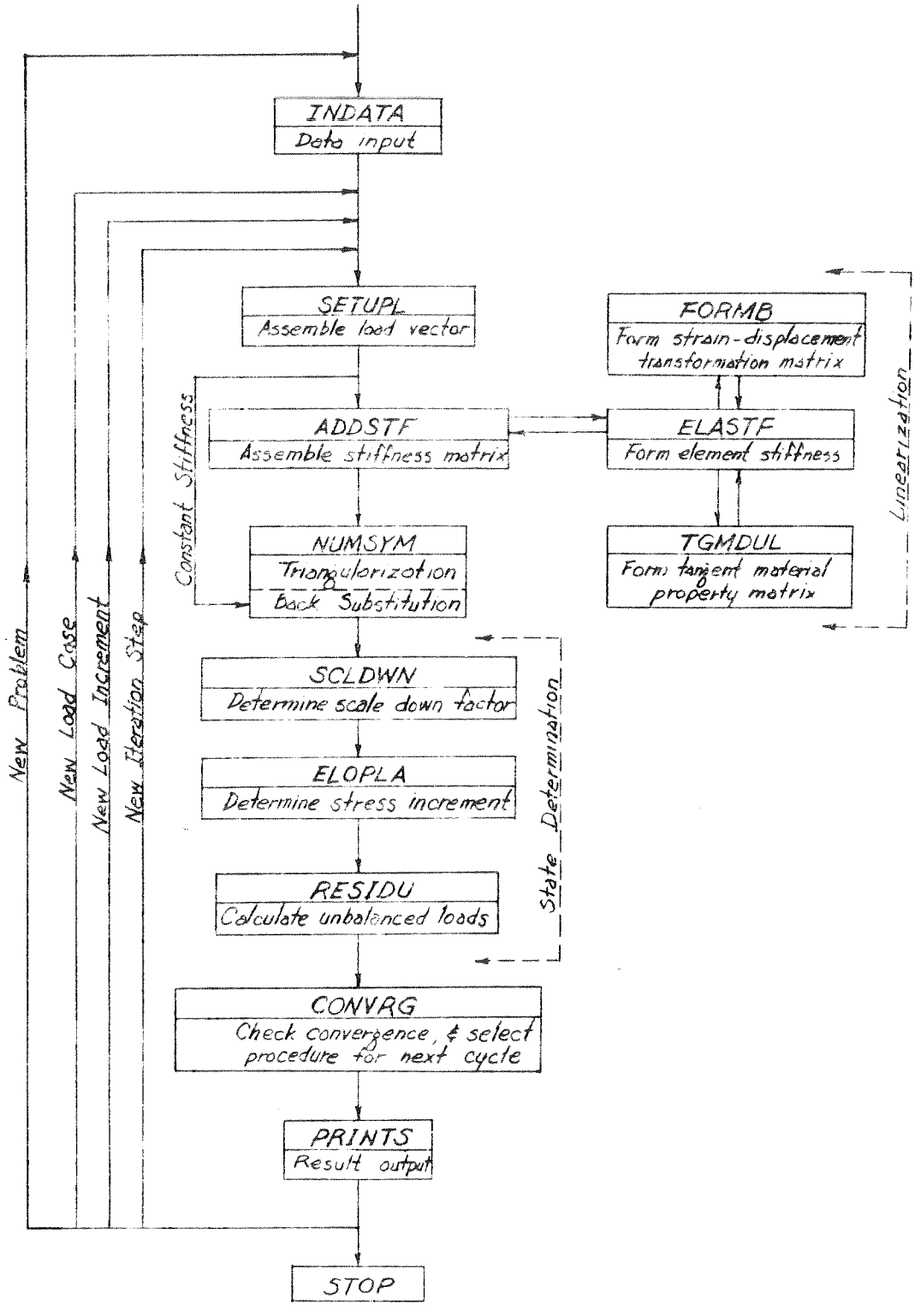

FIG 6-1 PROGRAM FLOW DIAGRAM

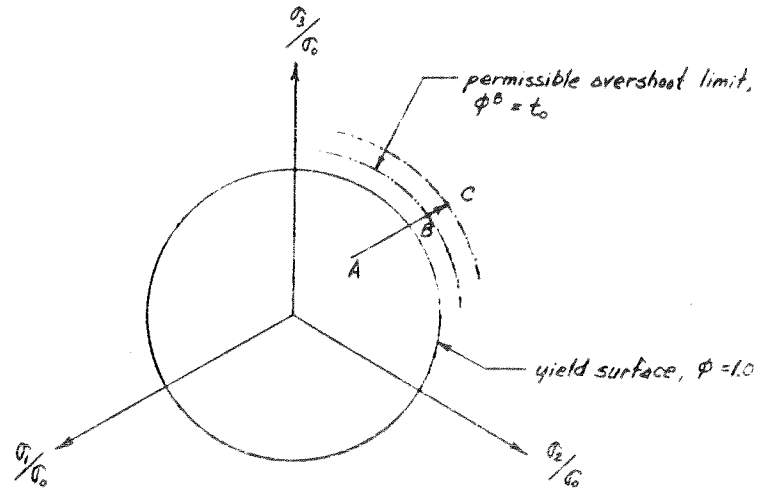

FIG 6-2 TRANSITIONAL CASE

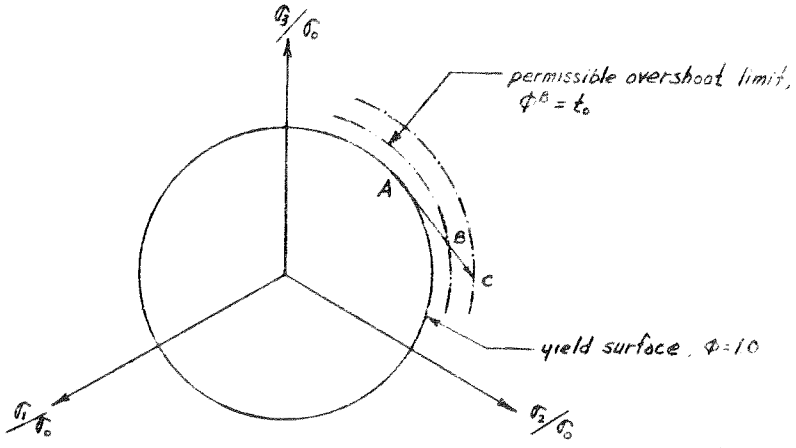

FIG 6-3 PLASTIC CASE

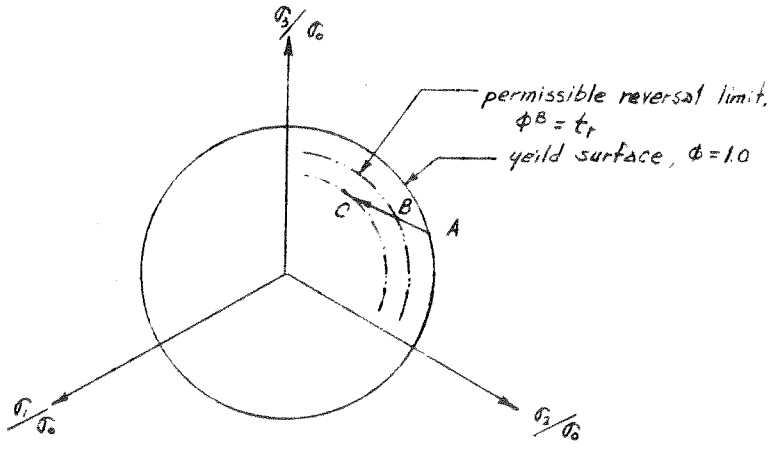

FIG 6-4 UNLOADING CASE

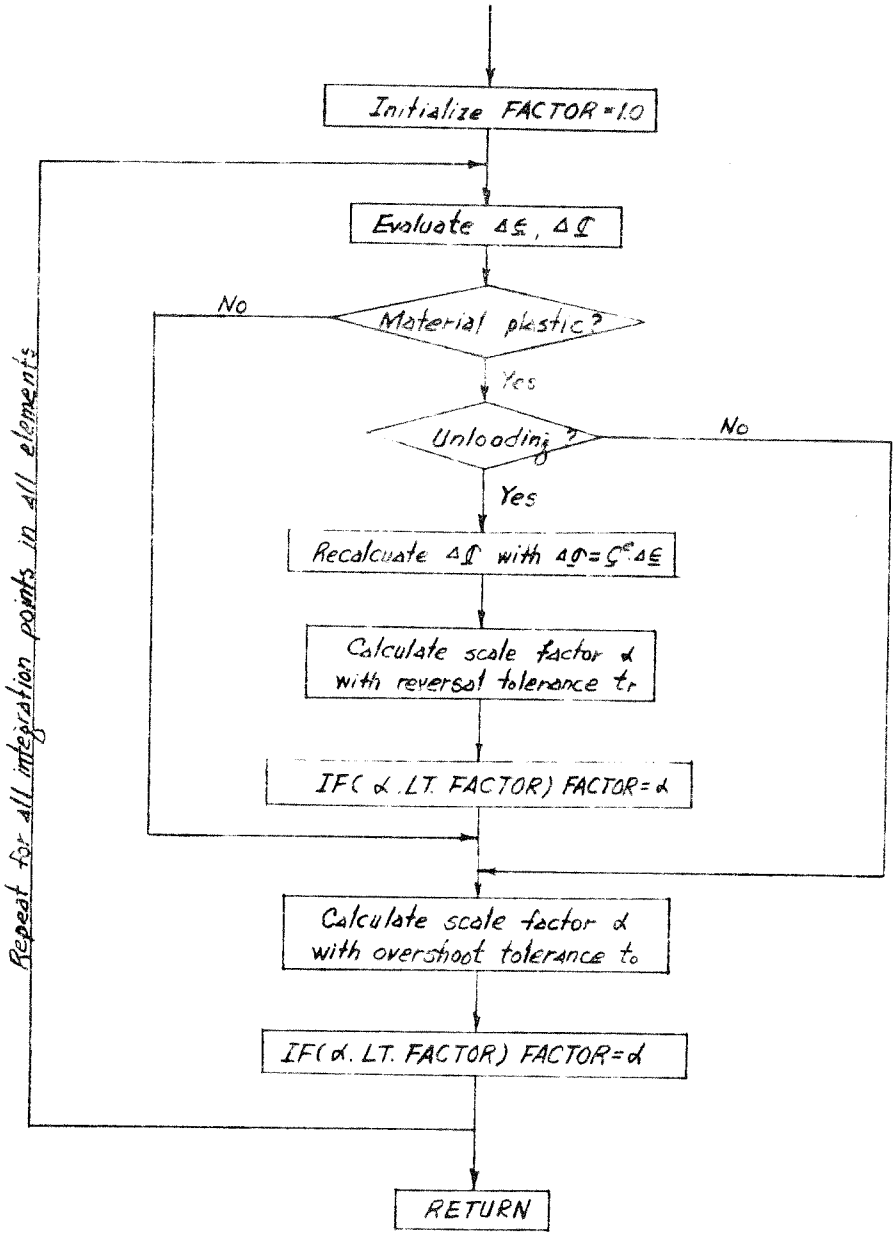

FIG 6-5 FLOW DIAGRAM FOR SCLDWN

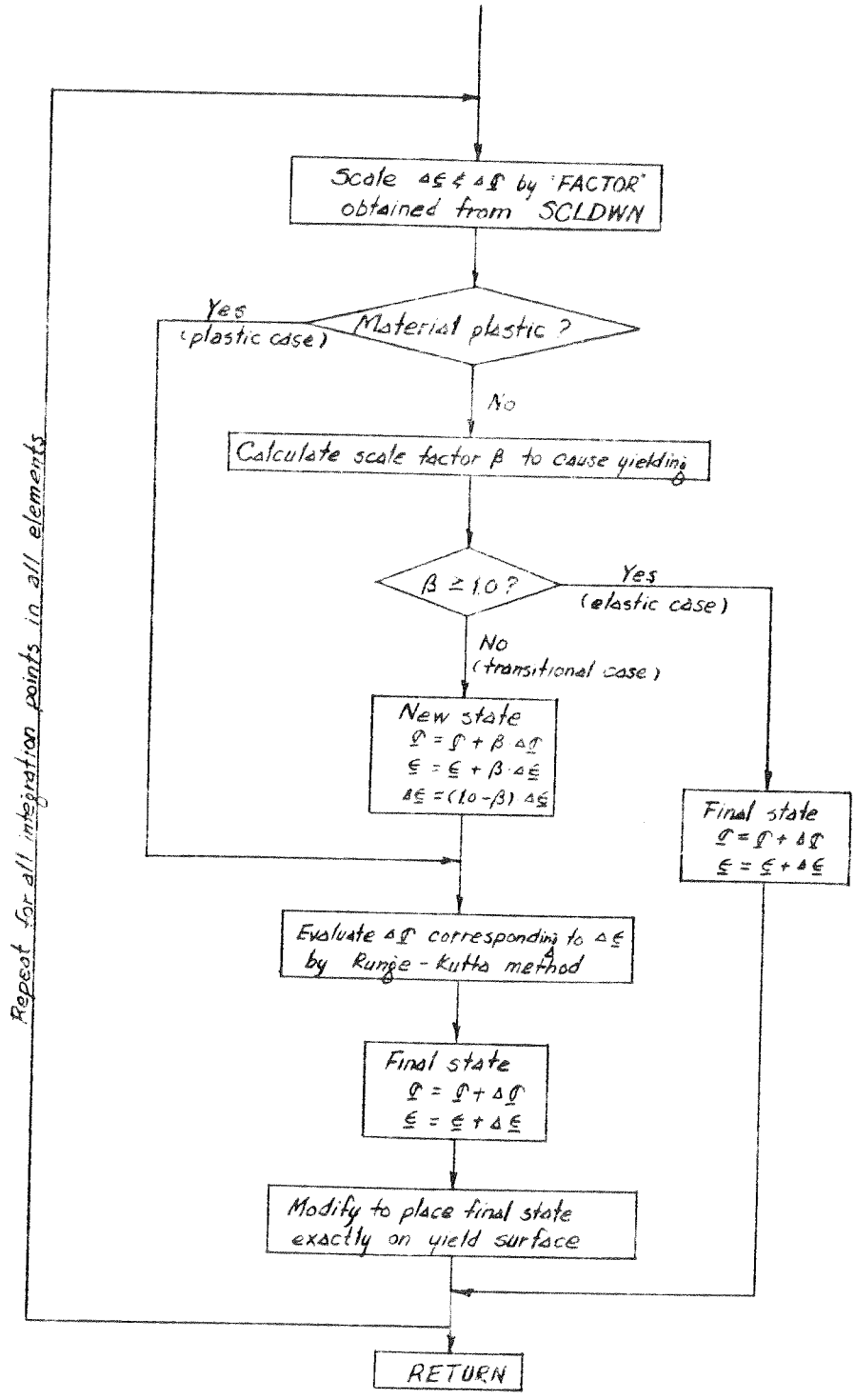

FIG 6-6 FLOW DIAGRAM FOR ELOPLA. VON MISES CRITERION

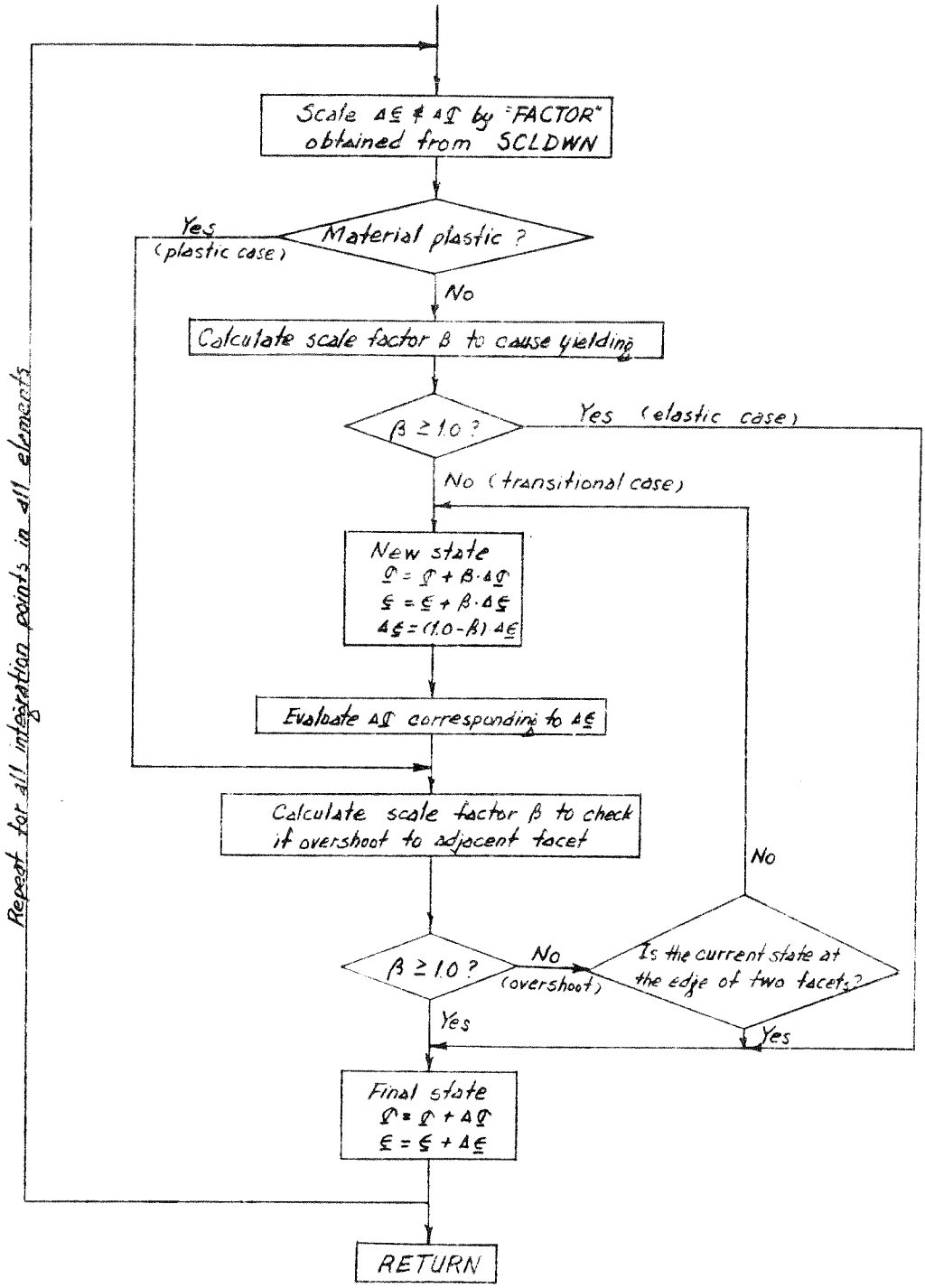

FIG 6-7 FLOW DIAGRAM FOR ELOPLA. TRESCA CRITERION

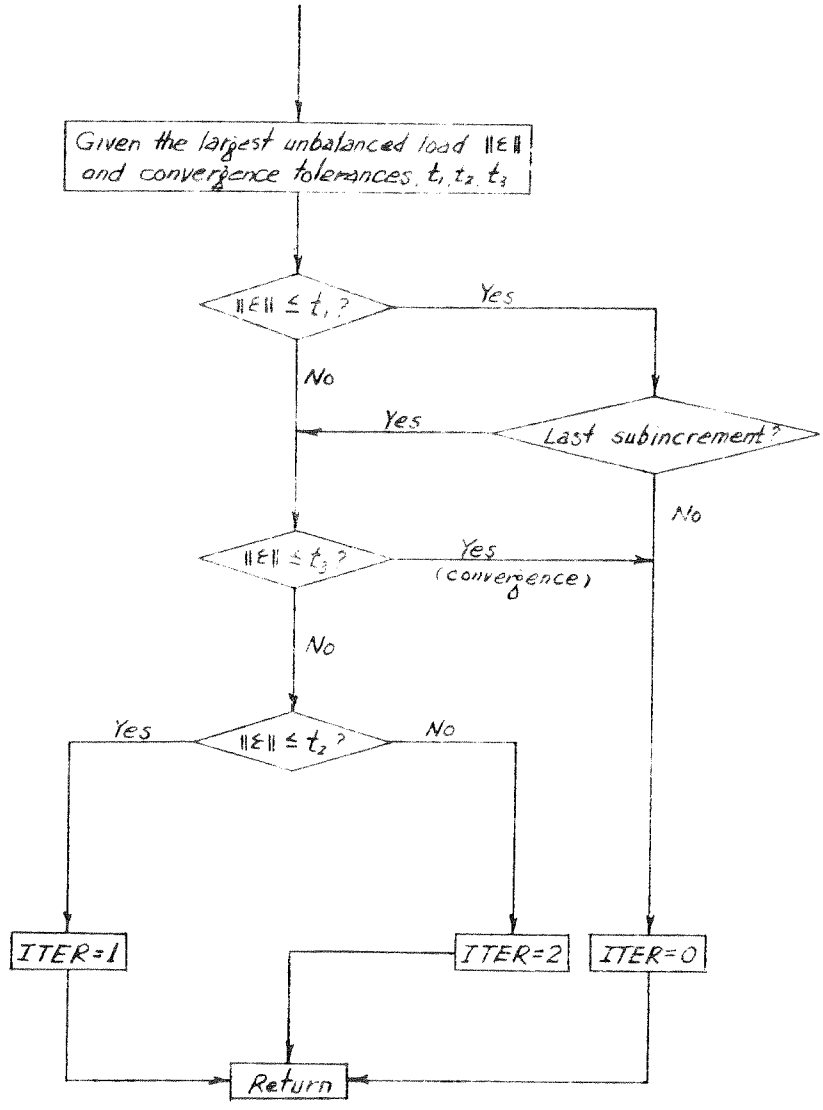

ITER = 0 Add next subincrement Reform stiffness.
ITER = 1 Iterate with constant stiffness
ITER = 2 Iterate with varying stiffness (Newton-Raphson method)

FIG 6-8 FLOW DIAGRAM FOR CONVRG

7. NUMERICAL EXAMPLES

7.1 CASES INVESTIGATED

In order to check the accuracy and efficiency of the method developed here, several elasto-plastic structures have been analyzed, as follows:

(1) A thick cylinder under internal pressure with its ends restrained in the axial direction.

(2) A perforated tension strip loaded by uniform tension at both ends.

(3) A torispherical pressure vessel subjected to internal pressure.

(4) A thin cylinder subjected to both axial load and internal pressure.

The first problem, for which a closed-form solution is known, and the second and third problems, for which experimental results are available, were selected to provide a check on the finite element results. The fourth problem was selected to investigate the behavior of the parallel material model for strain-hardening.

7.2 THICK CYLINDER

A thick cylinder under internal pressure and with its ends restrained in the axial direction has been studied. The cylinder has been analyzed in several different ways and the results have been compared with a closed-form solution derived by Hodge and White (4).

The cross section of the cylinder and the finite element idealization are shown in Fig. 7.1. The material was assumed to be elastic, perfectly plastic, with properties as follows:

Internal radius of the thick cylinder	$a = 1.0$
External radius of the thick cylinder	$b = 2.0$
Shearing modulus of elasticity	$G = 3.333 \times 10^4$
Poisson's ratio	$\nu = 0.3$
Yield stress in pure shear	$\kappa = 10.$

The following sequence of loading increments was applied:

(a) Internal pressure $\frac{p}{\kappa} = 1.0$ in one step.

(b) Increments $\frac{p}{\kappa} = 0.05$ continued until the plastic region penetrated through the complete thickness of the cylinder. The most accurate solution procedure was used, namely step by step with Newton-Raphson iteration within each load increment. Two different yield criteria were considered, namely the von Mises and Tresca criteria.

The variation of radial displacement with internal pressure is shown in Fig. 7.2. Fig. 7.3 shows the radial, circumferential and axial stress distributions at an internal pressure of $\frac{p}{\kappa} = 1.25$, when the plastic region had progressed through half of the thickness of the cylinder.

There is good agreement between the finite element and closed-form solutions. It is of interest to note that the finite element results using the two different yield criteria are almost identical, except for some stress discrepancies along the

elasto-plastic boundary, with the results from the von Mises criterion being closer to the closed-form solution. The closed-form solution was based on the von Mises criterion, but it has been shown by Hodge and White (4), Hill et al (2) and Marcal (30) that there should be little difference between the two yield criteria for this problem. The results obtained herein provide additional support for this observation.

Figures 7.4 and 7.5 show comparisons between the results obtained with the Q4I4 and Q4 elements, respectively. The Q4 element, which is fully compatible, but has an incomplete quadratic displacement function, is seen to provide a good displacement value, but to provide poor stress results at the integration points. The Q4I4 element exhibits stress errors of a similar type at the integration points, but to a less marked extent. Both elements provide accurate stress results at the element centers.

A comparison of Figs. 7.3 and 7.5 shows that better stress results are obtained by loading in several steps than by loading in a single step.

To demonstrate the application of the program for cases with reversed loading, a cyclic sequence of load increments was applied to the cylinder. This sequence is as follows:

$$\frac{p}{\kappa} = 0.0 \rightarrow 1.0 \rightarrow 1.25 \rightarrow 0.0 \rightarrow -1.0 \rightarrow -1.25 \rightarrow 0.0$$

Fig. 7.6 shows the radial displacements at each stage of the loading sequence, and Fig. 7.7 shows the corresponding stress distributions. The stresses are plotted for the element centers

only. It is of interest to note that the stress distributions associated with the first and second residual states are symmetric with respect to the initial state.

7.3 PERFORATED TENSION STRIP

7.3.1 Dimensions and Properties

Results of a test on a rectangular plate with a central hole have been reported by Theocaris and Marketos (20). This structure has also been studied with the finite element method by Marcal and King (38), and Zienkiewicz et al (50). Because this example has been studied both experimentally and theoretically, it is of value for assessing the effectiveness and accuracy of the present method.

The test material was aluminum. The following properties have been assumed for analysis:

Yield stress in pure tension	σ_o	= 24.3 kg/mm^2
Young's modulus	E	= 7000 kg/mm^2
Strain hardening modulus	H	= 225 kg/mm^2
Poisson's ratio	ν	= 0.2

The dimensions of the strip are shown in Fig. 7.8. Two different finite element meshes have been considered, namely a coarse mesh with 31 elements and a fine mesh with 92 elements, as shown in Figs. 7.9 and 7.10.

For a stepwise loading with Newton-Raphson iteration within each step, the variation of maximum strain with load is shown in Fig. 7.11. The strain from the finite element analyses are for the integration point which yielded first in each case.

The progression of the elastic-plastic boundary is illustrated in Figs. 7.12 and 7.13. The finite element results are generally in good agreement with the experimental results. The strains obtained here are somewhat larger than those computed by Marcal and King (38) and by Zienkiewicz et al (50). The progressive elastic-plastic boundaries from the analysis and experiment are in good agreement, even for the coarse finite element mesh. However, the results for the fine mesh agree more closely with the experimental results. It is of interest to note, in Fig. 7.13g, that the experimental results show yielding at the top of the hole, and that this yielding is also predicted by the analysis using the fine mesh. This yielding was not observed with the coarse mesh, and was not reported by Marcal and King or by Zienkiewicz et al.

7.3.2 Comparison of Solution Procedures

In order to compare the performance of different solution procedures, and to aid in the selection of the best method for practical analysis, analyses of the perforated strip have been carried out by the thirteen different procedures listed in Table 2.1, using the coarse mesh. The strain values, $E\epsilon/\sigma_0$, at the first yielded integration point for all procedures are summarized in Table 7.1 and Fig. 7.14. The number of times the stiffness was reformed and the number of iteration cycles for each procedure and each incremental load step are shown in Table 7.2. Central processor times on the CDC 6600 are also shown. The elastic-plastic boundaries for the loading $\frac{\sigma_\infty}{\sigma_0} = 1.0$ for each procedure are shown in Fig. 7.15.

The following conclusions may be drawn from this study:

(1) All procedures provide good final results, except Method 2, direct iteration with constant stiffness, and Method 4, step by step method with equilibrium correction. One reason why Method 2 did not provide a good final result is that it was terminated after 35 iteration cycles, prior to complete convergence.

(2) The final results are insensitive to the size of the load increment. Because of the influence of the load path, the elastic-plastic boundary computed by Methods 1, 2 and 3 (Fig. 7.15a) is slightly different from that computed by Methods 8, 9 and 10 (Fig. 7.15d). In general, however, the single step solutions give results which are very close from those obtained with several load increments.

(3) The methods making use of iteration with constant stiffness, namely Methods 2, 6, 9 and 12, are considerably more time comsuming for this example than those using iteration with varying stiffness. The methods using varying stiffness require the solution of both linearization and state determination problems in each step of the iteration, whereas those using constant stiffness require only that the state determination problem be solved. However, because the computer time required for solution of the linearization and state determination problems are similar for this example, and because the methods using varying stiffness require fewer cycles to converge, these methods prove to be more efficient. In other problems, particularly those with larger numbers of elements, the time for each linearization may substantially exceed the time for each state determination, and hence the relative efficiencies may change.

7.3.3 Convergence Rate

The convergence rate for maximum strain and maximum unbalanced nodal load are shown in Fig. 7.16 for Methods 1, 2 and 3. It can be seen that the rate of convergence is slow when a constant stiffness is used.

7.3.4 Use of Q4 and Q4I4 Elements

To investigate the differences between results obtained with the Q4I4 and Q4 elements, the analyses for the coarse and fine meshes have been repeated by Method 1 using the Q4 element. The convergence rates and final results are shown in Table 7.3 and the elastic-plastic boundaries are shown in Fig. 7.17. The results obtained with the Q4 element are inferior to those for the Q4I4 element in the case of the coarse mesh, but there is close agreement for the fine mesh. The Q4I4 element appears to be a superior element on the basis of this example.

7.3.5 Unbalanced Load Computation and Path Independent Approach

In all of the methods considered, the unbalanced load has been computed using the equation

$$\underline{R}^I = \int_V \underline{B}_1^{*T} \underline{\sigma} \, dV$$

in which $\underline{B}_1^*$ is the strain-displacement transformation matrix at the beginning of the current step. As noted in Chapter 5, the internal resisting force, $\underline{R}^I$, may also be computed by

$$\underline{R}^I = \int_V \underline{B}_0^{*T} \underline{\sigma} \, dV$$

in which $\underline{B}_o^*$ is the transformation matrix corresponding to the elastic state.

The procedure used to compute the strains and stresses in these examples has also been the "path dependent" approach based on the equations,

$$\delta \underline{\epsilon}_n = \underline{B}_i^* \, \delta \underline{r}_n$$

$$\delta \underline{\sigma}_n = \underline{h}_n \, \delta \underline{\epsilon}_n$$

$$\Delta \underline{\sigma}_n = \Delta \underline{\sigma}_{n-1} + \delta \underline{\sigma}_n$$

$$\underline{\sigma}_n = \underline{\sigma}_{n-1} + \Delta \underline{\sigma}_n$$

$$\underline{R}^x = \int_v \underline{B}_i^{*T} \underline{\sigma}_n \, dv$$

As noted in Section 5.3.9, the stresses and strains may also be determined by a "path independent" approach within any load increment.

To investigate these alternative methods of computation, the perforated strip has been analyzed, for the coarse mesh, using several variations of Method 1, in which the state determination problem was solved in several different ways. The alternative procedures are shown in Table 7.4.

The most rapid convergence was obtained with procedure type 2. In this case, the strain increments were determined using a transformation matrix $\underline{B}_i^*$ which is consistent with that used for the linearization, and a constant transformation matrix $\underline{B}_o^*$, was used for the calculation of the internal resisting force. Procedure type 3 also converged rapidly. However, it was noted that unloading at previously yielded integration points occured with this procedure, leading to small oscillating values of the

unbalanced load. If the unbalanced load tolerance were set very small, convergence might not be obtained with this procedure. To avoid this, a provision was included in the program to prevent unloading at previously yielded points at all iteration cycles except the first one in any load increment. The convergence rate shown in Table 7.5 was obtained with this provision. No such unloading was observed with procedure type 2, and for practical computation this procedure is recommended.

It may be noted that procedures types 1 and 6 do not converge. The reason why type 1 diverges is that the constant transformation matrix, $\underline{B}_o^*$, which is used to evaluate the strain increments is inconsistent with that used to form the stiffness and obtain the displacement increment. In both the type 5 and type 6 analyses, the use of the matrix $\underline{B}_i^*$ to determine the total strains would appear to be inconsistent, because this transformation changes progressively. However, procedure type 5 converged whereas type 6 did not. The reason for this is not clear. It can be seen, nevertheless, that even where convergence is obtained by any path independent procedure, this convergence is likely to be slow. Hence, it may be concluded that path independent procedures should not be used for practical computation.

Procedure type 7 demonstrates that the basic Q4 element, which has a constant transformation matrix in all cases, exhibits convergence with a path independent procedure. However, more rapid convergence was previously obtained using a path dependent procedure.

TABLE 7.1

STRAIN ($E\epsilon/\sigma_0$) AT POINT OF FIRST YIELD

Method Type \ $\frac{\sigma_u}{\sigma_0}$	0.5	0.6	0.7	0.8	0.9	1.0	Remark
1						4.561425	
2						3.884088	No convergence after 35 cycles
3						4.555528	
4	0.928814	1.114577	1.593967	2.241999	3.296554	4.297315	
5	0.928814	1.114577	1.593967	2.241999	3.296554	4.609688	
6	0.928814	1.114577	1.593967	2.241999	3.296554	4.599701	
7	0.928814	1.114577	1.593967	2.241999	3.296554	4.609560	
8	0.928814	1.228785	1.857356	2.555872	3.431419	4.575259	
9	0.928814	1.217414	1.687917	2.496428	3.393974	4.456471	
10	0.928814	1.228730	1.860693	2.556379	3.432010	4.575667	
11	0.928814	1.114577	1.593967	2.553513	3.435872	4.587026	
12	0.928814	1.114577	1.593967	2.557521	3.471997	4.553072	
13	0.928814	1.114577	1.593967	2.553589	3.436878	4.587700	

TABLE 7.2

COMPARISON OF OPERATIONS

Step	1		2		3		4		5		6		Total		Central Processor Time (sec) (CDC 6600)
$\frac{\sigma_u}{\sigma_o}$	0.5		0.6		0.7		0.8		0.9		1.0				
Method Type	N.R.S*	N.I*	N.R.S.	N.I.	N.R.S.	N.I.	N.R.S.	N.I.	N.R.S.	N.I.	N.R.S.	N.I.	N.R.S.	N.I.	
1											7	7	7	7	15.8
2											1	>35	1	>35	>80.0
3											2	15	2	15	23.4
4	1	1	1	1	1	1	1	1	1	1	1	1	6	6	11.9
5	1	1	1	1	1	1	1	1	1	1	4	4	9	9	18.4
6	1	1	1	1	1	1	1	1	1	1	1	15	6	20	34.4
7	1	1	1	1	1	1	1	1	1	1	3	4	8	9	17.7
8	1	1	3	3	5	5	3	3	4	4	4	4	20	20	38.9
9	1	1	1	8	1	8	1	8	1	14	1	15	6	54	88.5
10	1	1	3	3	3	4	2	3	3	4	4	4	16	19	35.7
11	1	1	1	1	1	1	4	4	4	4	4	4	15	15	29.6
12	1	1	1	1	1	1	1	8	1	15	1	15	6	41	67.7
13	1	1	1	1	1	1	2	3	3	4	4	4	12	14	27.4

*N.R.S. = No. of times structure stiffness reformed.
N.I. = No. of Iteration cycles

TABLE 7.3

CONVERGENCE RATES FOR SINGLE LOAD STEP. COMPARISON OF Q4 AND Q4I4 ELEMENTS

Iteration Cycle	Max. Residual Force				$E\epsilon/\sigma_0$ at Point of First Yield			
	Q4 Element Coarse Mesh	Q4I4 Coarse Mesh	Q4 Element Fine Mesh	Q4I4 Element Fine Mesh	Q4 Element Coarse Mesh	Q4I4 Coarse Mesh	Q4 Fine Mesh	Q4I4 Fine Mesh
1	9.2168	8.7567	7.2554	7.4357	1.84585	1.85763	1.99521	2.01372
2	5.0491	7.0399	5.2338	5.9474	3.36510	3.46135	3.91052	4.06626
3	1.5476	1.5284	1.1460	1.1390	3.72173	4.49165	4.47800	4.71729
4	0.0105	0.2794	0.0740	0.0445	3.82849	4.56121	4.58734	4.80722
5	0.0000	0.0242	0.0154	0.0000	3.82940	4.56206	4.58925	4.80239
6		0.0.08	0.0000			4.56183	4.58957	
7		0.0008				4.56143		

Loading: $\frac{\sigma_u}{\sigma_0} = 1$

Scheme : Direct N-R Iteration Method

TABLE 7.4

ALTERNATIVE PROCEDURES FOR STATE DETERMINATION

Type	Element	State Determination	Transformation Matrix for Evaluation of $\Delta \underline{\epsilon}$	Transformation Matrix for Evaluation of $\underline{R}^r$
1	Q4I4	Path-Dependent	$\underline{B}_c^*$	$\underline{B}_o^*$
2	Q4I4	Path-Dependent	$\underline{B}_1^*$	$\underline{B}_o^*$
3	Q4I4	Path-Dependent	$\underline{B}_t^*$	$\underline{B}_t^*$
4	Q4I4	Path-Independent	$\underline{B}_o^*$	$\underline{B}_o^*$
5	Q4I4	Path-Independent	$\underline{B}_1^*$	$\underline{B}_o^*$
6	Q4I4	Path-Independent	$\underline{B}_t^*$	$\underline{B}_t^*$
7	Q4	Path-Independent	$\underline{B}$	$\underline{B}$

$\underline{B}_o^*$ = transformation matrix corresponding to elastic state.

$\underline{B}_t^*$ = transformation matrix corresponding to state of beginning of linear step.

$\underline{B}$ = transformation matrix without static condensation.

TABLE 7.5

MAXIMUM UNBALANCED LOADS FOR DIFFERENT STATE DETERMINATION PROCEDURES

Single step N-R iteration in all cases, $\frac{\sigma_u}{\sigma_o} = 1.0$.
Strain = $E\epsilon/\sigma_o$. See Table 7.4 for definition of procedures

Iterative Cycle	Type 1	Type 2	Type 3	Type 4	Type 5	Type 6	Type 7
1	8.7567	8.7567	8.7567	8.7567	8.7567	8.7567	9.2167
2	7.0914	7.0483	7.0399	7.1945	7.1476	7.1436	5.0430
3	1.6313	1.5926	1.5284	2.2022	2.1091	4.5879	1.5213
4	0.8383	0.0126	0.2794	1.9278	1.7049	5.1731	0.3874
5	1.4779	0.0000	0.0241	1.7390	1.4435	5.1949	0.2712
6	1.9565		0.0108	1.5360	1.1990	12.2001	0.1826
7	3.5273		0.0008	1.4085	1.0036	15.2330	0.1372
8	3.6003			1.2538	0.8385	33.6724	0.1016
9	5.7980			1.1502	0.7006	24.8541	0.0746
10	3.8461			1.0305	0.5857	47.1228	0.0543
11	4.7889			0.9444	0.4895	63.7916	0.0393
12	3.7194			0.8496	0.4092	61.2234	0.0283
13	5.2855			0.7777	0.3421	77.1607	0.0203
14	3.9027			0.7015	0.2859	70.6628	0.0145
15	5.0203			0.6414	0.2390	105.0266	0.0104
16	3.7899			0.5795	0.1997	113.1733	0.0074
17	5.1257			0.5294	0.1670	113.3245	
18	3.8825			0.4790	0.1396	107.8183	
19	5.1144			0.4372	0.1167	108.8824	
20	3.8178			0.3959	0.0975	106.8961	

TABLE 7.6

STRAINS AT POINT OF FIRST YIELD FOR DIFFERENT STATE DETERMINATION PROCEDURES

Single step N-R iteration in all cases, $\frac{\sigma_2}{\sigma_0} = 1.0$.
Strain = $E\epsilon/\sigma_0$. See Table 7.4 for definition of procedures

Type 1	Type 2	Type 3	Type 4	Type 5	Type 6	Type 7
———	4.41198	4.56134	4.08968	4.16316	——	3.89451

7.4 TORISPHERICAL PRESSURE VESSEL

A torispherical pressure vessel head subjected to internal pressure has been tested by Stoddart and Owen (21), and analyzed by Marcal (35, 46) using axisymmetric curved shell elements. The relevant dimensions of the vessel head are as follows:

Mean diameter of cylindrical barrel of vessel	D = 24"
Mean radius of sphere	R = 24"
Mean radius of torus	r = 2"
Thickness of the shell	t = 1/4"

The vessel tested by Stoddart and Owen was made of mild steel with the following properties:

Young's modulus	$E = 30.4 \times 10^3$ ksi
Uniaxial yield stress	$\sigma_0 = 40.197$ ksi
Poisson's ratio	$\nu = 0.31$

Elastic perfectly plastic behavior was assumed by both Stoddart and Owen and Marcal, with yield according to the von Mises criterion.

The structure has been idealized with thirty-eight elements of Q4I4 type, as shown in Fig. 7.18. The element stiffnesses were obtained using a 2x8 integration order, with 8 integration points through the thickness of the shell.

The elastic stress distributions on the internal and external surfaces of the vessel for a pressure of 0.1 ksi are shown on Fig. 7.19. The experimental results of Stoddart and Owen and the finite element results are seen to be in excellent

agreement. This demonstrates the applicability of the Q4I4 element to the analyses of thin shells of this type. A similar demonstration has been given by Wilson et al (54).

The maximum equivalent stress occurs at an angle $\theta = 45°$, on the internal surface of the torus. In the finite element analysis, yielding is predicted to occur first at this point at a pressure of 0.22 ksi. This compares well with the experimental pressure of 0.20 ksi at first yield reported by Stoddart and Owen. For the elasto-plastic analysis, a pressure of 0.215 ksi was first applied, followed by increments of 0.043 ksi until the pressure reached 0.473 ksi (2.15 times first yield).

The computed surface strains at an angle $\theta = 44.44°$ are shown for increasing pressure in Table 7.7 and Figs. 7.20 and 7.21. These results are at a slightly different location from those reported by Stoddart and Owen and Marcal, which corresponded to $\theta = 45°$, but the difference is believed to be negligible.

The agreement with Marcal's results are seen to be close, and the agreement with the experimental results to be reasonable. The main discrepancies are between the numerical results and the experimental results on the external surface of the vessel, especially the circumferential strains. It may be noted that Marcal (35) has questioned the accuracy of the experimental results.

The computed progression of the elastic-plastic boundary is shown in Figs. 7.22 and 7.23. Yielding occurs first on the internal surface near the point $\theta = 45°$. As the pressure is increased the yielded region spreads through the thickness and

along the shell. At higher pressure, yielding begins at the external surface of the torus. At a pressure of 0.387 ksi, the full thickness becomes plastic. Yielding then spreads into the sphere and cylinder.

For the purpose of design, it is important to determine an ultimate pressure. In the test, the values of strain showed a sudden increase at a pressure of 0.375 ksi, and it was concluded that a pressure of 0.375 ksi was the experimental ultimate pressure. The upper and lower bounds calculated by limit analysis methods (15, 17) were 0.456 ksi and 0.375 ksi, respectively. If deflection were used as the criterion for defining the ultimate load, than a pressure of 0.450 ksi might be taken as the ultimate pressure from the present analysis, because the slope of the deflection curve beyond this pressure became very flat. The maximum strain at $\phi = 45°$ also increased rapidly from 0.6% at 0.430 ksi pressure to 1.7% at 0.473 ksi. On the other hand, if the ultimate load were defined more conservatively, then a pressure of 0.387 ksi might be selected, because the plastic region had spread through the whole thickness at this pressure. These calculated ultimate pressures are consistent with the limit analysis and experimental results.

The analysis required 313 seconds of effective time (178 seconds of C.P. time) on the CDC 6600, with a field length of 64000 octal.

TABLE 7.7

TORISPHERICAL VESSEL. COMPUTED STRAINS AT $\theta = 44.44°$. OUTER INTEGRATION POINTS

Internal Pressure p (ksi)	$\epsilon_{max} \times 10^{-2}$		$\epsilon_{min} \times 10^{-2}$		$\epsilon_{normal} \times 10^{-2}$		$\epsilon_{merid} \times 10^{-2}$		$\epsilon_{circumf.} \times 10^{-2}$	
	Internal Surface	External Surface	Internal Surface	External Surface	Internal Surface	External Surface	Internal Surface	External Surface	Internal Surface	External Surface
0.215	0.1234276	0.0478931	-0.0229374	-0.0394508	-0.0227400	0.0478326	0.1232303	-0.0393905	-0.0657940	-0.0626703
0.258	0.1558309	0.0581136	-0.0311311	-0.0492841	-0.0308786	0.0579984	0.1555783	-0.0491689	-0.0800234	-0.0735349
0.301	0.2028080	0.0726763	-0.0475116	-0.0615021	-0.0471688	0.0725285	0.2024652	-0.0613543	-0.0973123	-0.0893569
0.344	0.2677171	0.0918604	-0.0735867	-0.0752406	-0.0731033	0.0916732	0.2672337	-0.0750534	-0.1191039	-0.1092558
0.387	0.3789074	0.1384381	-0.1261317	-0.1021736	-0.1253520	0.1381870	0.3781277	-0.1019225	-0.1540310	-0.1409434
0.430	0.6039802	0.2608709	-0.2558240	-0.1590870	-0.2543865	0.2604558	0.6025427	-0.1586719	-0.2261007	-0.2064287
0.473	1.7167860	0.8856619	-0.9622697	-0.4422293	-0.9576044	0.8842406	1.7121200	-0.4408080	-0.5794208	-0.5298447

7.5 THIN CYLINDER

A thin cylinder subjected to both axial load and internal pressure has been selected to investigate the behavior of the parallel material procedure for consideration of strain hardening. The dimensions and material properties of the cylinder are shown in Fig. 7.24. For the purposes of demonstration, a material with a high strain hardening modulus, $H = 0.1\ E$, has been used.

Figure 7.25 shows the manner in which the projection of the yield surface on the π - plane translates with increasing axial stress. An axial load was applied beyond the initial yield limit, to σ_z/σ_o = 1.25, 1.50, and 1.75, respectively, and in each case the load was removed. The positive and negative internal pressures required to cause yield were then found. Hence, three points were found on each loading surface, and the surfaces were constructed. As expected, the surface translates parallel to the σ_z axis.

Figure 7.26 shows the movement of the yield surface in the π - plane when an axial stress of 1.5 σ_o is first imposed, followed by unloading and addition of internal pressure up to a hoop stress of 1.4 σ_o . Under axial load the surface translates parallel to the σ_z axis, as before. Under internal pressure, producing yielding in the σ_θ direction, the center of the surface migrates towards the σ_θ axis. Fig. 7.27 shows successive locations of the yield surface and its center. From the path of the center of the surface, it appears that the strain hardening in this case corresponds closely to Prager's kinematic

hardening model (11). Further studies are needed, however, to investigate in greater detail the characteristics of this strain hardening model.

(a) Cross Section of Thick Cylinder

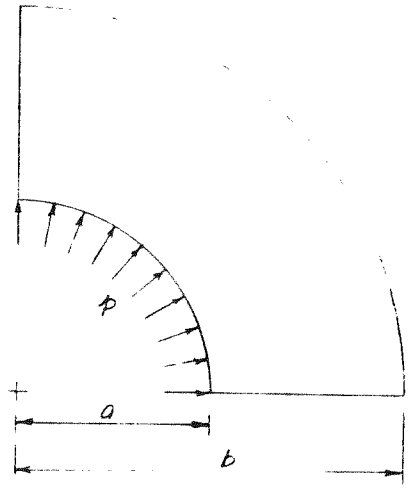

(b) Idealization of Structure

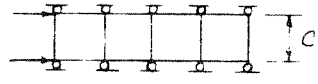

(c) Parameters of Material Properties

$b/a = 2$

$\nu = 0.3$

$K/G = 0.003$

(d) Input Data

$a = 10.$

$b = 20.$

$c = 1.0$

$G = 3.3334 \times 10^4$ $E = 8.6658 \times 10^4$

$K = 10.$, $\sigma_0 = 20.$ for Tresca Criterion,

$\sigma_0 = 17.32$ for von Mises Criterion

FIG 7-1 THICK CYLINDER

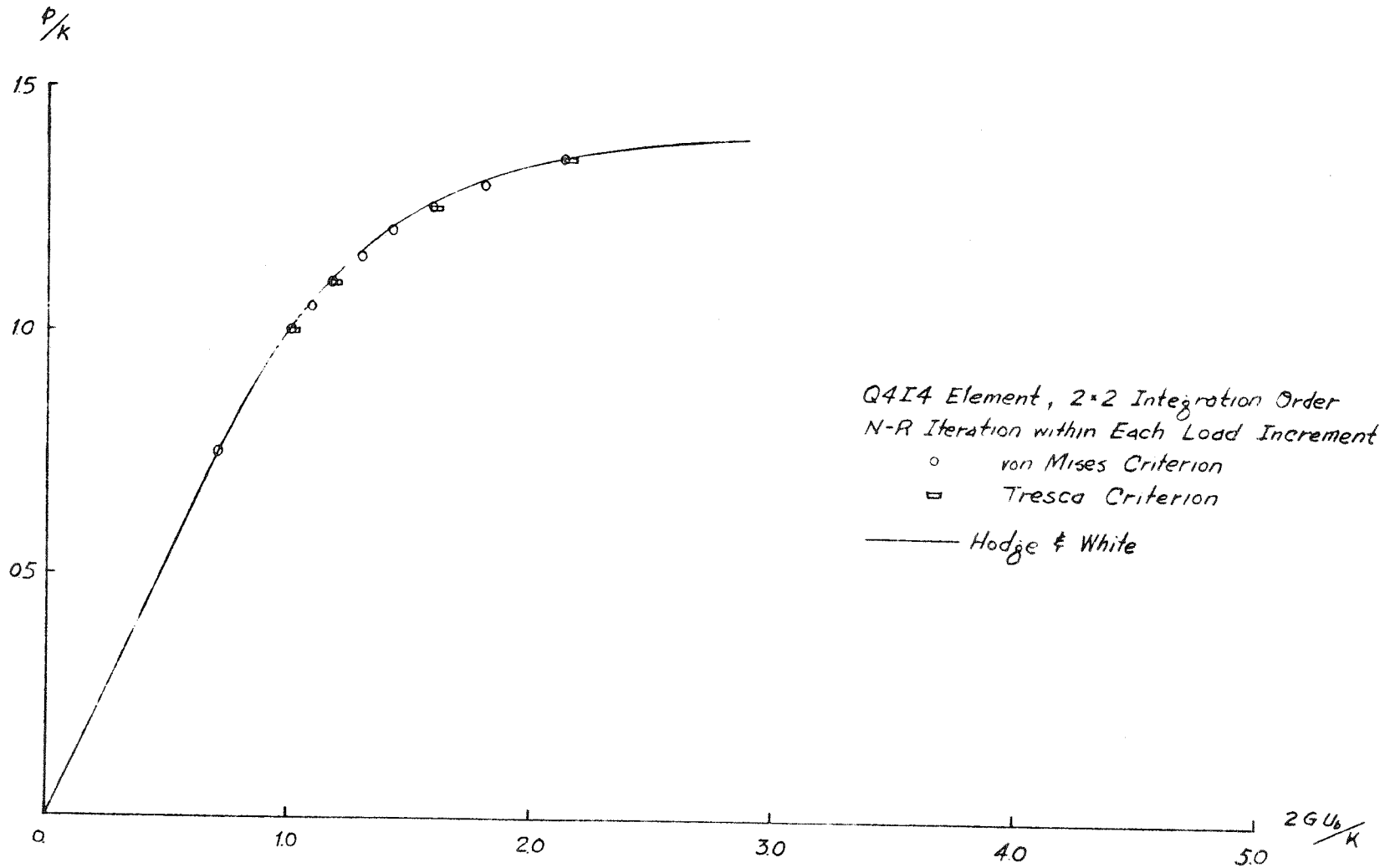

FIG 7-2 RADIAL DISPLACEMENTS OF THICK CYLINDER COMPARISON OF YIELD CRITERIA

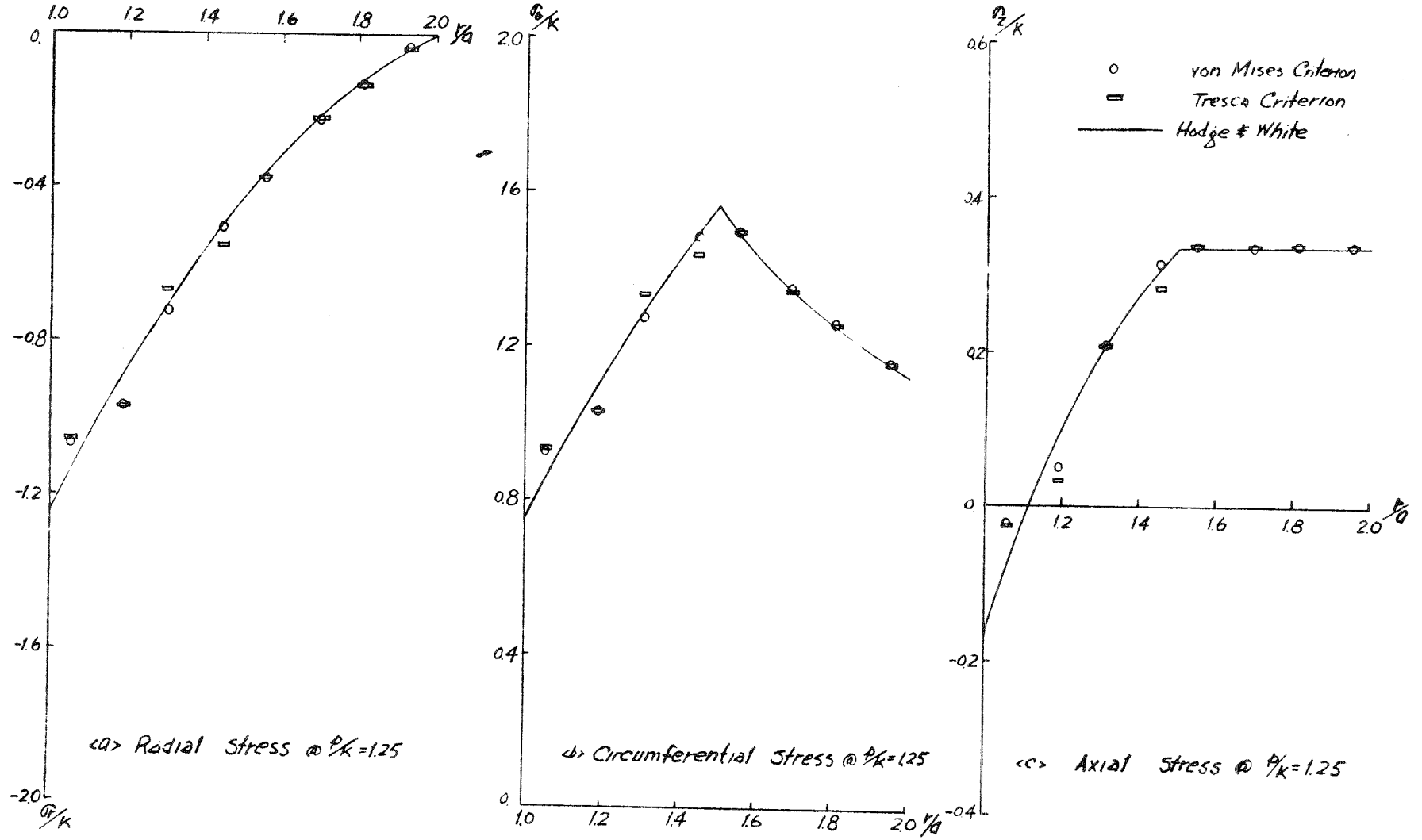

FIG 7-3 STRESSES IN THICK CYLINDER COMPARISON OF YIELD CRITERIA

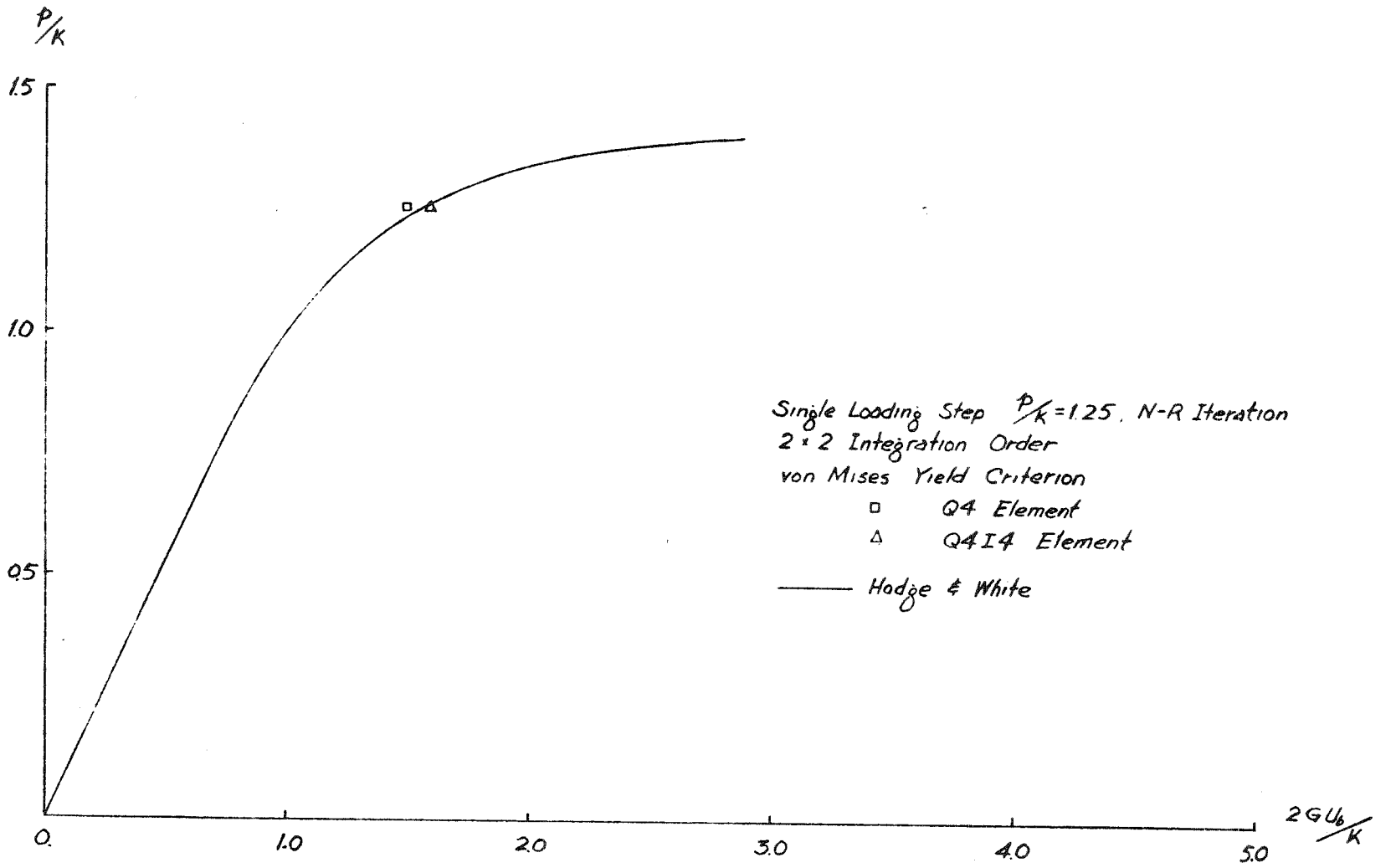

FIG 7-4 RADIAL DISPLACEMENTS OF THICK CYLINDER. COMPARISON OF Q4I4 AND Q4 ELEMENTS

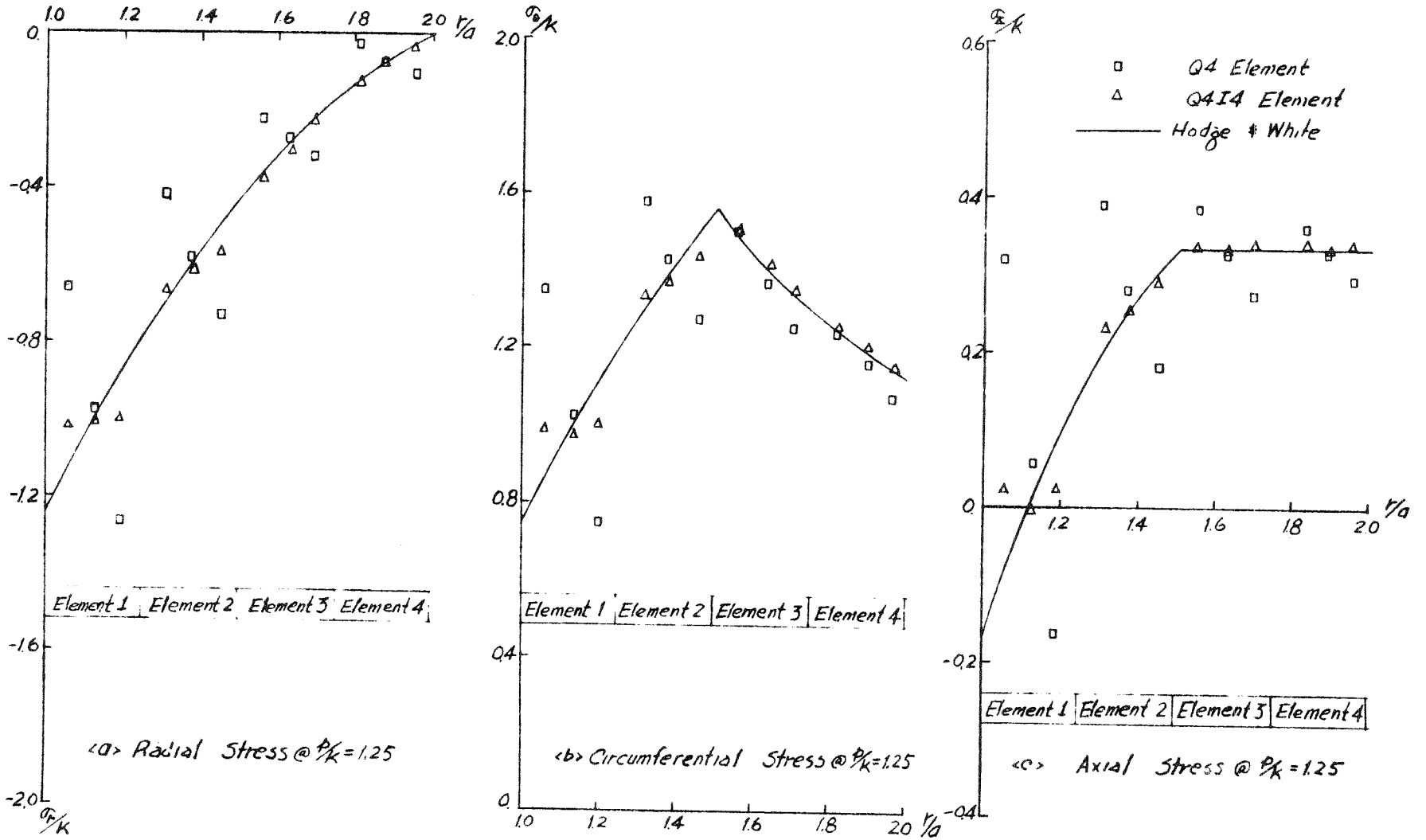

FIG 7-5 STRESSES IN THICK CYLINDER COMPARISON OF Q4I4 AND Q4 ELEMENTS

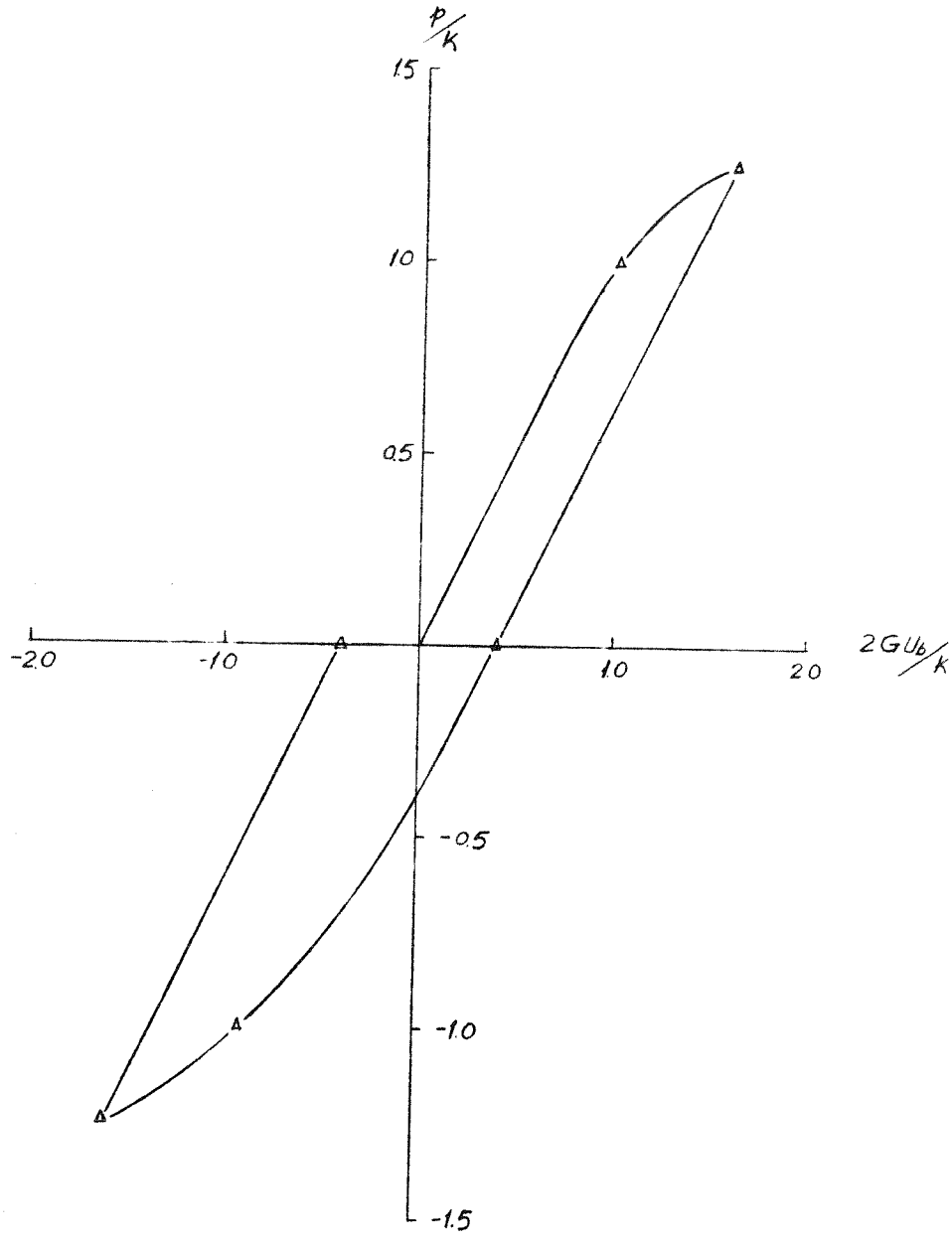

Loading Path p/k = 0.0 → 1.0 → 1.25 → 0.0 → -1.0 → -1.25 → 0.0

Q4I4 Element, 2 x 2 Integration Order
Tresca Yield Criterion
N-R Iteration Within Each Load Increment

FIG 7-6 RADIAL DISPLACEMENT OF THICK CYLINDER WITH LOAD REVERSAL

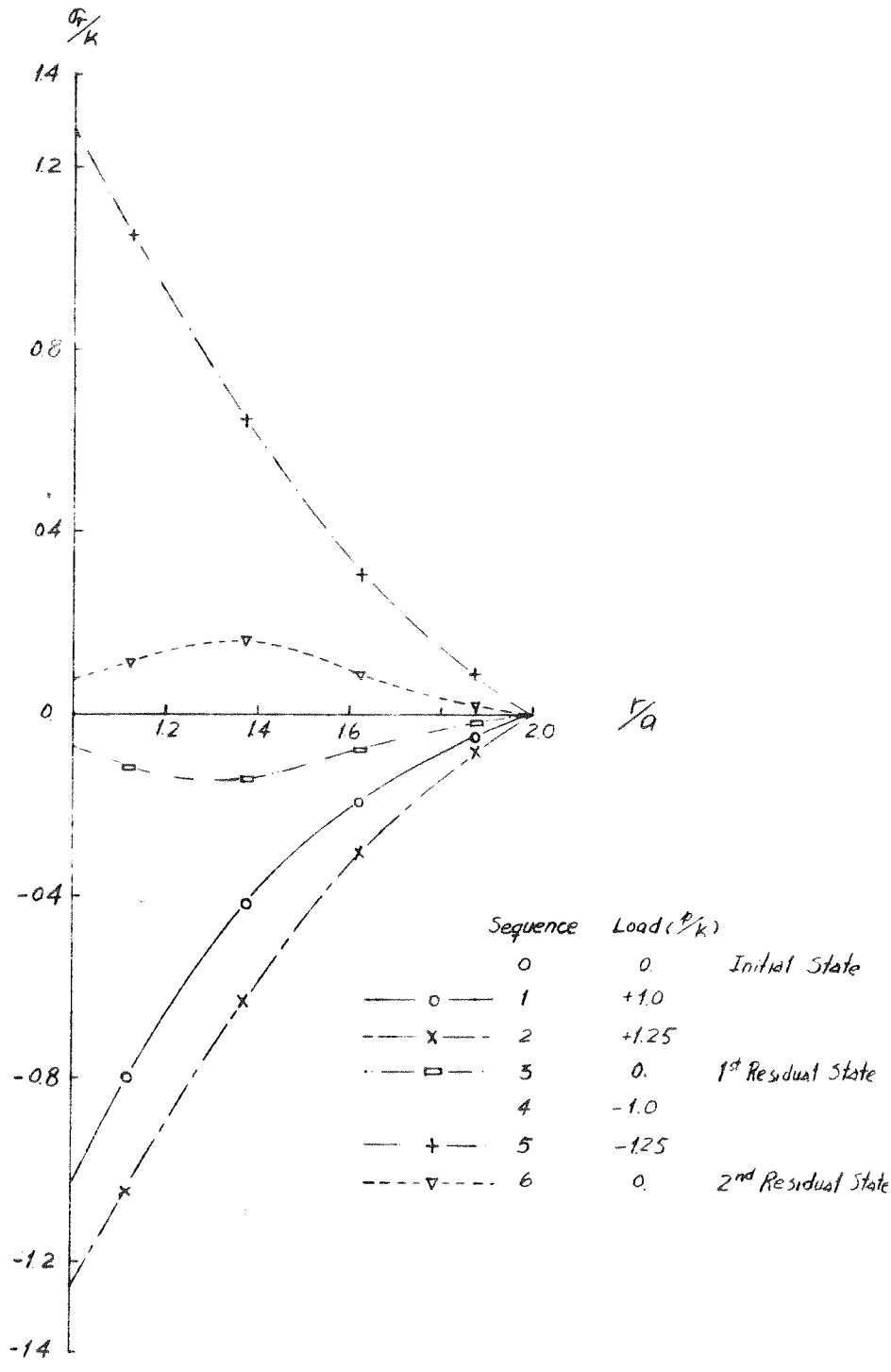

(a) Radial Stress

FIG 7-7 STRESSES IN THICK CYLINDER WITH LOAD REVERSAL

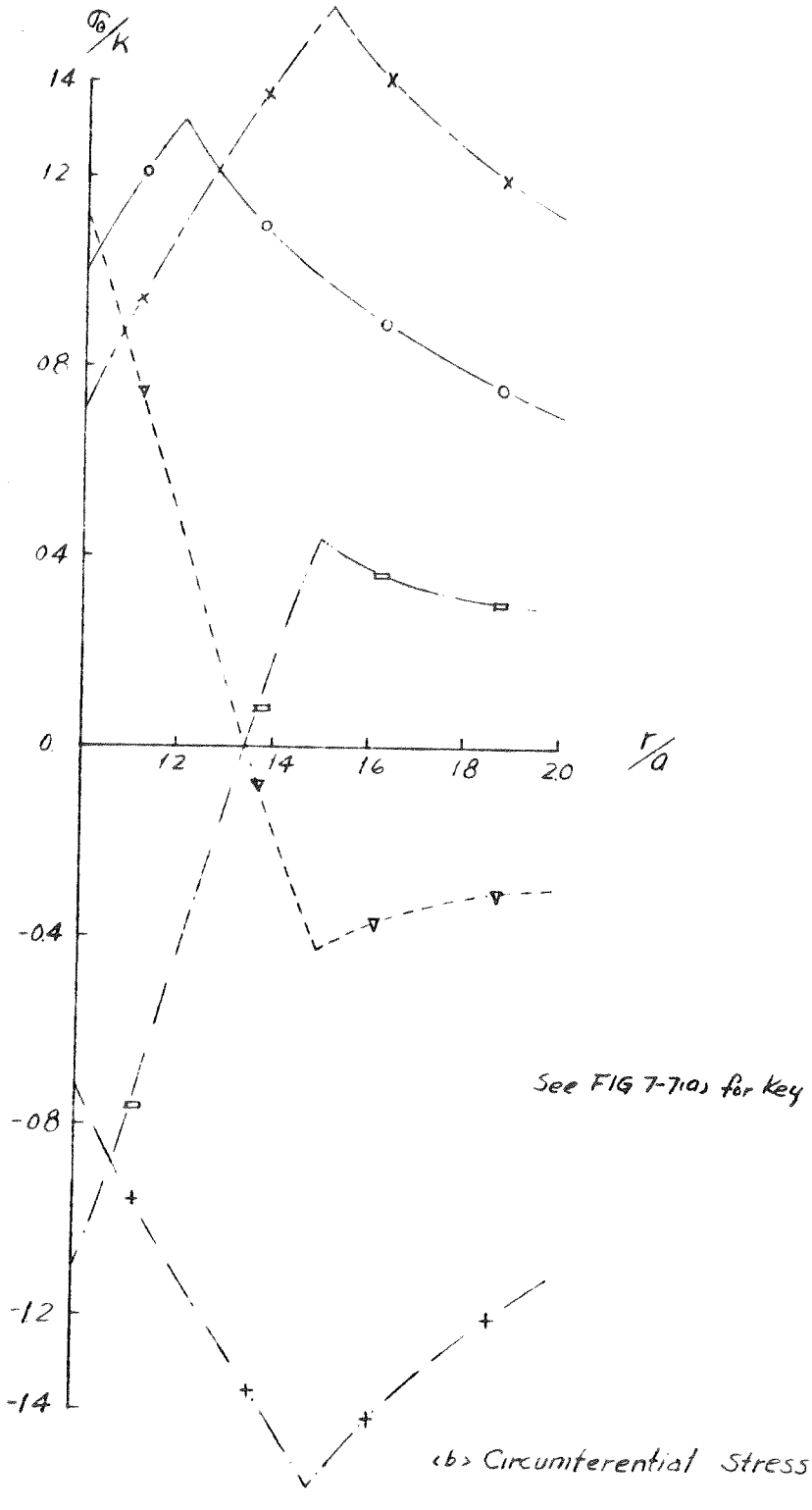

FIG 7-7 STRESSES IN THICK CYLINDER WITH LOAD REVERSAL

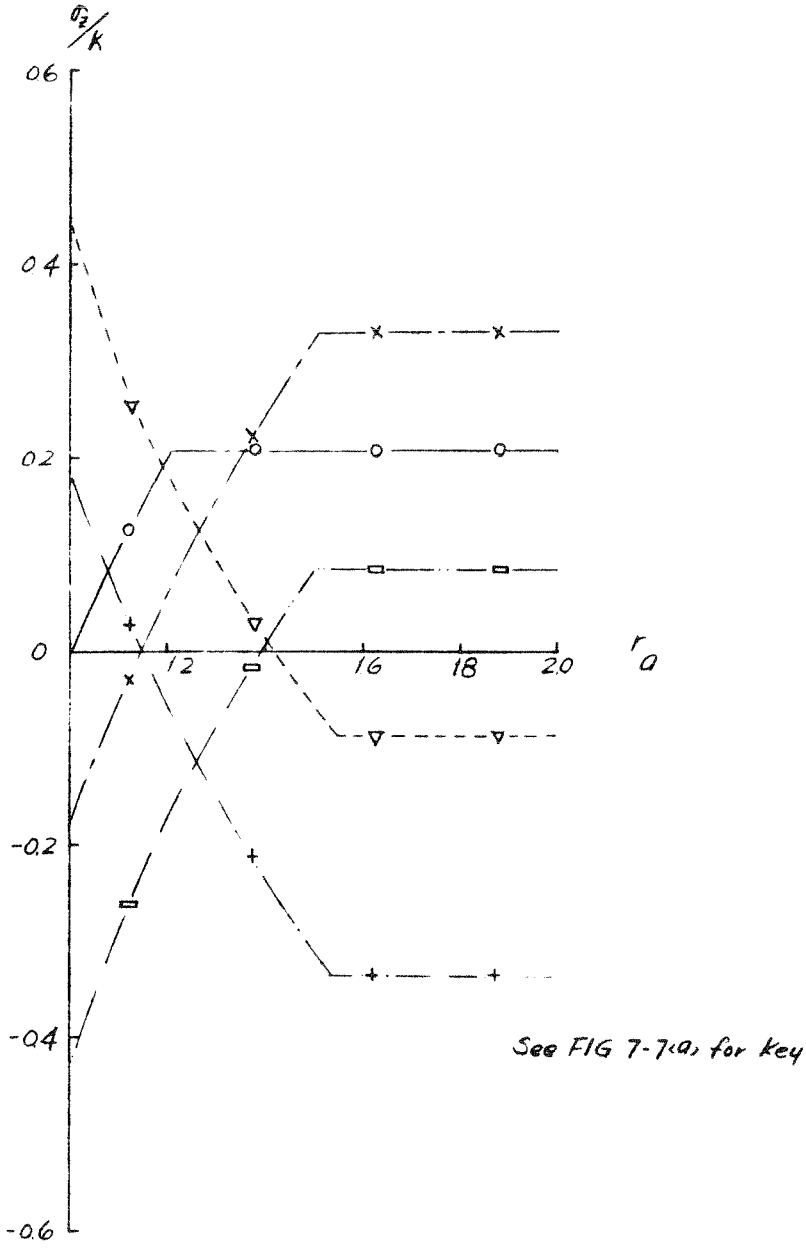

(c) Axial Stress

FIG 7-7 STRESSES IN THICK CYLINDER WITH LOAD REVERSAL

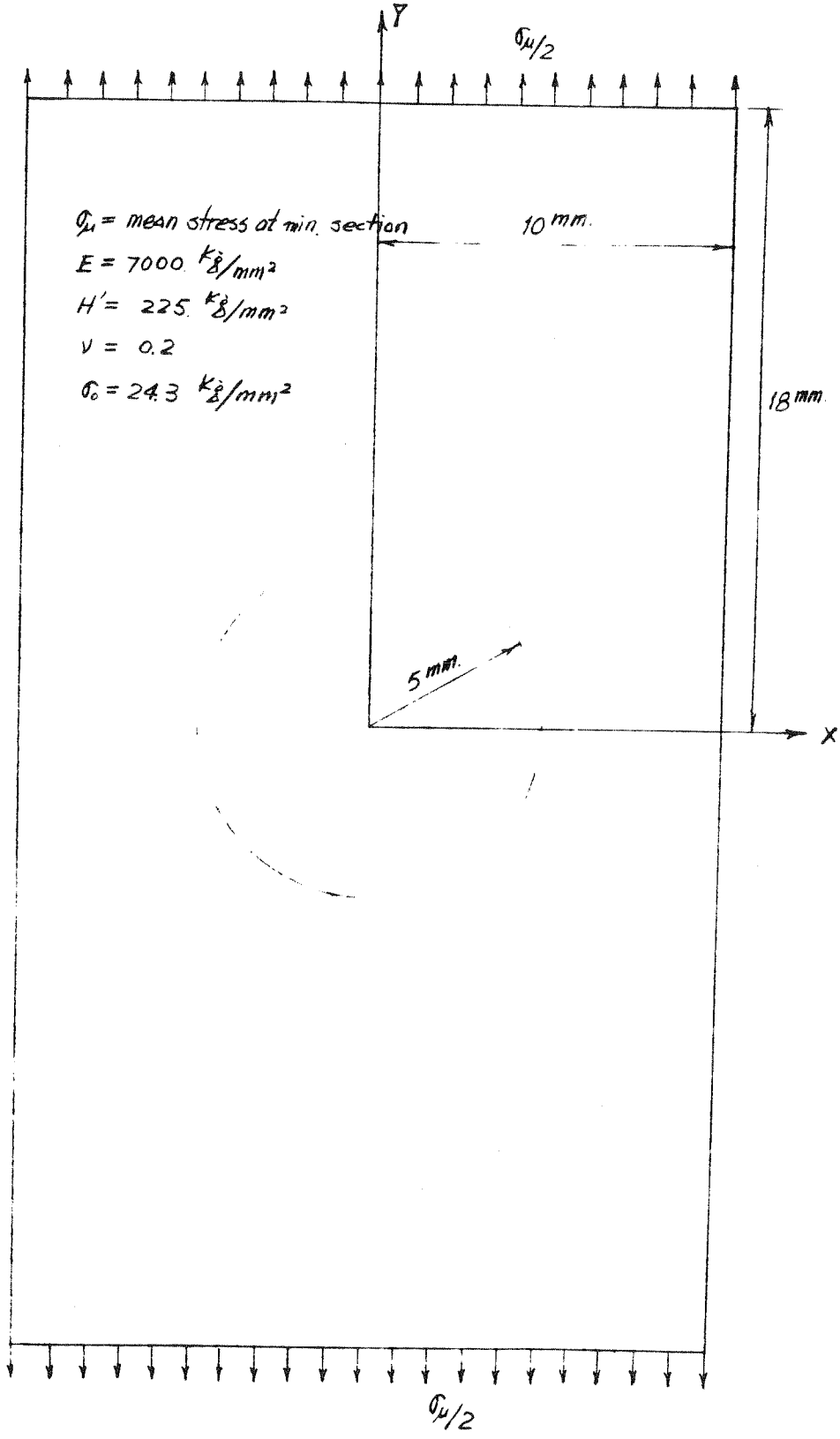

FIG 7-8 PERFORATED TENSION STRIP

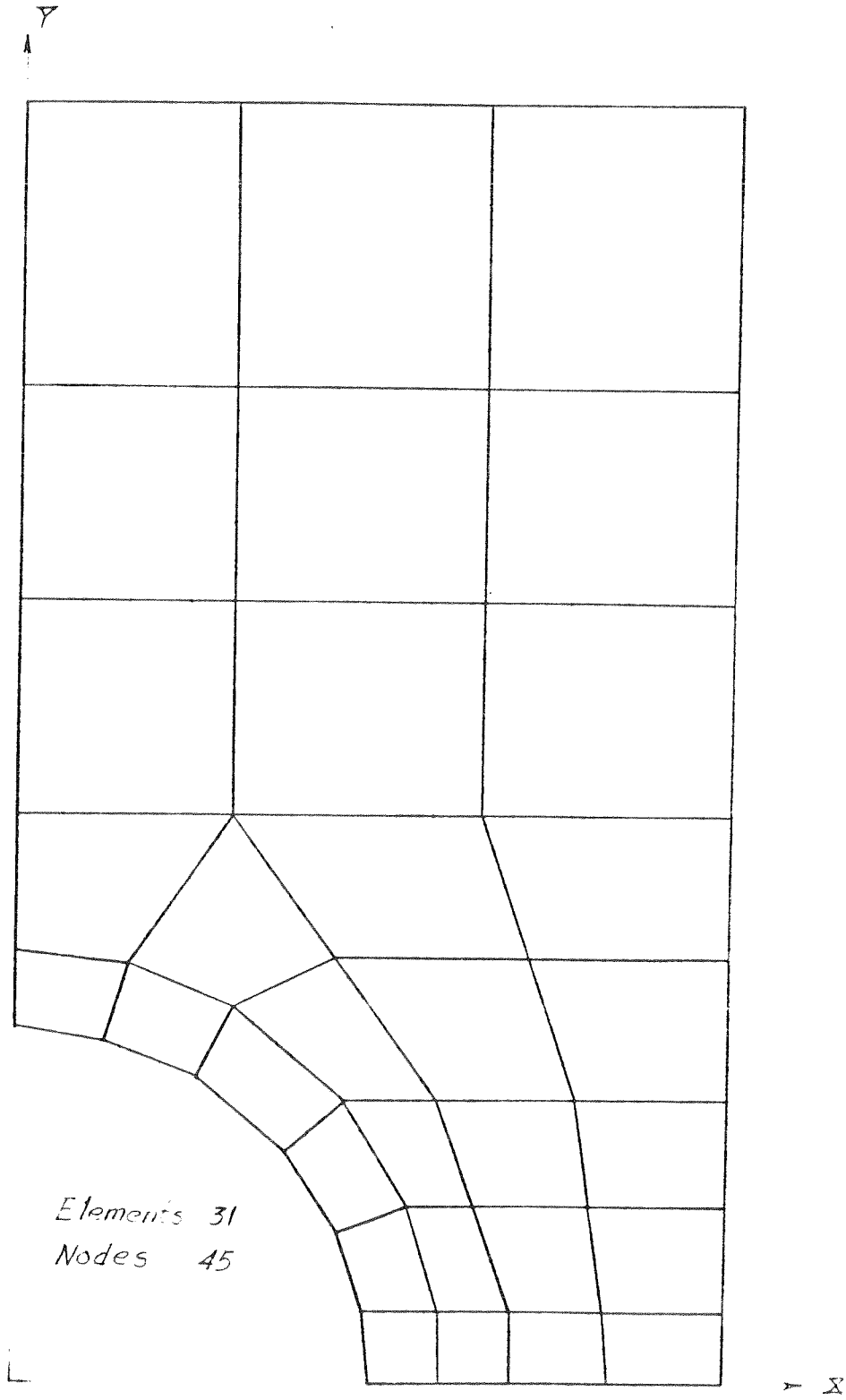

FIG 7-9 COARSE MESH

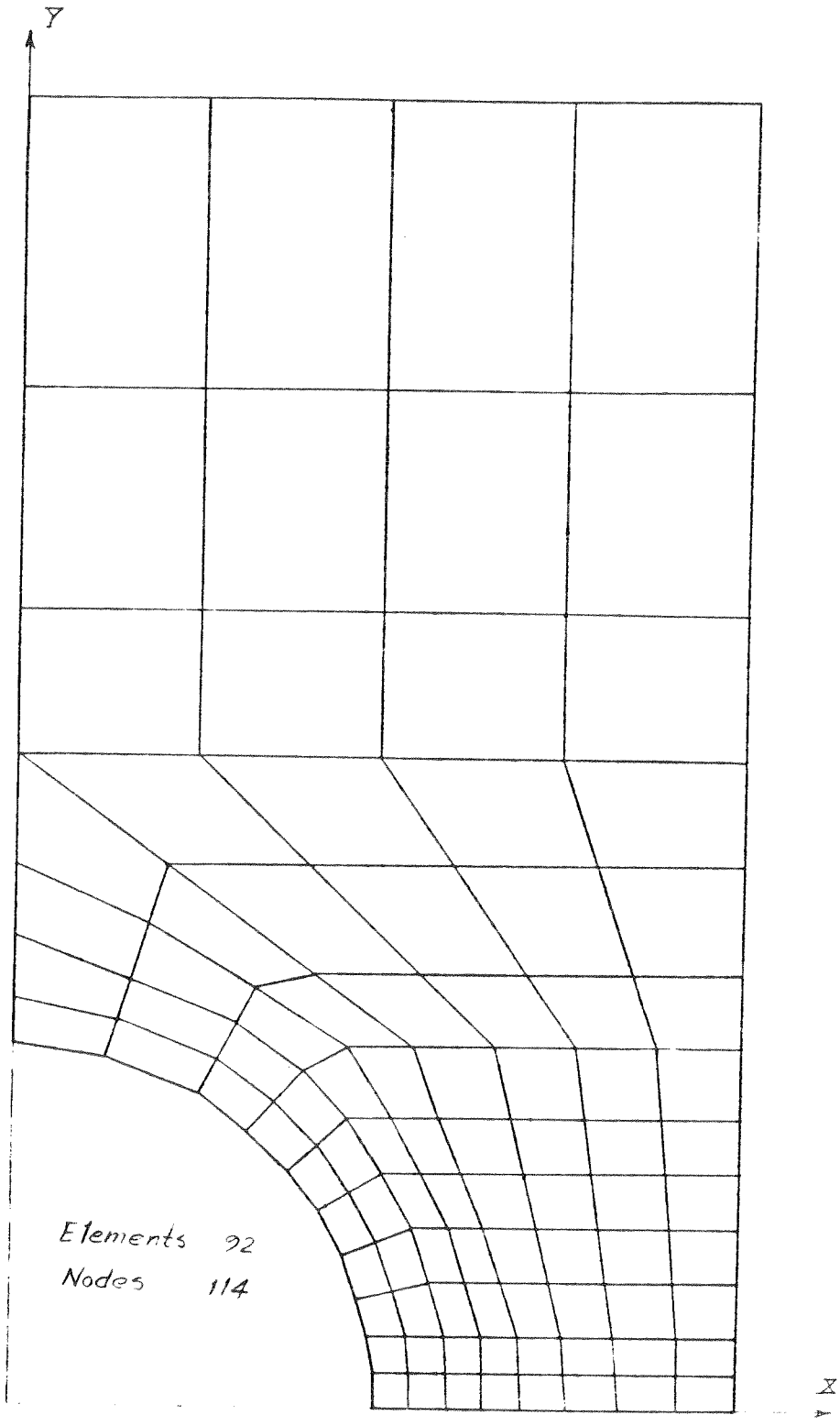

FIG 7-10 FINE MESH

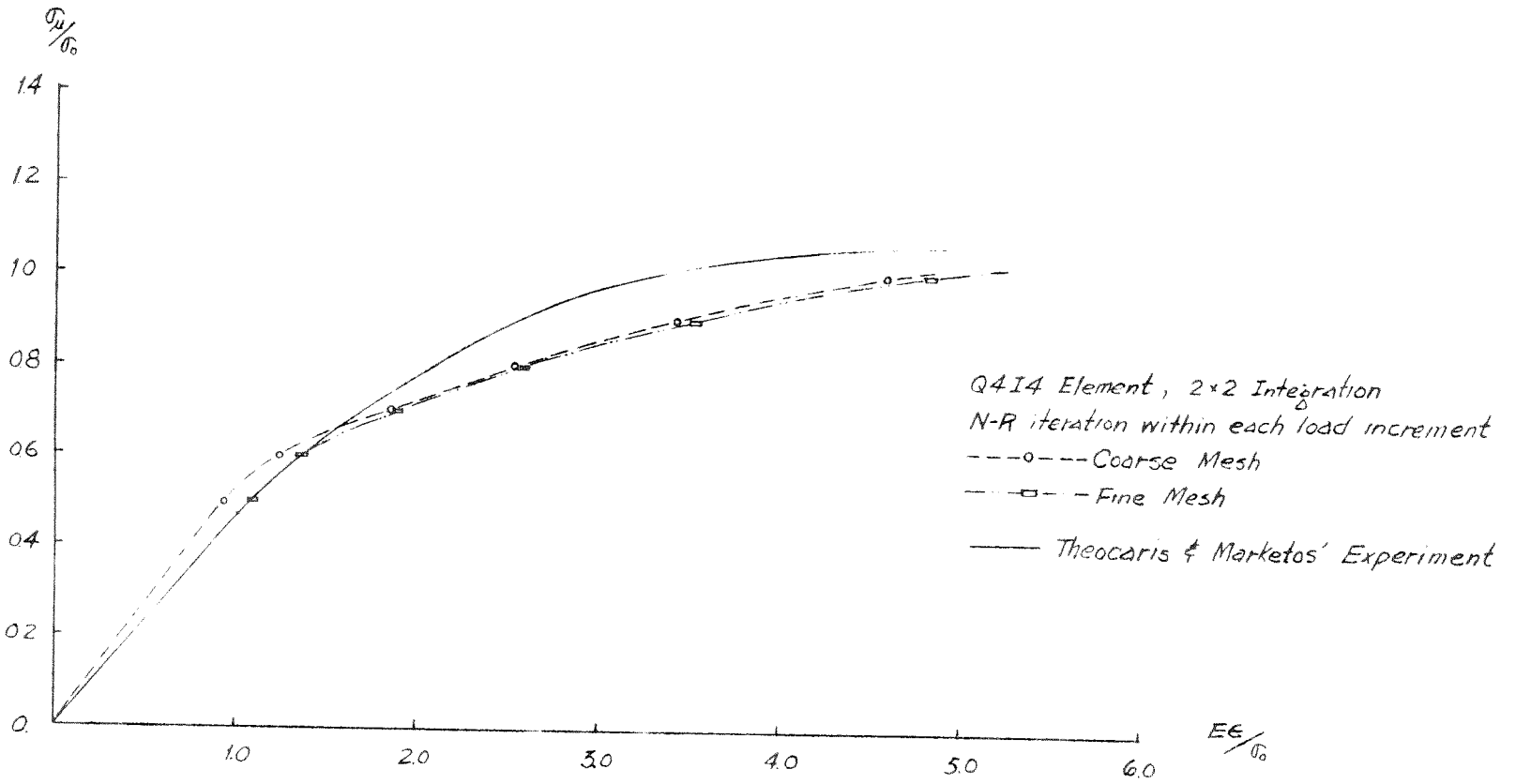

FIG 7-11 STRAIN AT POINT OF FIRST YIELD

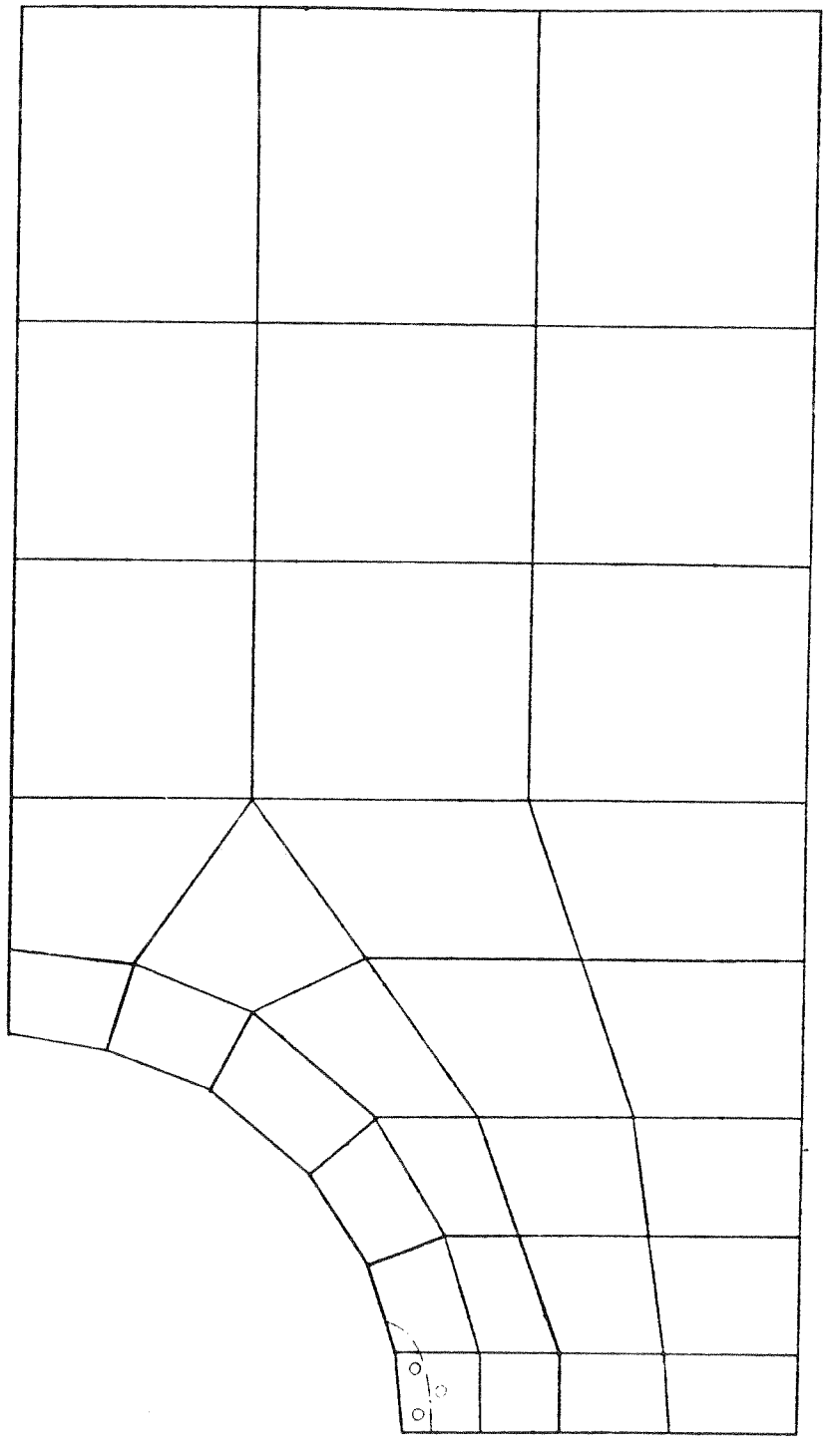

—·—·— Theocaris & Marketos' Experiment @ $\sigma_y/\sigma_0 = 0.54$

o Yielded Integration Point @ $\sigma_y/\sigma_0 = 0.60$

FIG 7-12(a) SPREAD OF PLASTIC ZONE, COARSE MESH

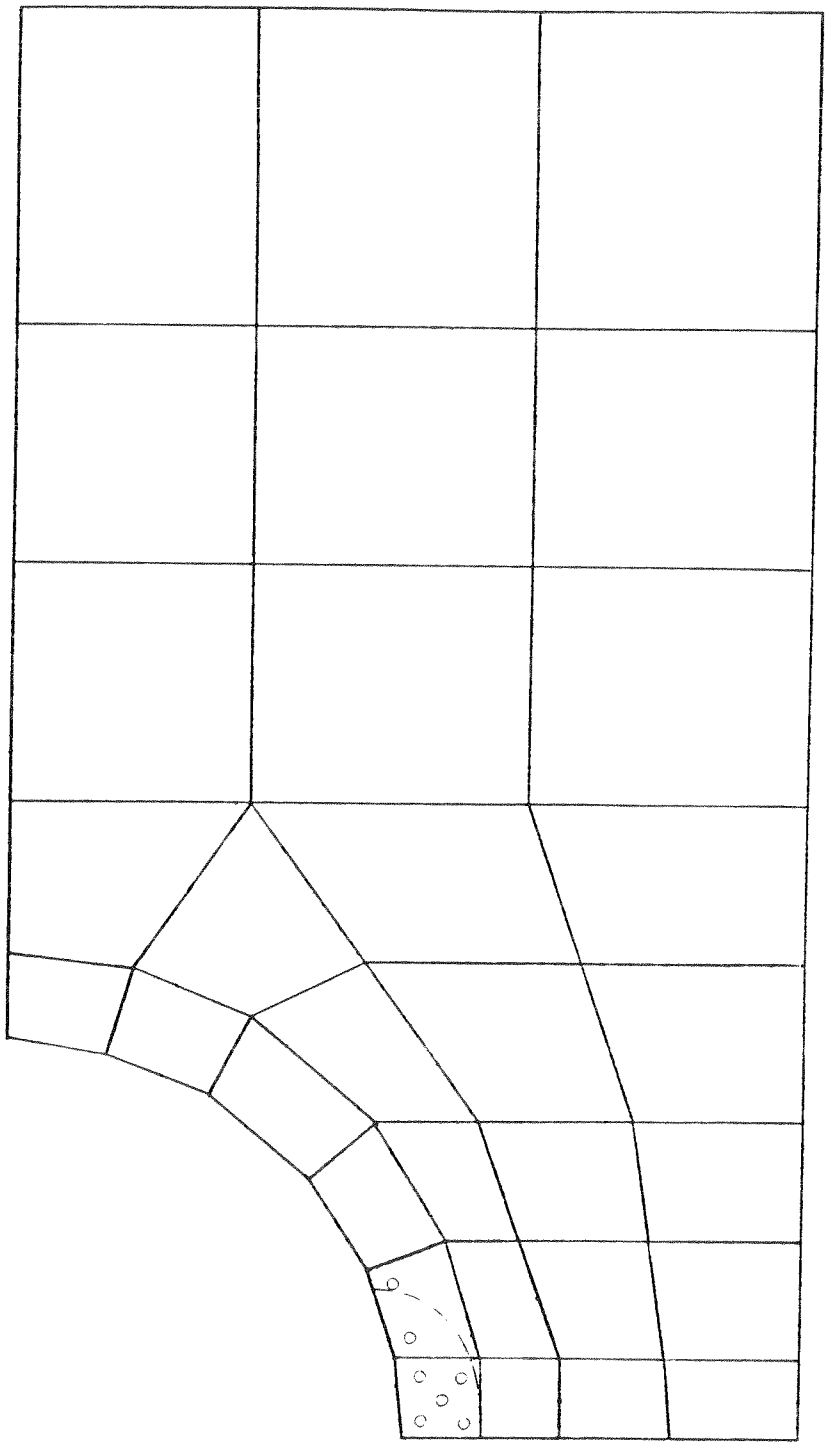

——— Theocaris & Marketos' Experiment @ $P_u/P_o = 0.665$

o Yielded Integration Point @ $P_u/P_o = 0.7$

FIG 7-12(6) SPREAD OF PLASTIC ZONE, COARSE MESH

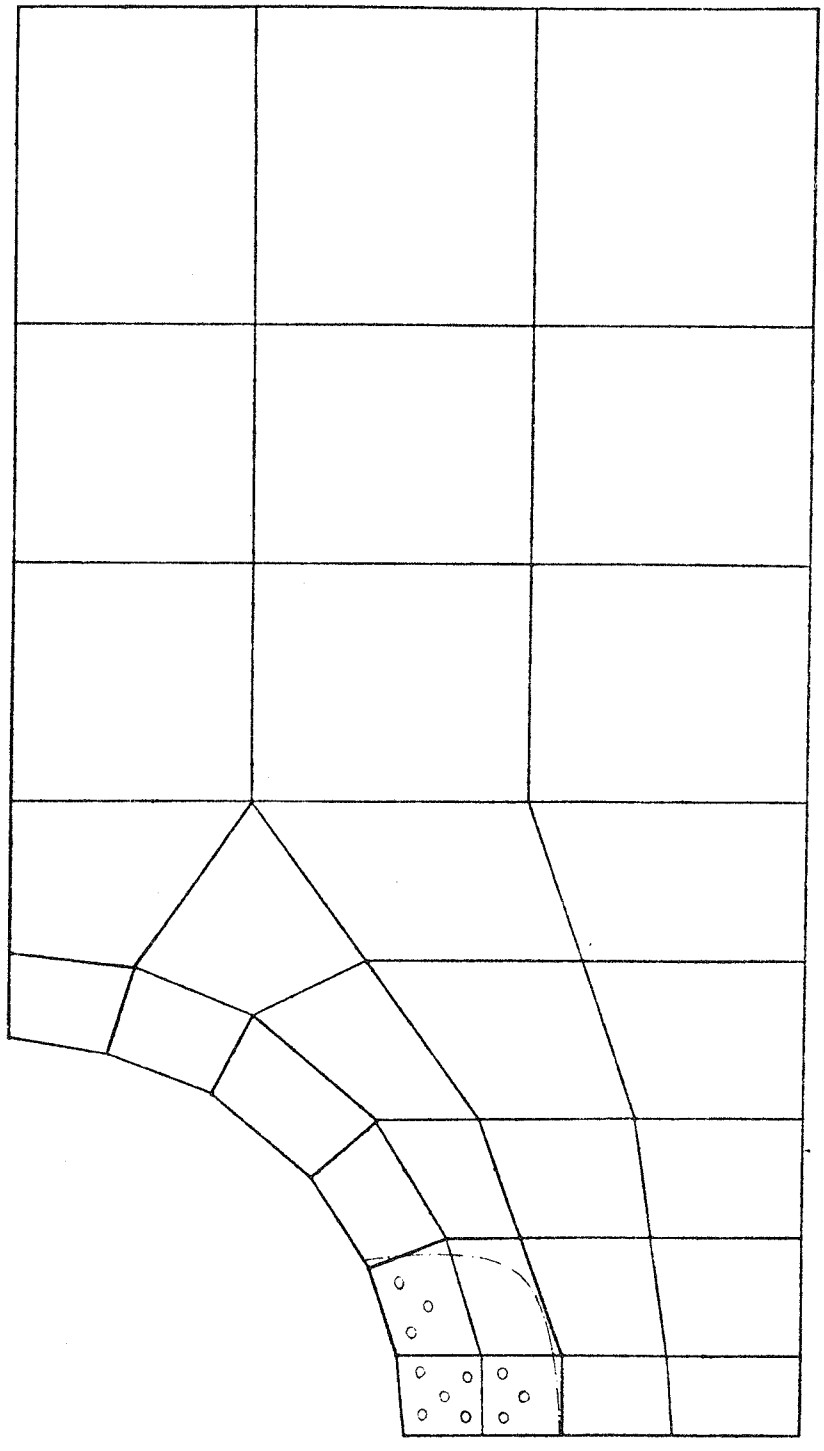

—·—·— Theocaris & Marketos' Experiment @ $\sigma_2/\sigma_0 = 0.875$

o Yielded Integration Point @ $\sigma_2/\sigma_0 = 0.80$

FIG 7-12 <c> SPREAD OF PLASTIC ZONE, COARSE MESH

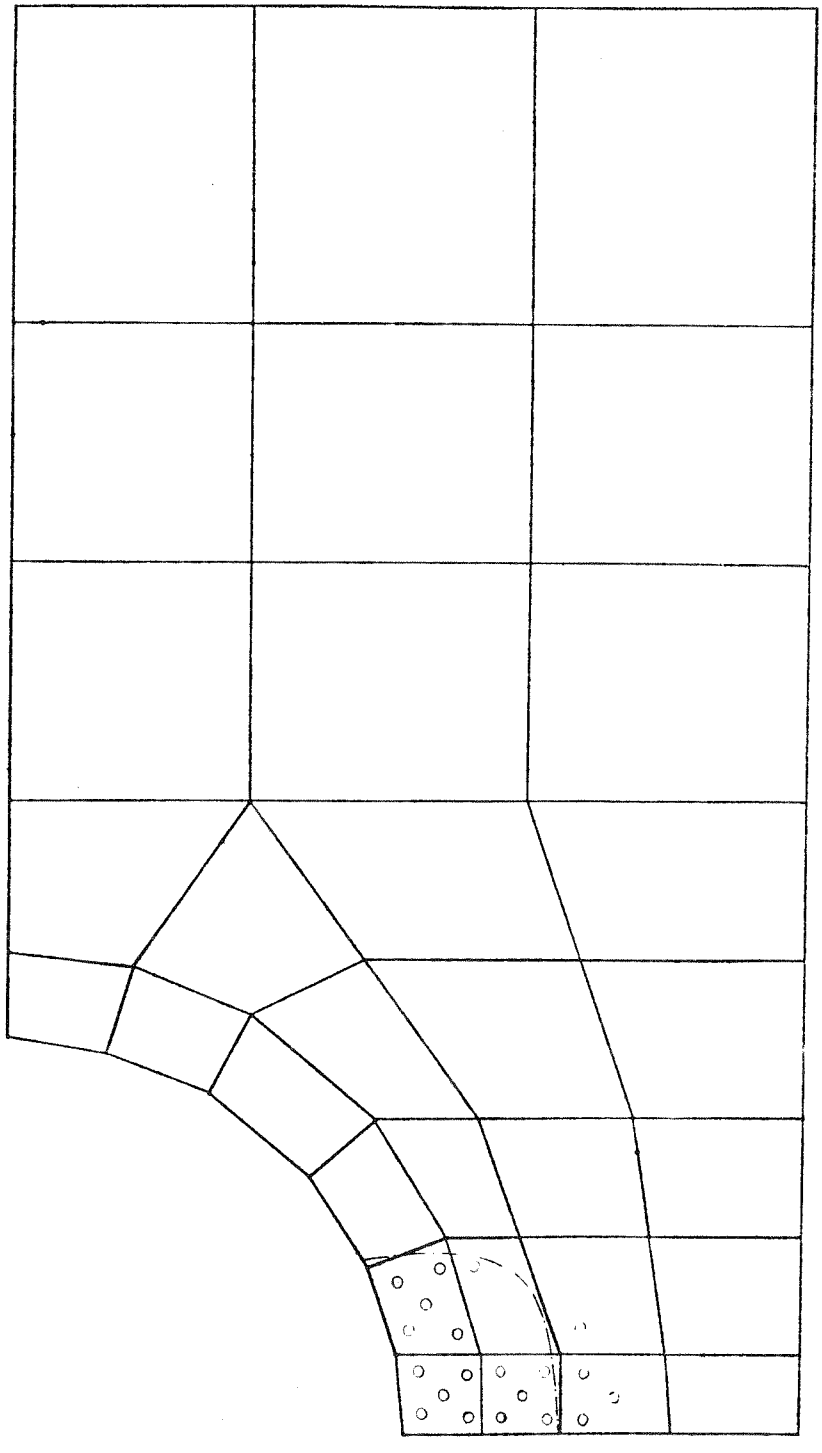

— · — · — Theocaris & Marketos' Experiment @ $\sigma_y/\sigma_0 = 0.825$

○ Yielded Integration Point @ $\sigma_y/\sigma_0 = 0.90$

FIG 7-12 <d> SPREAD OF PLASTIC ZONE, COARSE MESH

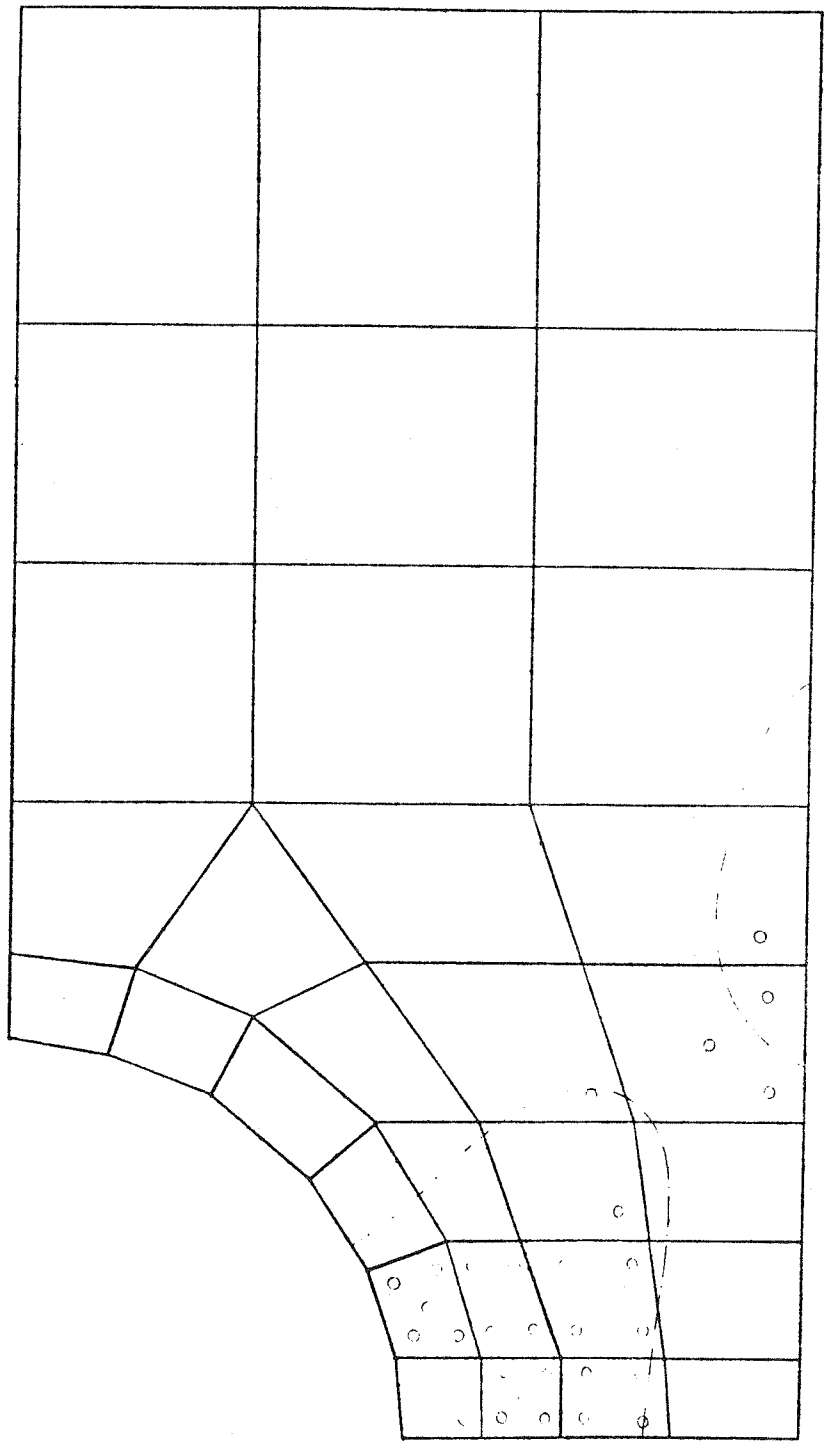

—·—·— Theocaris & Marketos' Experiment @ $P_u/\sigma_0 = 0.145$

o Yielded Integration Point @ $P_u/\sigma_0 = 1.0$

FIG 7-12(e) SPREAD OF PLASTIC ZONE, COARSE MESH

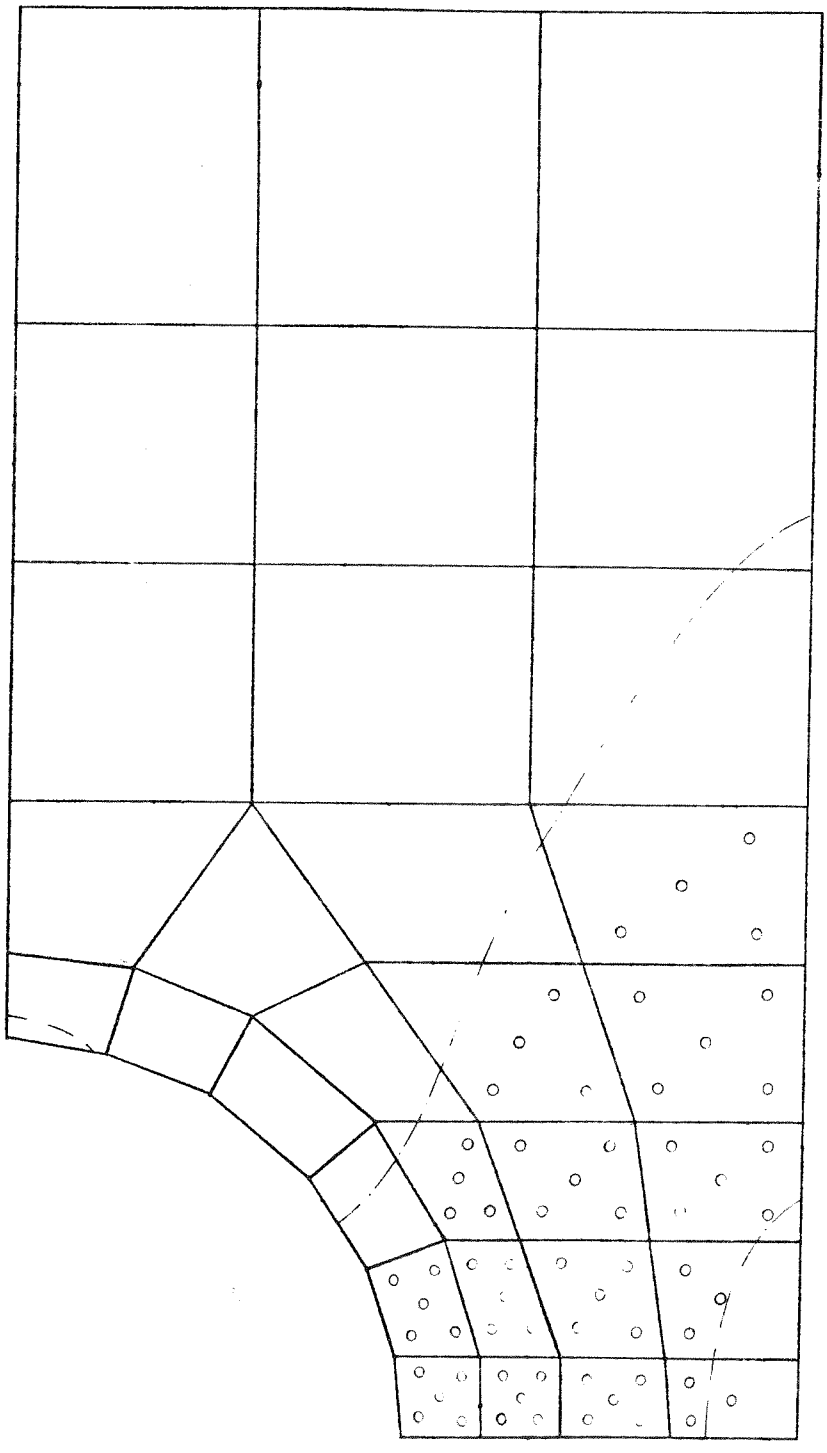

—·—·— Theocaris & Marketos' Experiment @ $\sigma_y/\sigma_0 = 1.07$

o Yielded Integration Point @ $\sigma_y/\sigma_0 = 1.10$

FIG 7-12<f> SPREAD OF PLASTIC ZONE, COARSE MESH

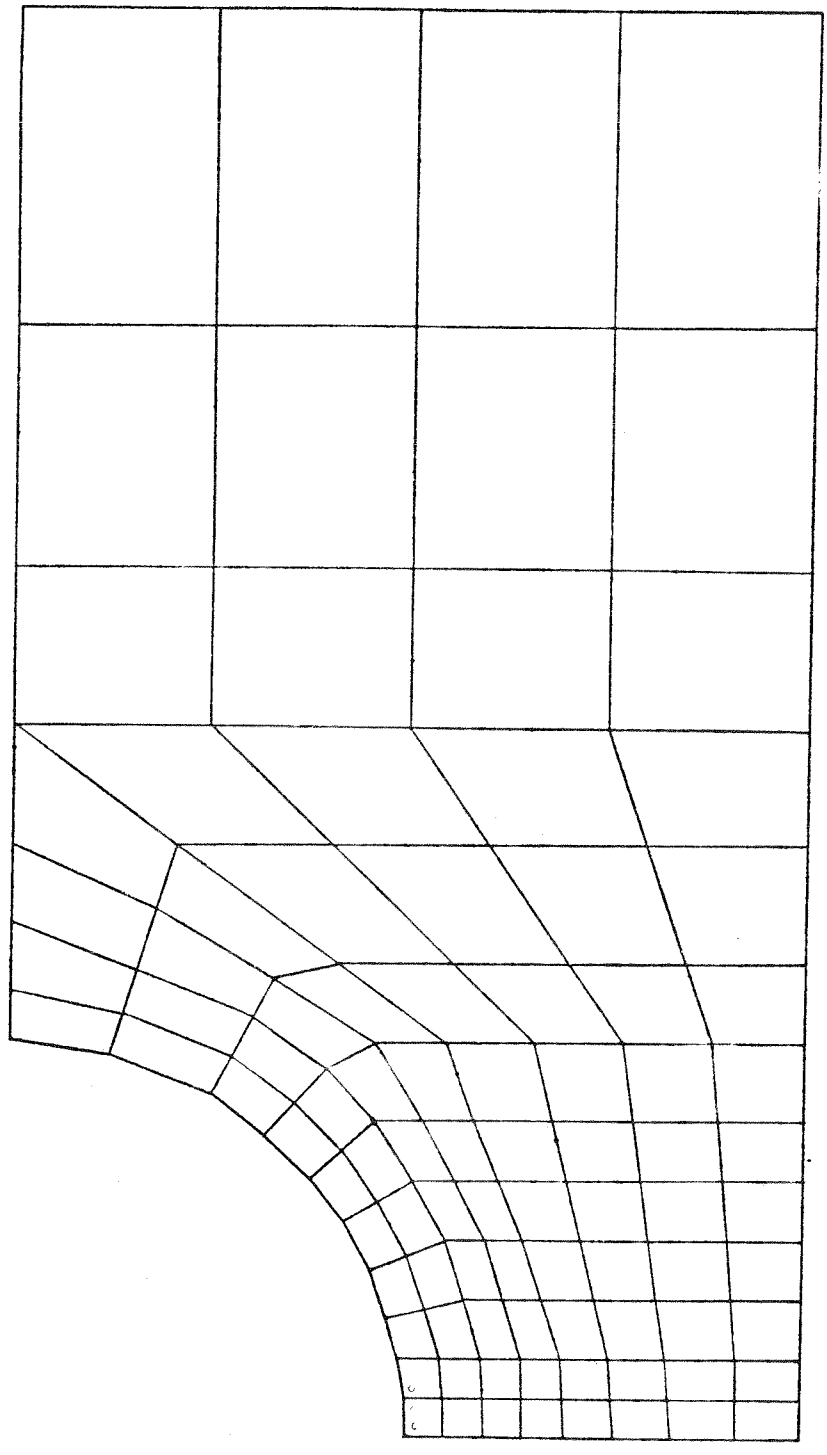

(1st Yield Occured) Theocaris & Marketos' Experiment @ $\sigma_y/\sigma_0 = 0.46$

o Yielded Integration Point @ $\sigma_y/\sigma_0 = 0.50$

FIG 7-13<a> SPREAD OF PLASTIC ZONE, FINE MESH

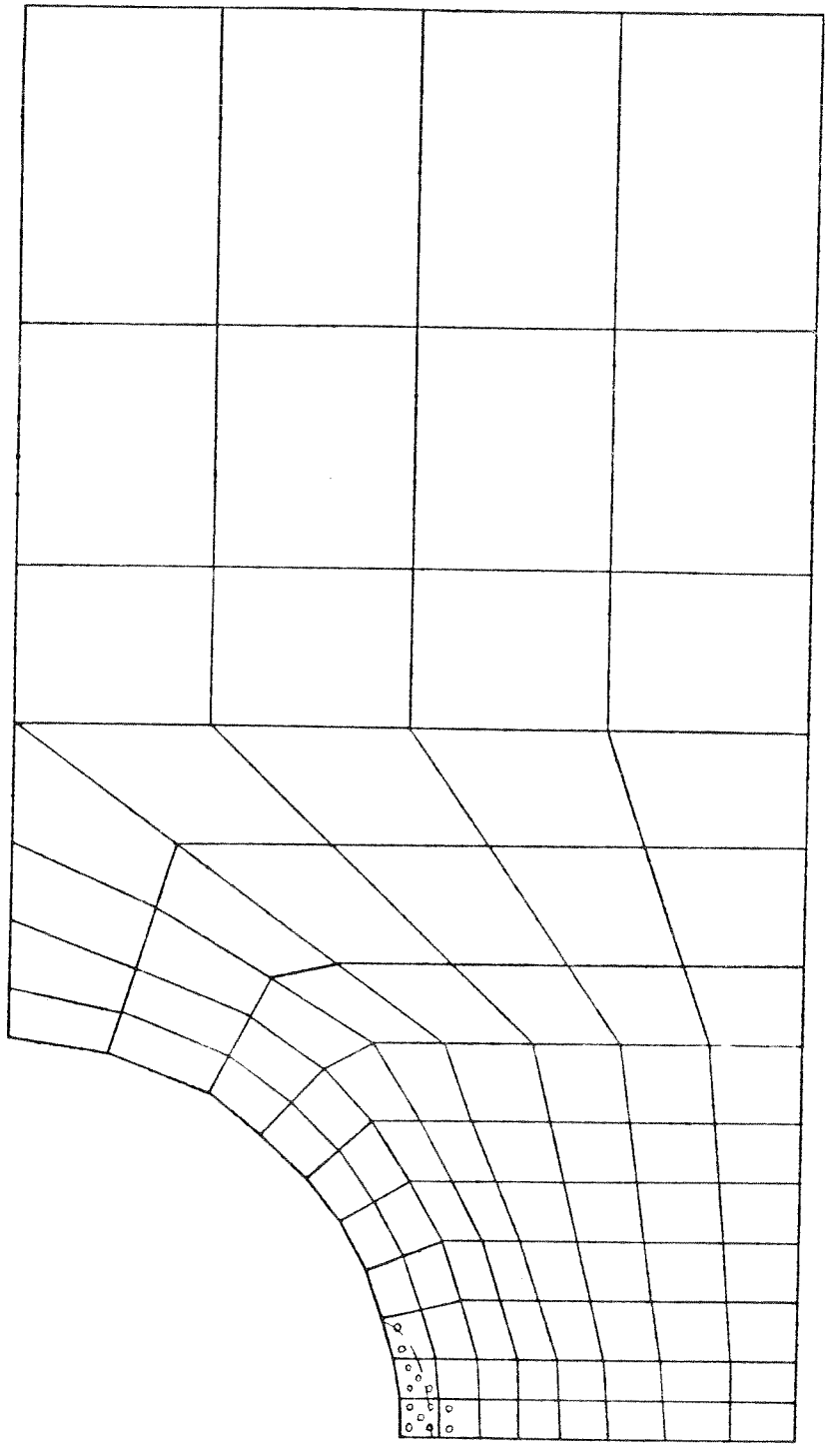

—·—·— Theocaris & Marketos' Experiment @ $\sigma_u/\sigma_o = 0.54$

o Yielded Integration Point @ $\sigma_u/\sigma_o = 0.60$

FIG 7-13<b> SPREAD OF PLASTIC ZONE. FINE MESH

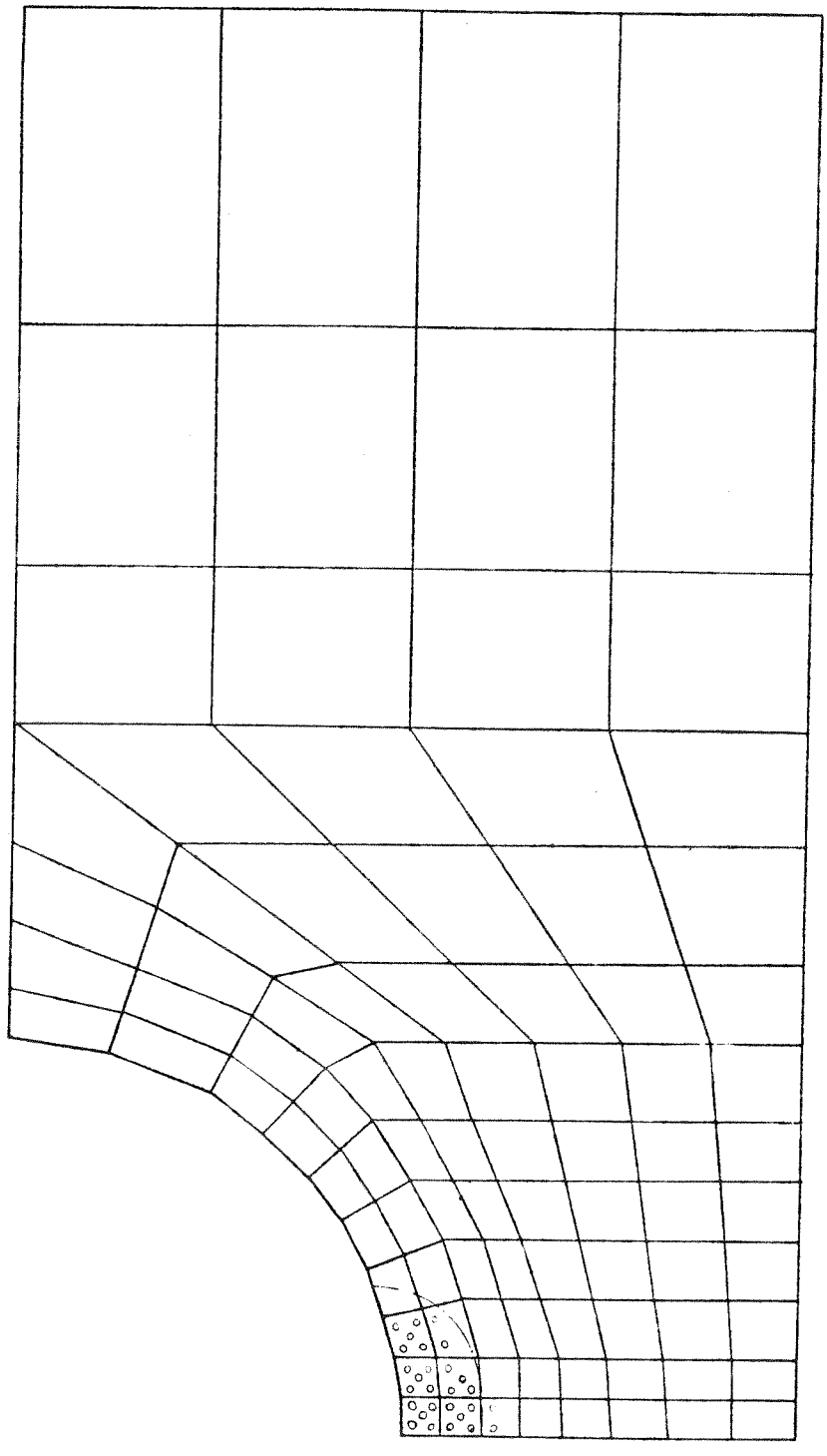

— · — · — Theocaris & Marketos' Experiment @ $\sigma_u/\sigma_o = 0.665$

o Yielded Integration Point @ $\sigma_u/\sigma_o = 0.7$

FIG 7-13<c> SPREAD OF PLASTIC ZONE, FINE MESH

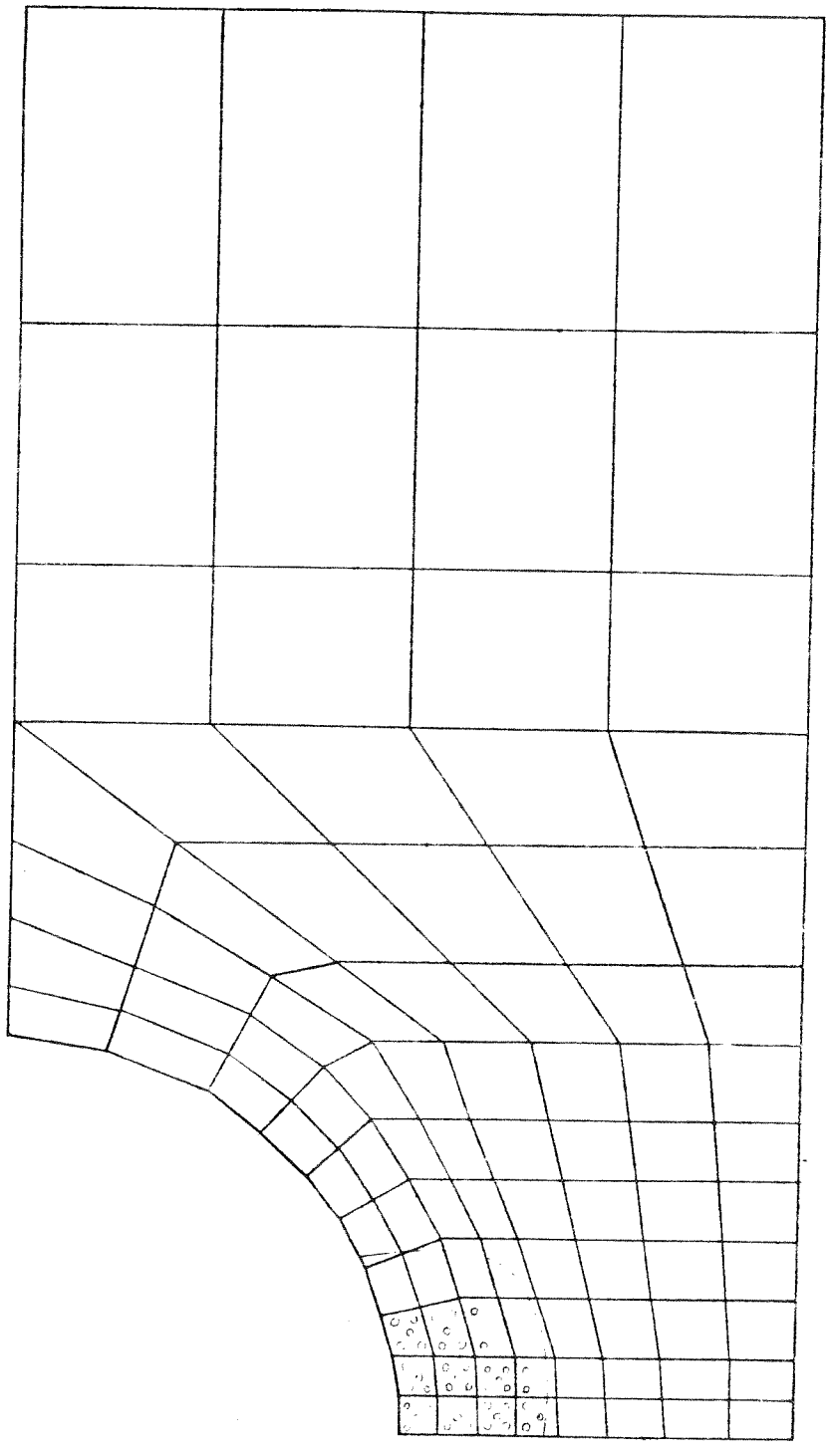

—·—·— Theocaris & Marketos' Experiment @ $\sigma_2/\sigma_0 = 0.8$

o Yielded Integration Point @ $\sigma_2/\sigma_0 = 0.8$

FIG 7-13(d) SPREAD OF PLASTIC ZONE, FINE MESH

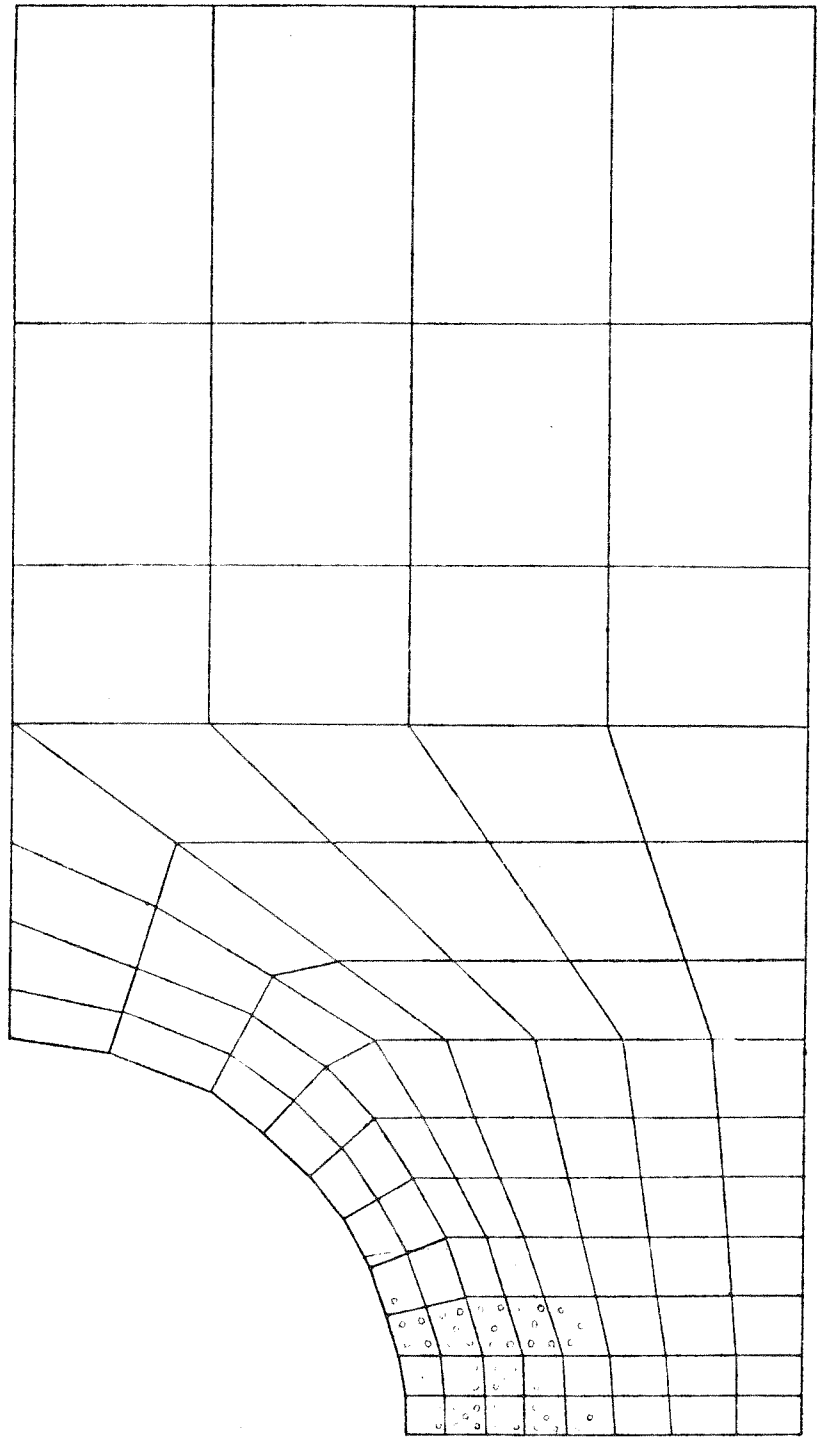

— — — Theocaris & Marketos' Experiment @ σ_u/σ_o = 0.82

o Yielded Integration Point @ σ_u/σ_o = 0.81

FIG 7-13(e) SPREAD OF PLASTIC ZONE, FINE MESH

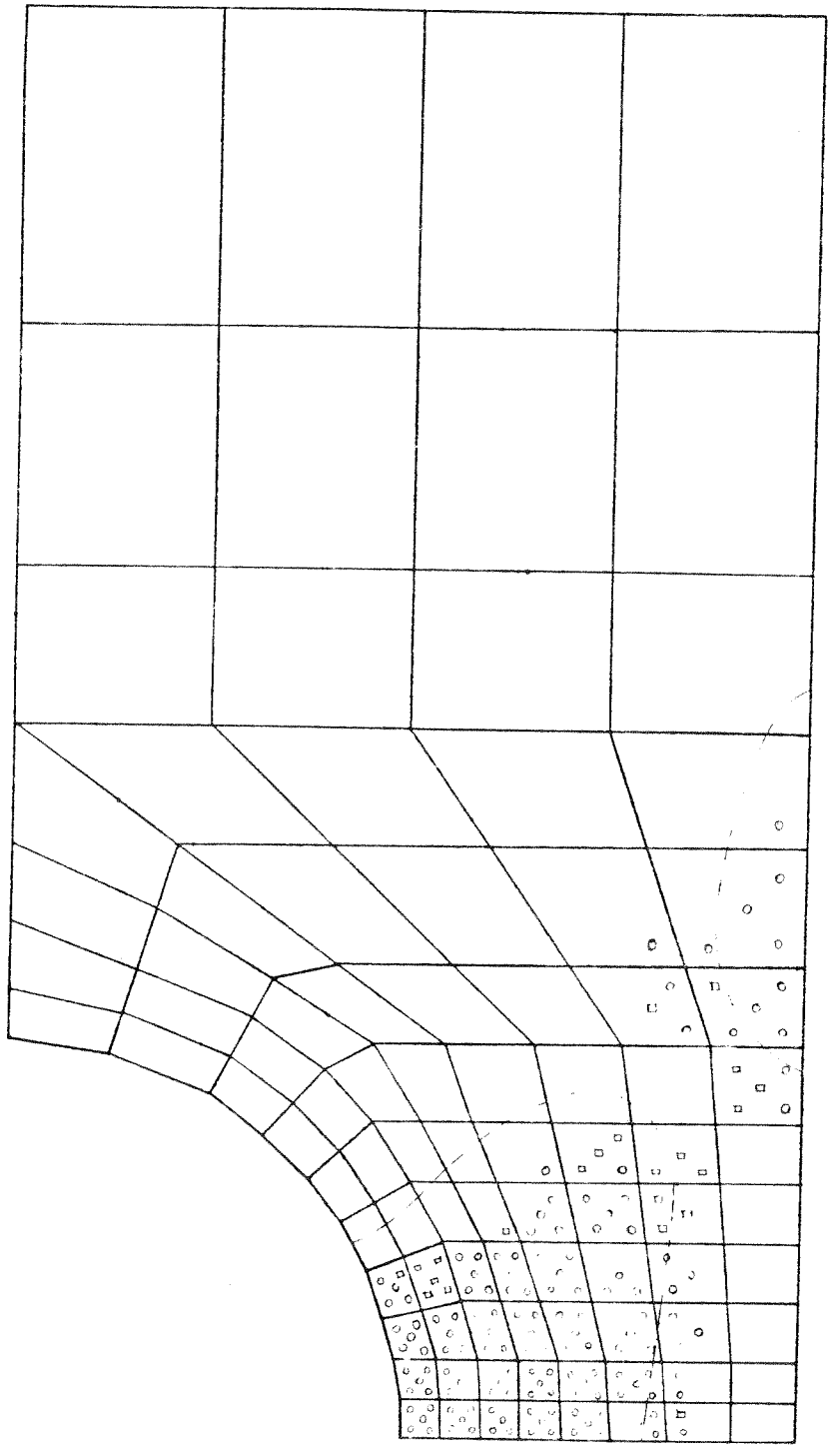

—·—·— Theocaris & Marketos' Experiment @ $\frac{\sigma_2}{\sigma_0} = .994$

o Yielded Integration Point @ $\frac{\sigma_2}{\sigma_0} = 1.00$

□ Within 5% of Yield Limit

FIG 7-13<f> SPREAD OF PLASTIC ZONE, FINE MESH

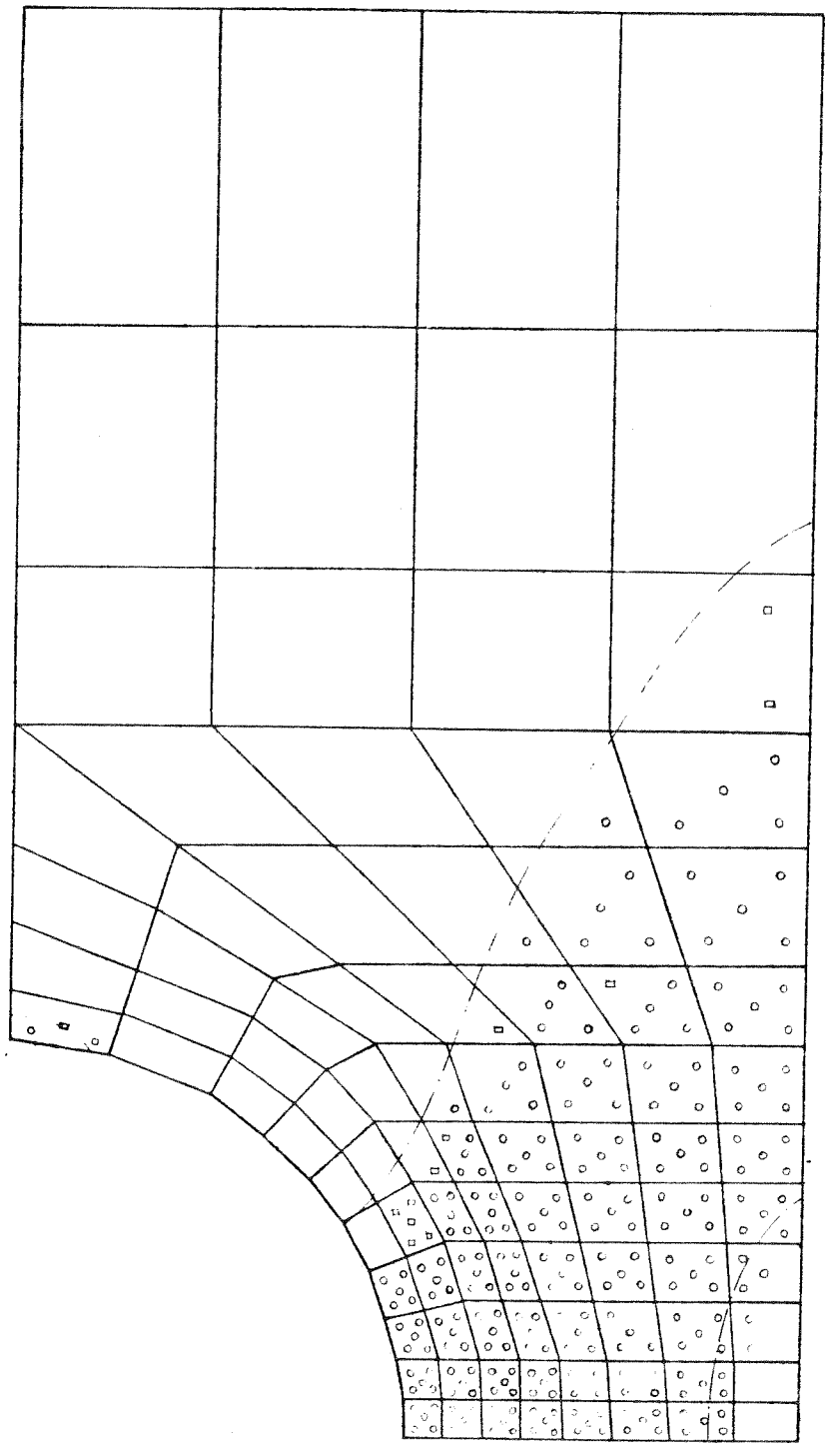

— · — · — Theocaris & Marketos' Experiment @ $\sigma_u/\sigma_o = 1.07$

○ Yielded Integration Point @ $\sigma_u/\sigma_o = 1.10$

□ Within 5% of Yield Limit

FIG 7-13(a) SPREAD OF PLASTIC ZONE, FINE MESH

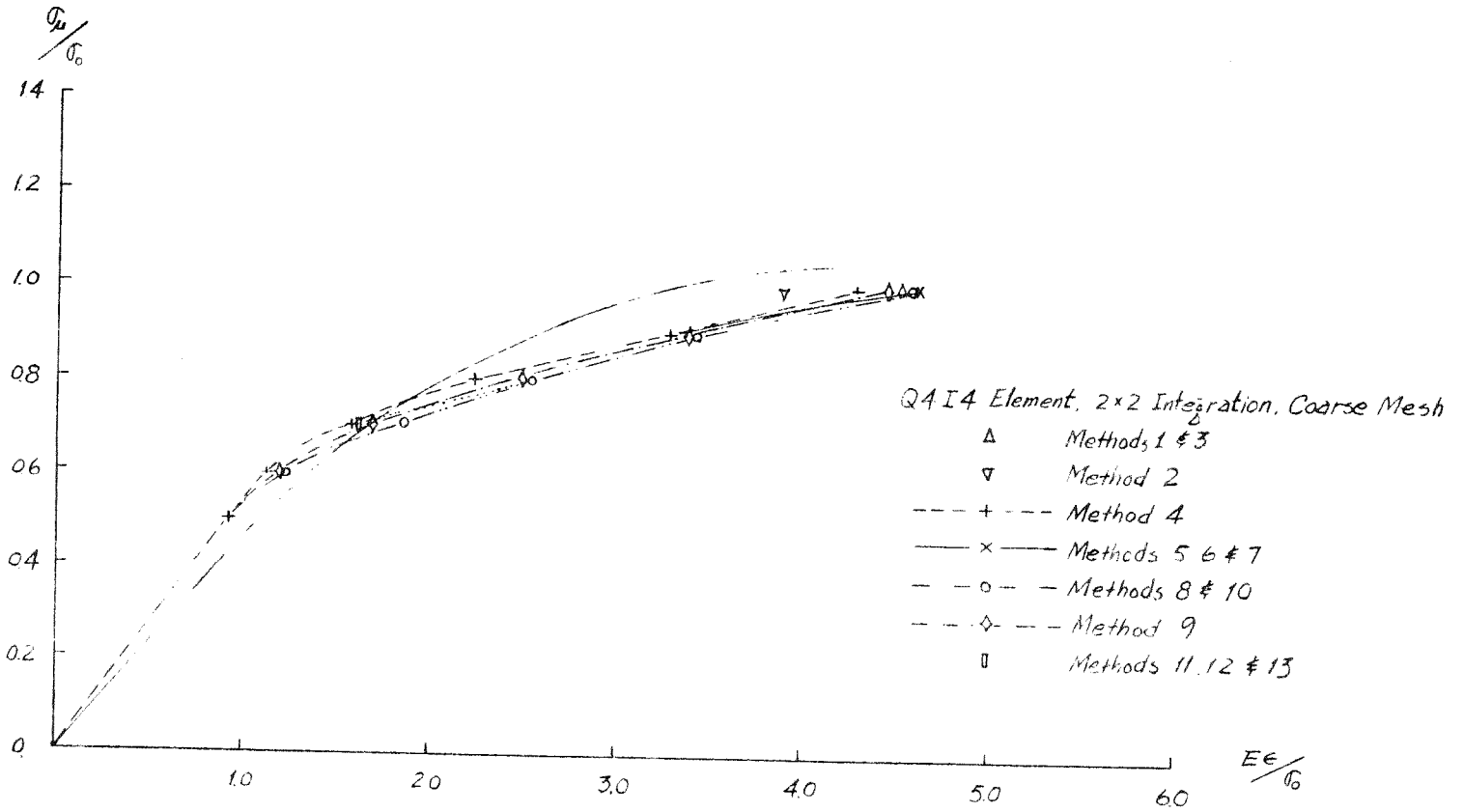

FIG 7-14 STRAIN AT POINT OF FIRST YIELD COMPARISON OF SOLUTION PROCEDURES

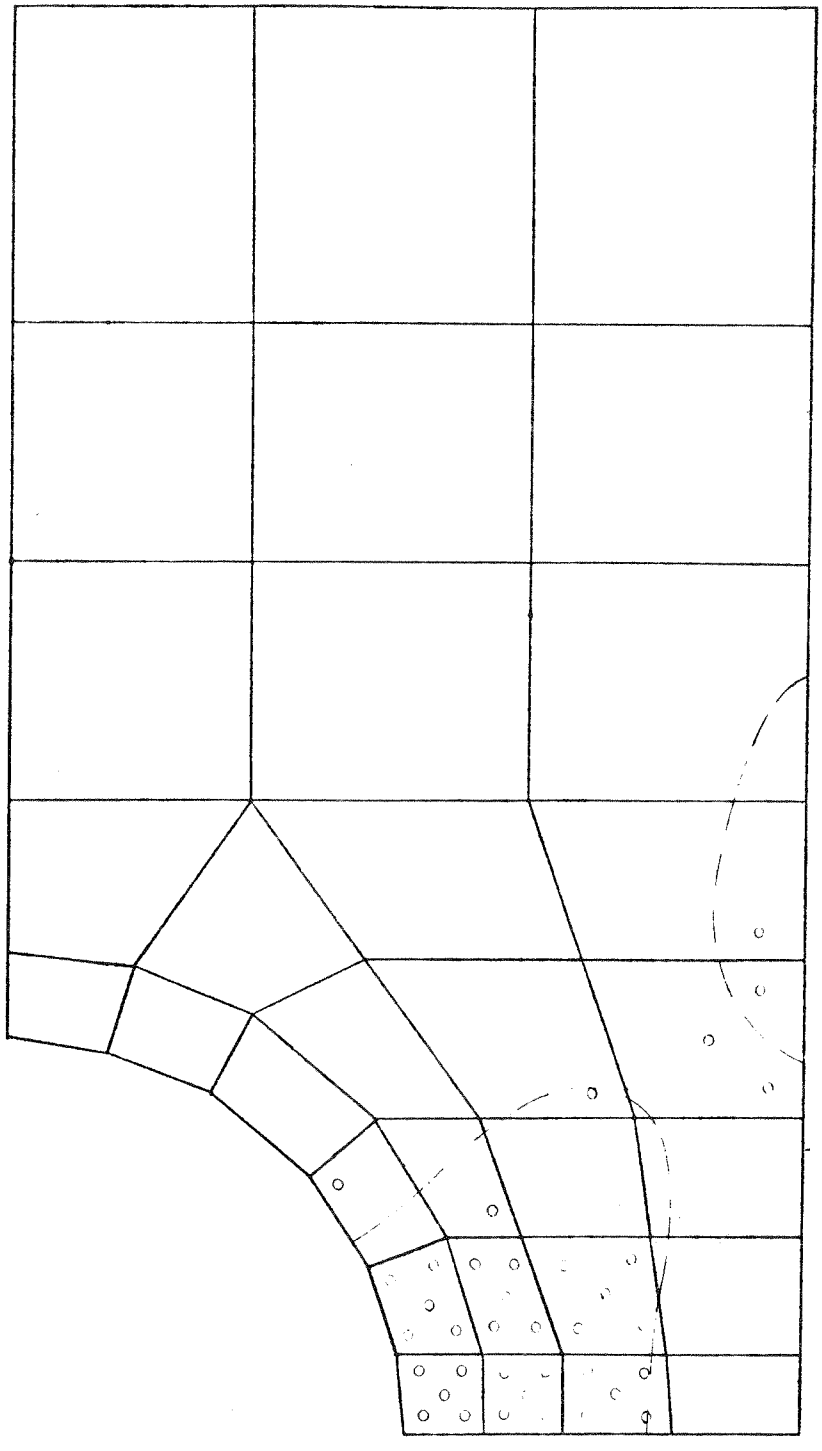

—·—·— Theocaris & Marketos' Experiment @ $\sigma_u/\sigma_o = 0.945$

o Yielded Integration Point @ $\sigma_u/\sigma_o = 1.0$

FIG 7-15(a) SPREAD OF PLASTIC ZONE, METHODS 1,2,3

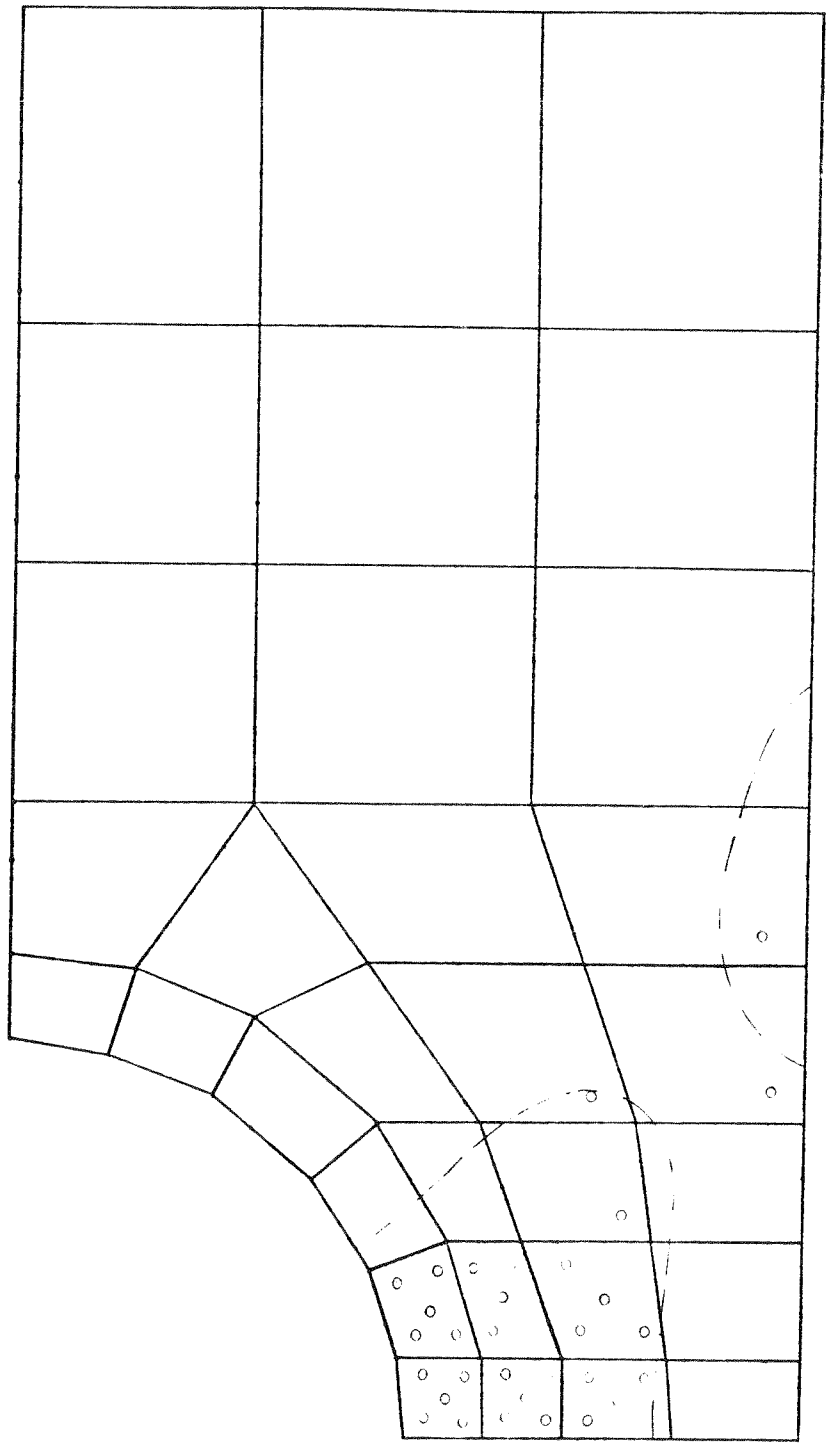

—·—·— Theocaris & Marketos' Experiment @ $P_y/\sigma_o = 0.945$

o Yielded Integration Point @ $P_y/\sigma_o = 1.0$

FIG 7-15<b> SPREAD OF PLASTIC ZONE, METHOD 4

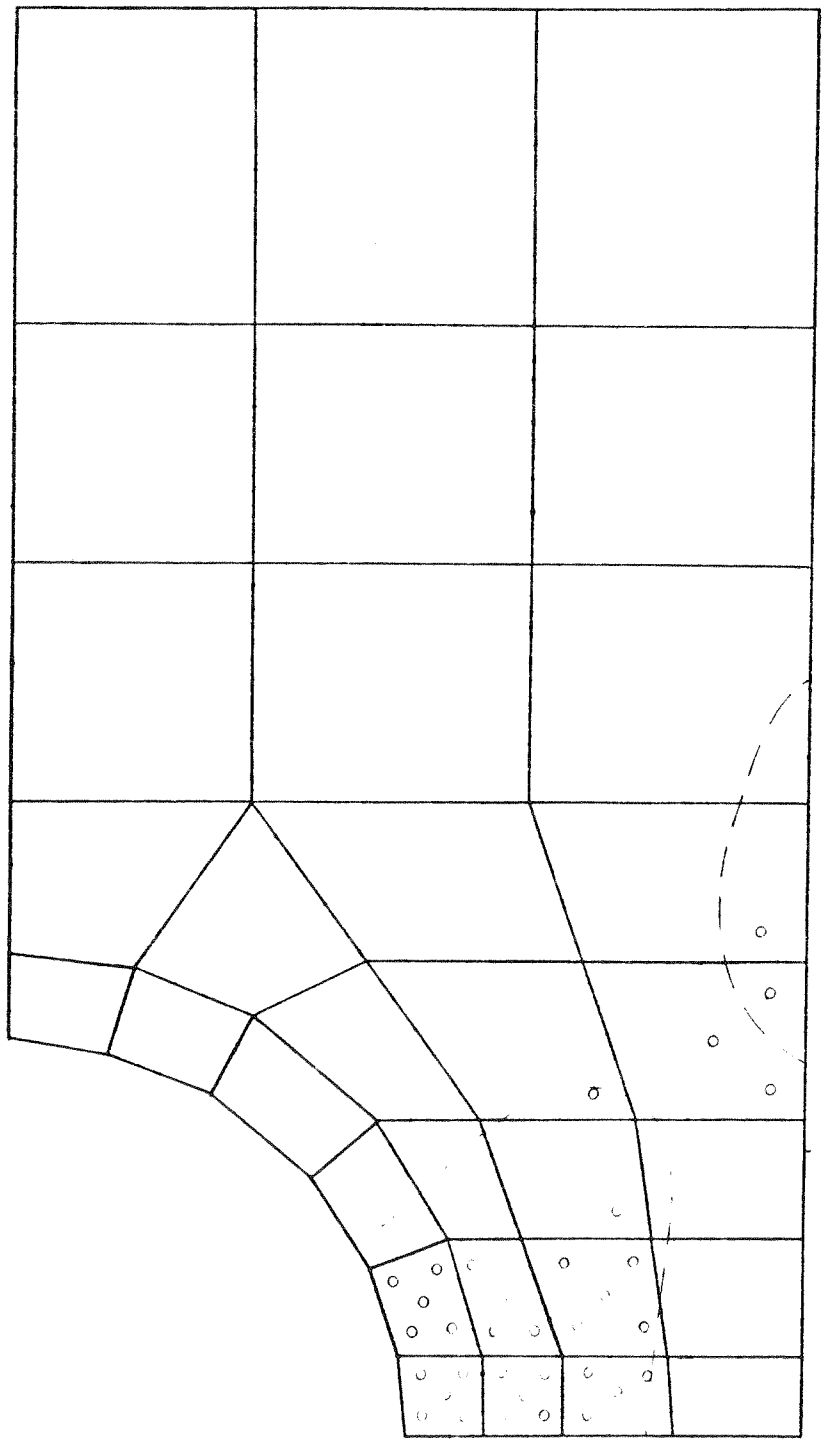

— — — — Theocaris & Marketos' Experiment @ $\sigma_y/\sigma_0 = 0.945$

o Yielded Integration Point @ $\sigma_y/\sigma_0 = 10$

FIG 7-15(c) SPREAD OF PLASTIC ZONE, METHODS 5.6.7

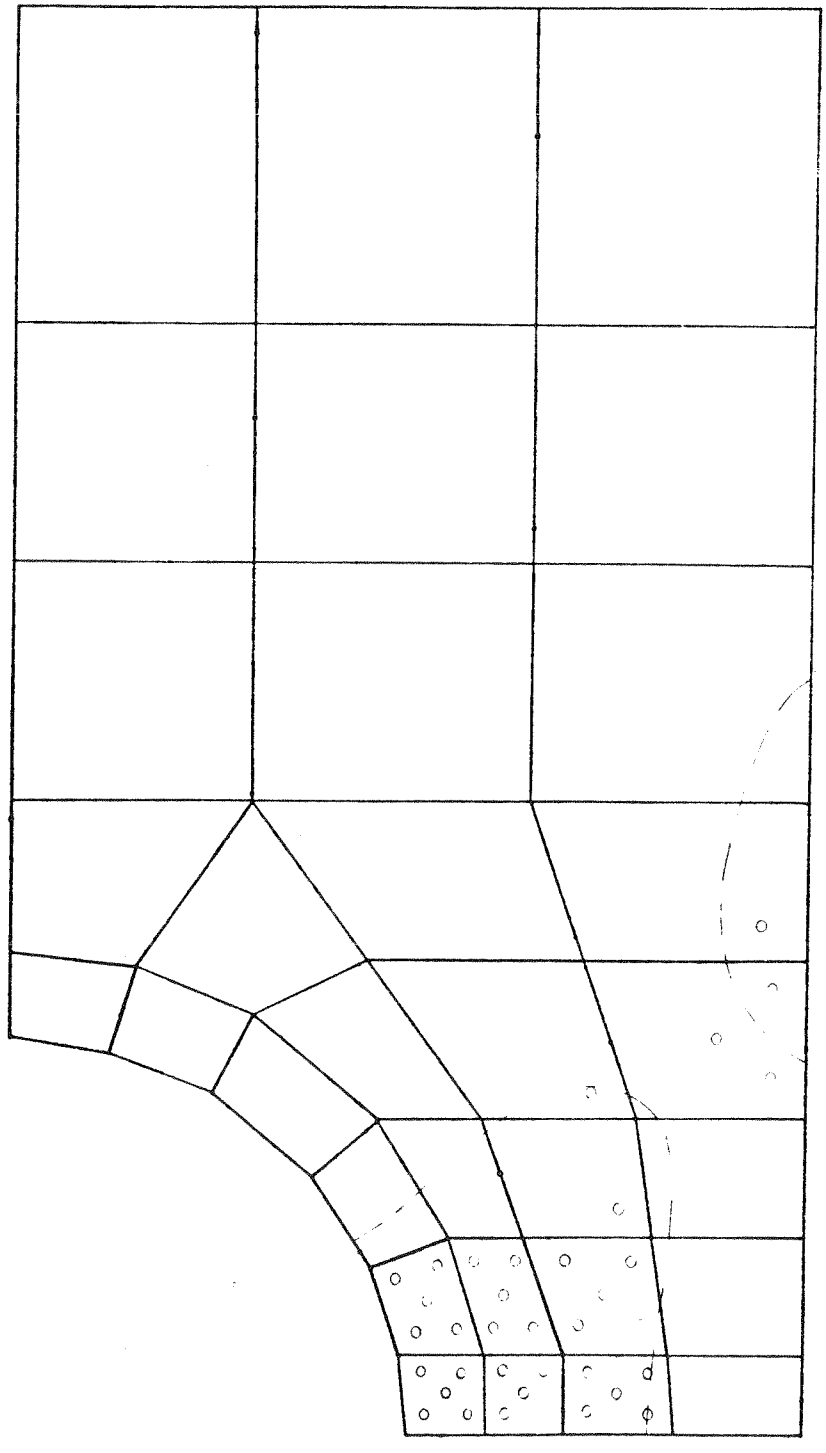

—·—·— Theocaris & Marketos' Experiment @ $\sigma_u/\sigma_o = 0.945$

o Yielded Integration Point @ $\sigma_u/\sigma_o = 1.0$

FIG 7-15<d> SPREAD OF PLASTIC ZONE, METHODS 8,9,10

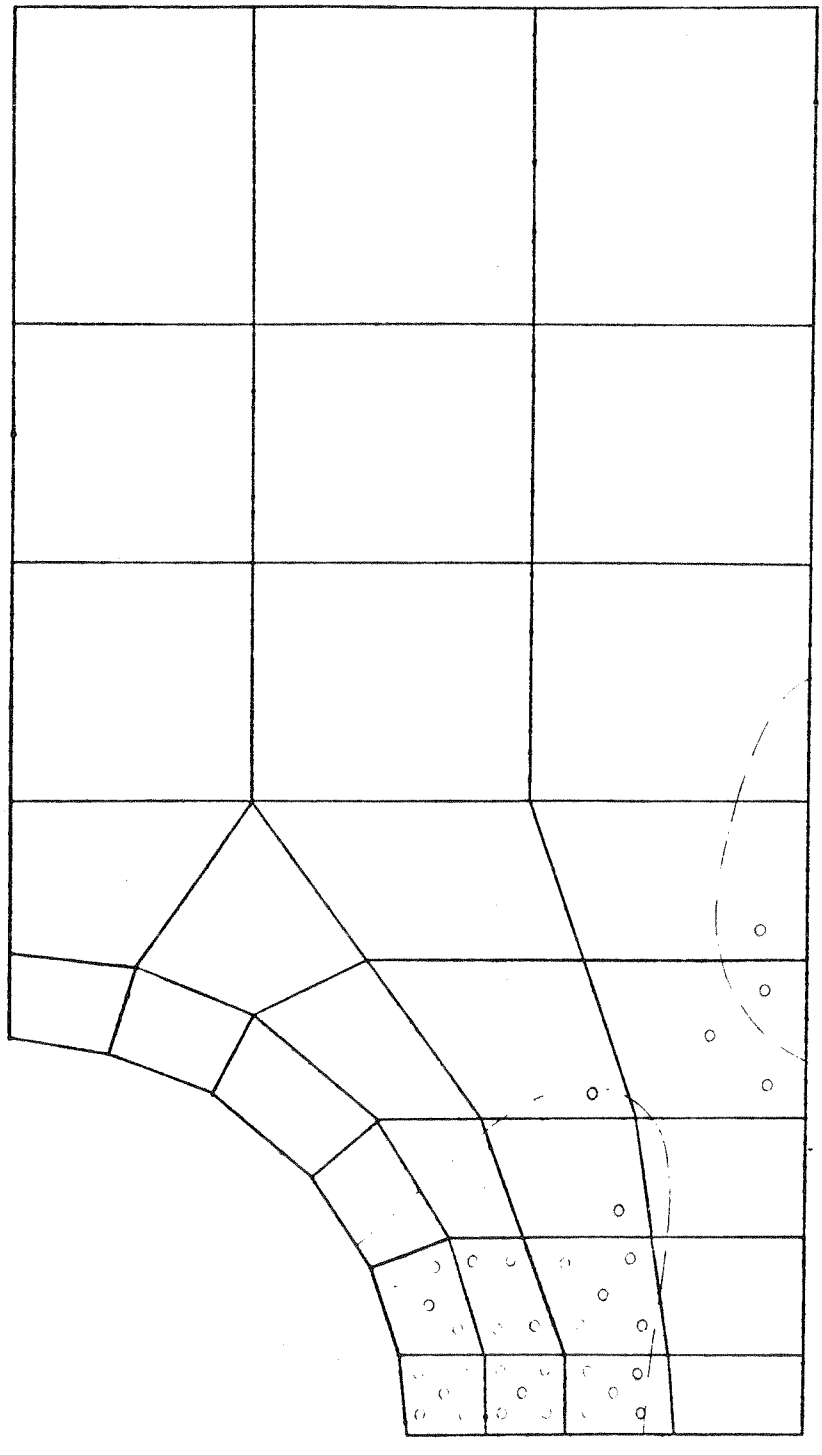

— · — · — Theocaris & Marketos' Experiment @ $\bar{\sigma}/\sigma_0 = 0.945$

o Yielded Integration Point @ $\bar{\sigma}/\sigma_0 = 1.0$

FIG T-15(e) SPREAD OF PLASTIC ZONE, METHODS 11, 12, 13

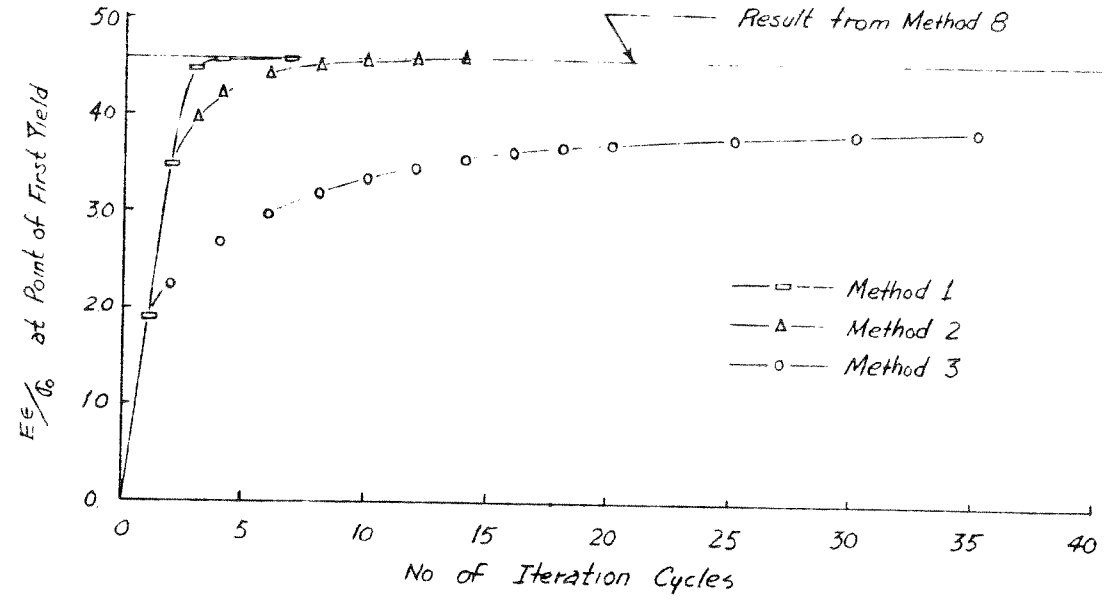

(a) STRAIN CONVERGENCE

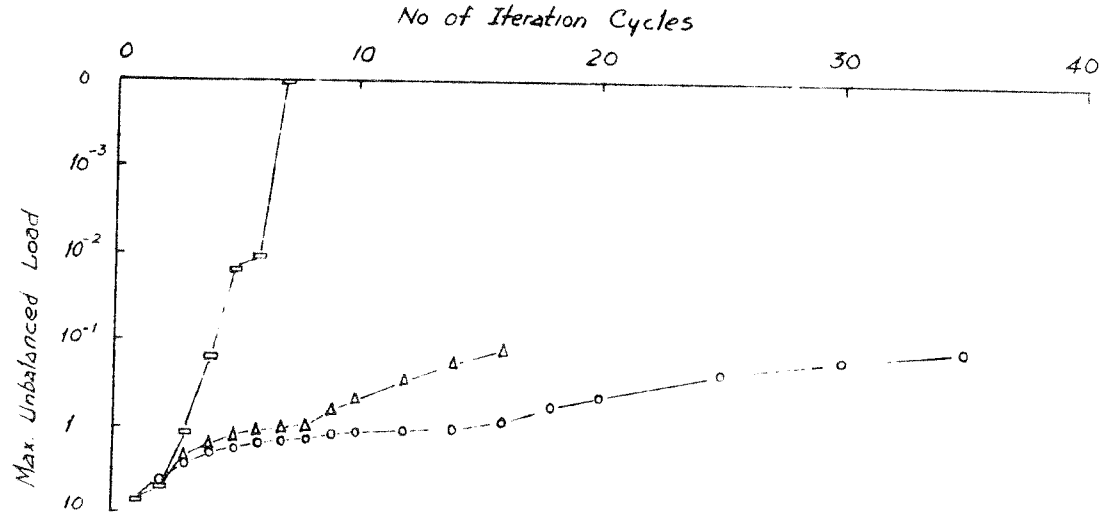

(b) UNBALANCED LOAD CONVERGENCE

FIG 7-16 CONVERGENCE RATES OF SINGLE STEP METHODS

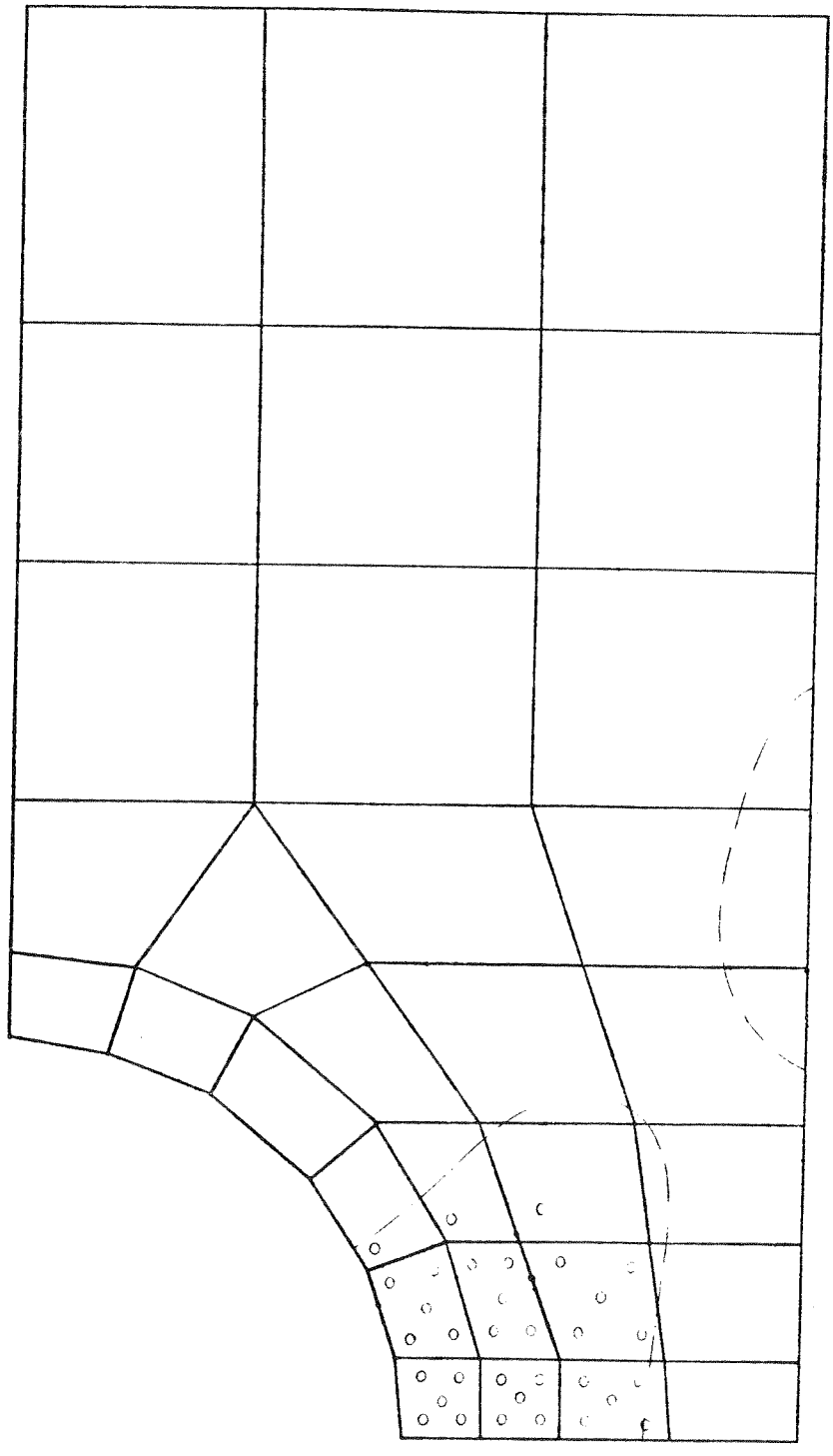

—·—·— Theocaris & Marketos' Experiment @ $\sigma_y/\sigma_0 = 0.945$

o Yielded Integration Point @ $\sigma_y/\sigma_0 = 1.0$

FIG 7-17(a) SPREAD OF PLASTIC ZONE. Q4 ELEMENT

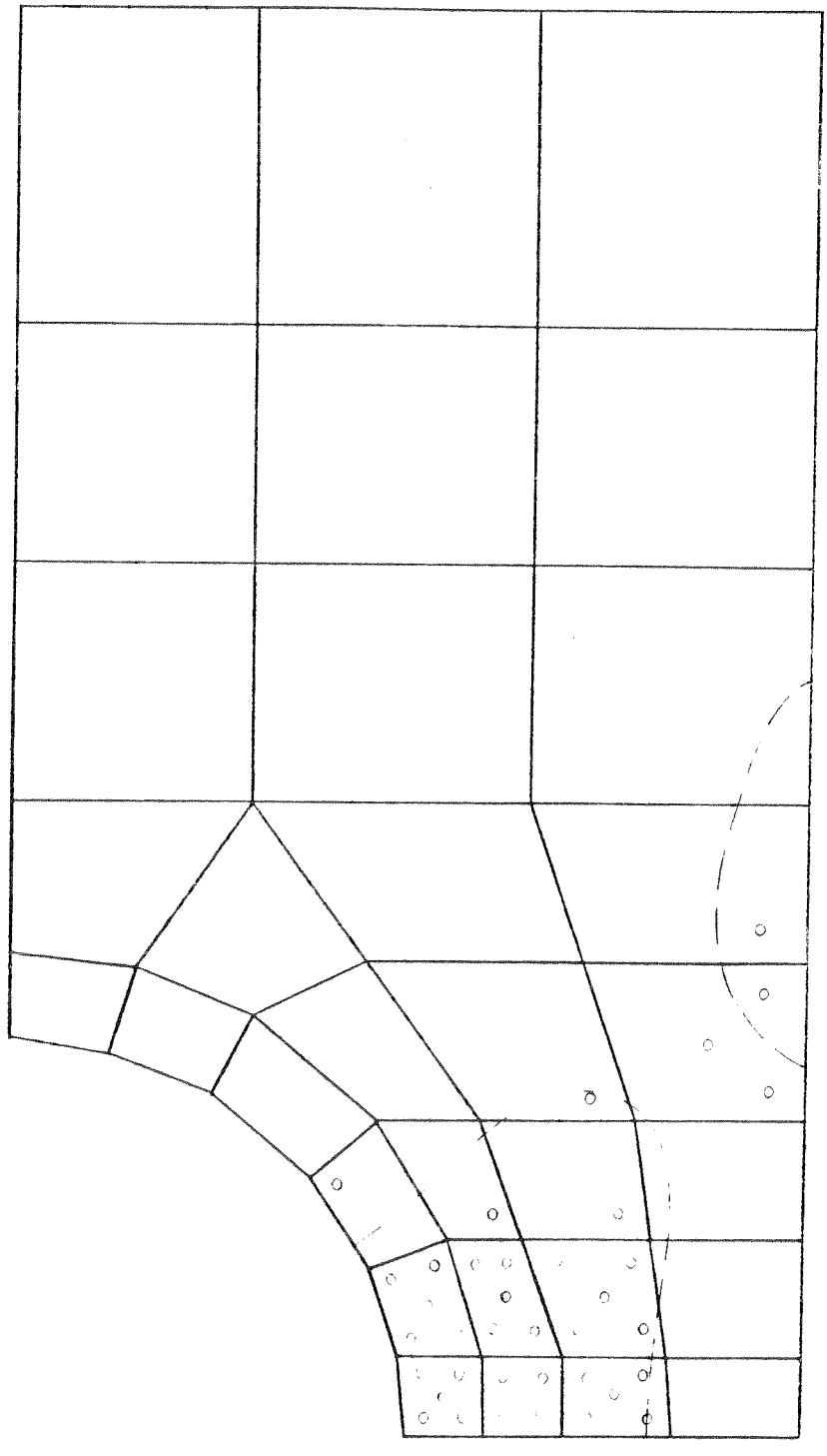

— · — · — Theocaris & Marketos' Experiment @ $\sigma_y/\sigma_0 = 0.945$

o Yielded Integration Point @ $\sigma_y/\sigma_0 = 1.0$

FIG 7-17(b) SPREAD OF PLASTIC ZONE, Q4I4 ELEMENT

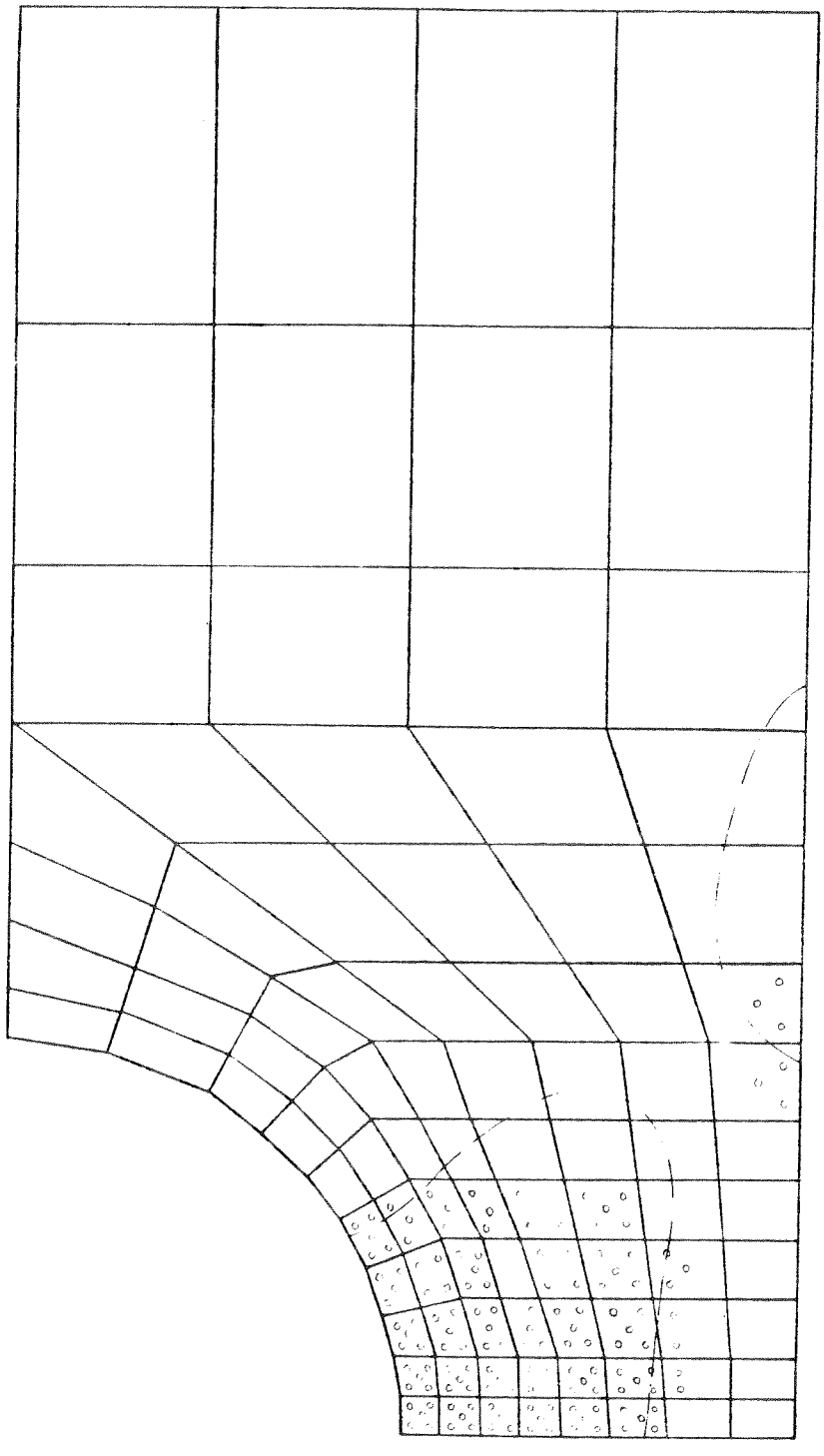

—·—·— Theocaris & Marketos' Experiment @ $\sigma_y/\sigma_0 = 0.945$

o Yielded Integration Point @ $\sigma_y/\sigma_0 = 1.0$

FIG 7-17(c) SPREAD OF PLASTIC ZONE, Q4 ELEMENT

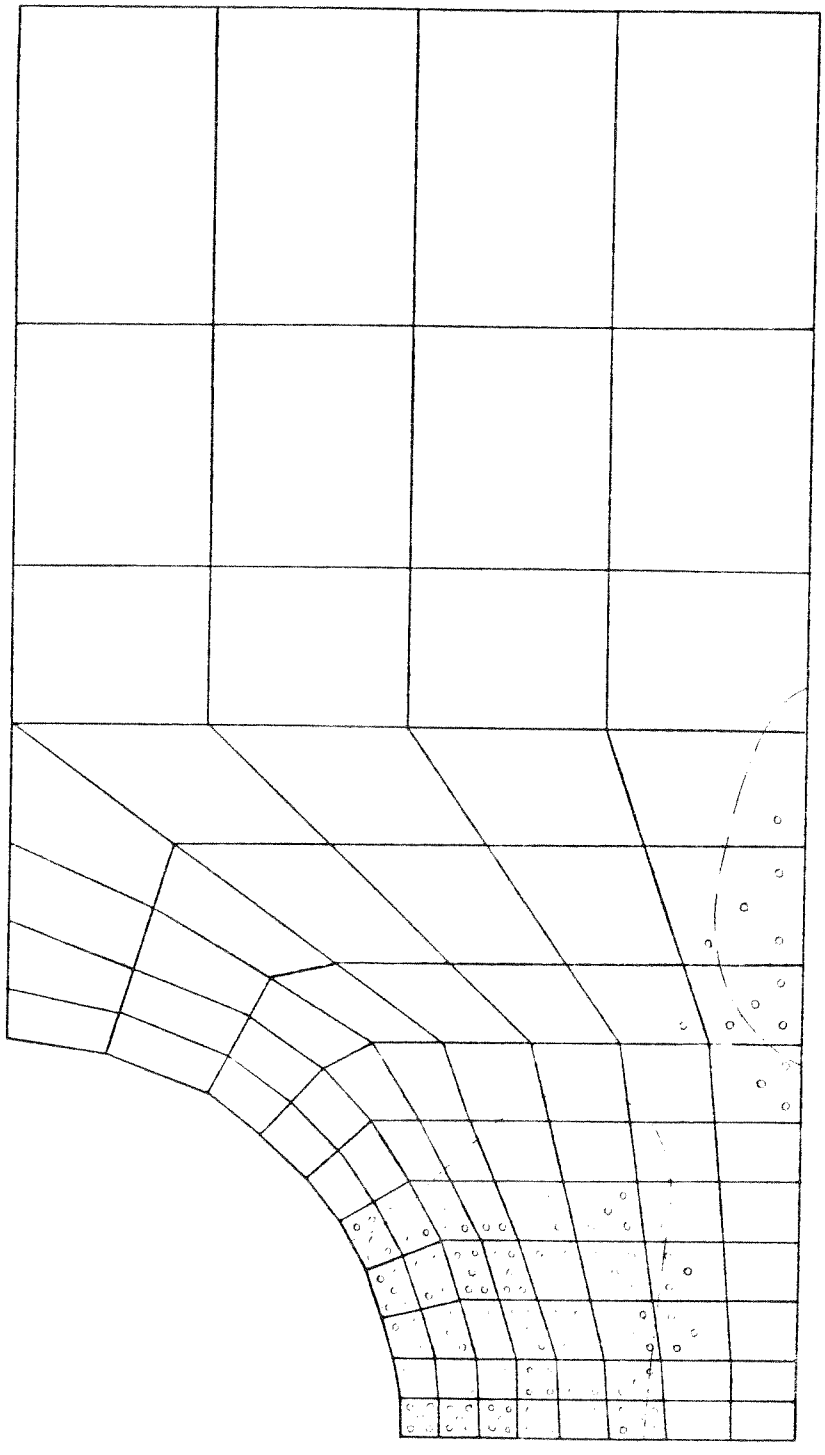

— · — · — Theocaris & Marketos' Experiment @ $\sigma_y/\sigma_0 = 0.945$

o Yielded Integration Point @ $\sigma_y/\sigma_0 = 1.0$

FIG 7-17(d). SPREAD OF PLASTIC ZONE, Q4I4 ELEMENT

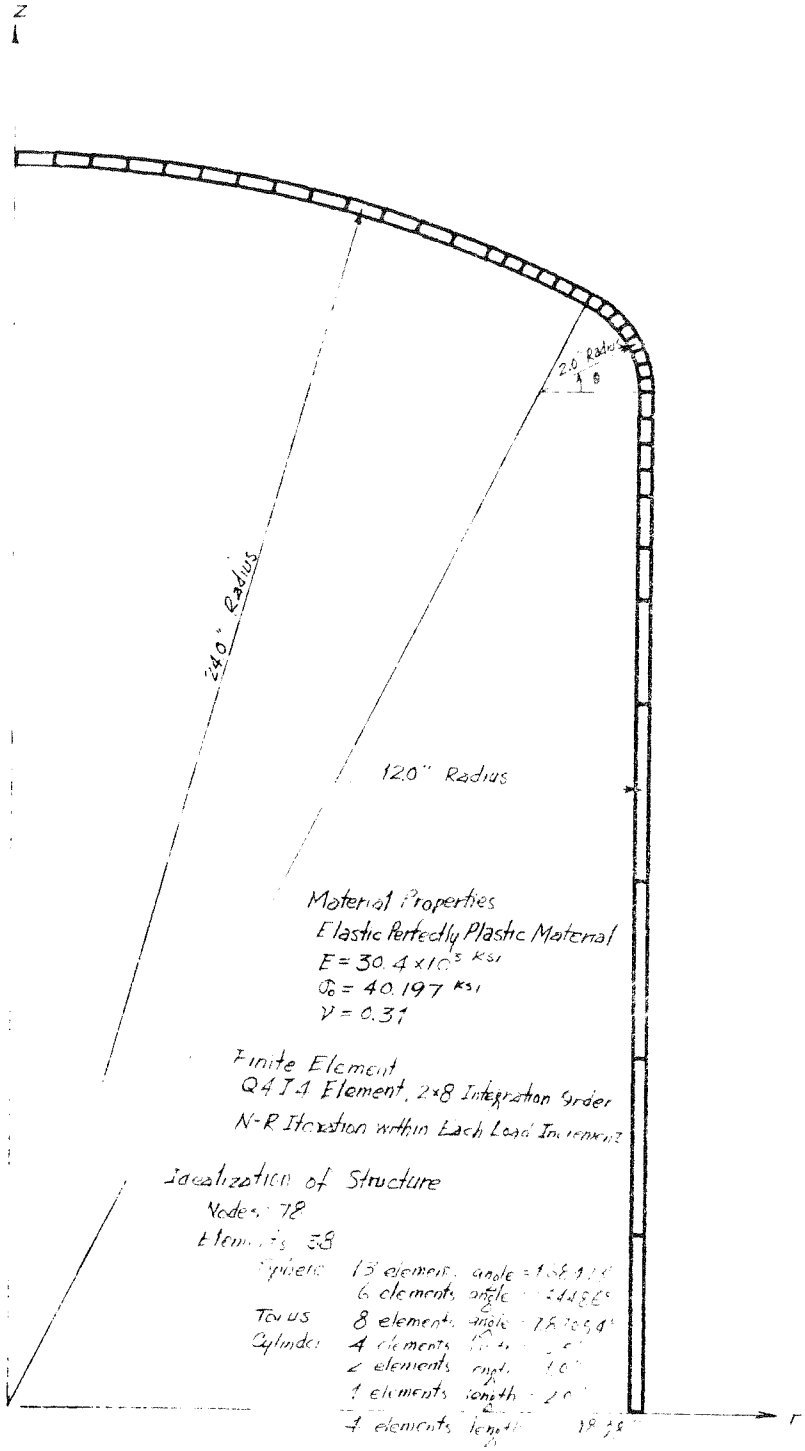

FIG 7-18 TORISHERICAL PRESSURE VESSEL

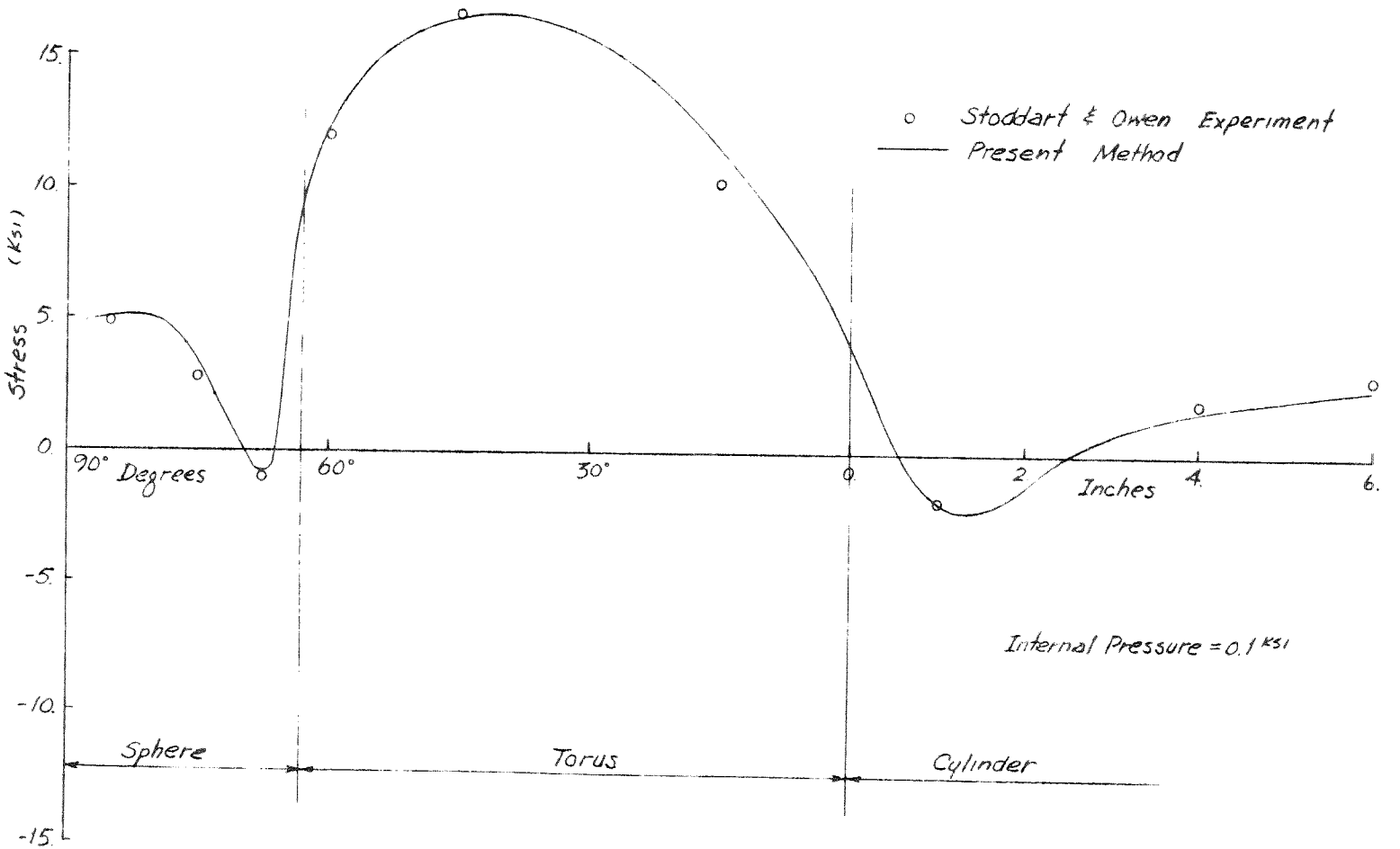

FIG 7-19 (a) TORISPHERICAL VESSEL ELASTIC ANALYSIS INNER SURFACE MERIDIONAL STRESS

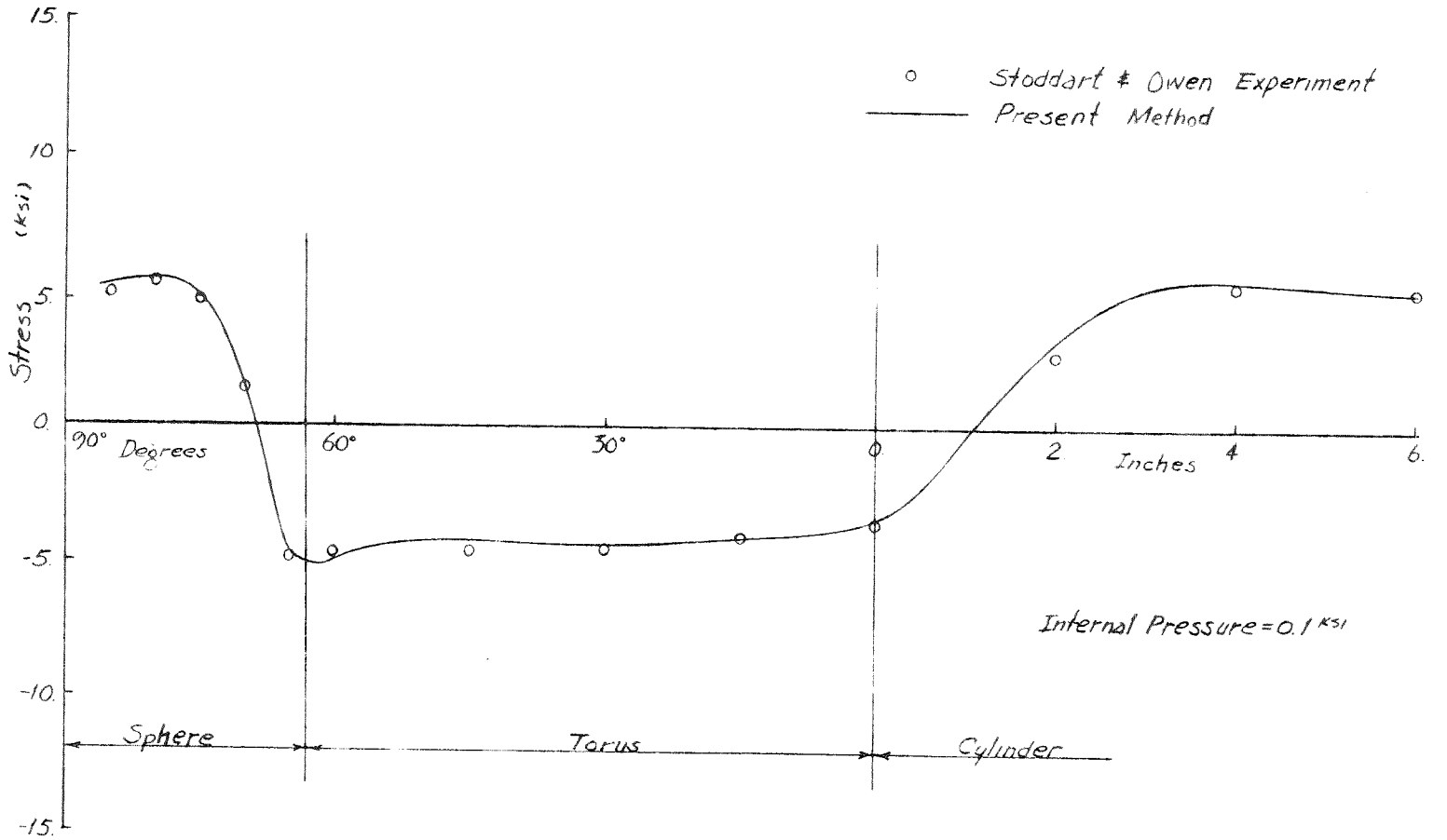

FIG 7-19 <b> TORISPHERICAL VESSEL. ELASTIC ANALYSIS INNER SURFACE CIRCUMFERENTIAL STRESS

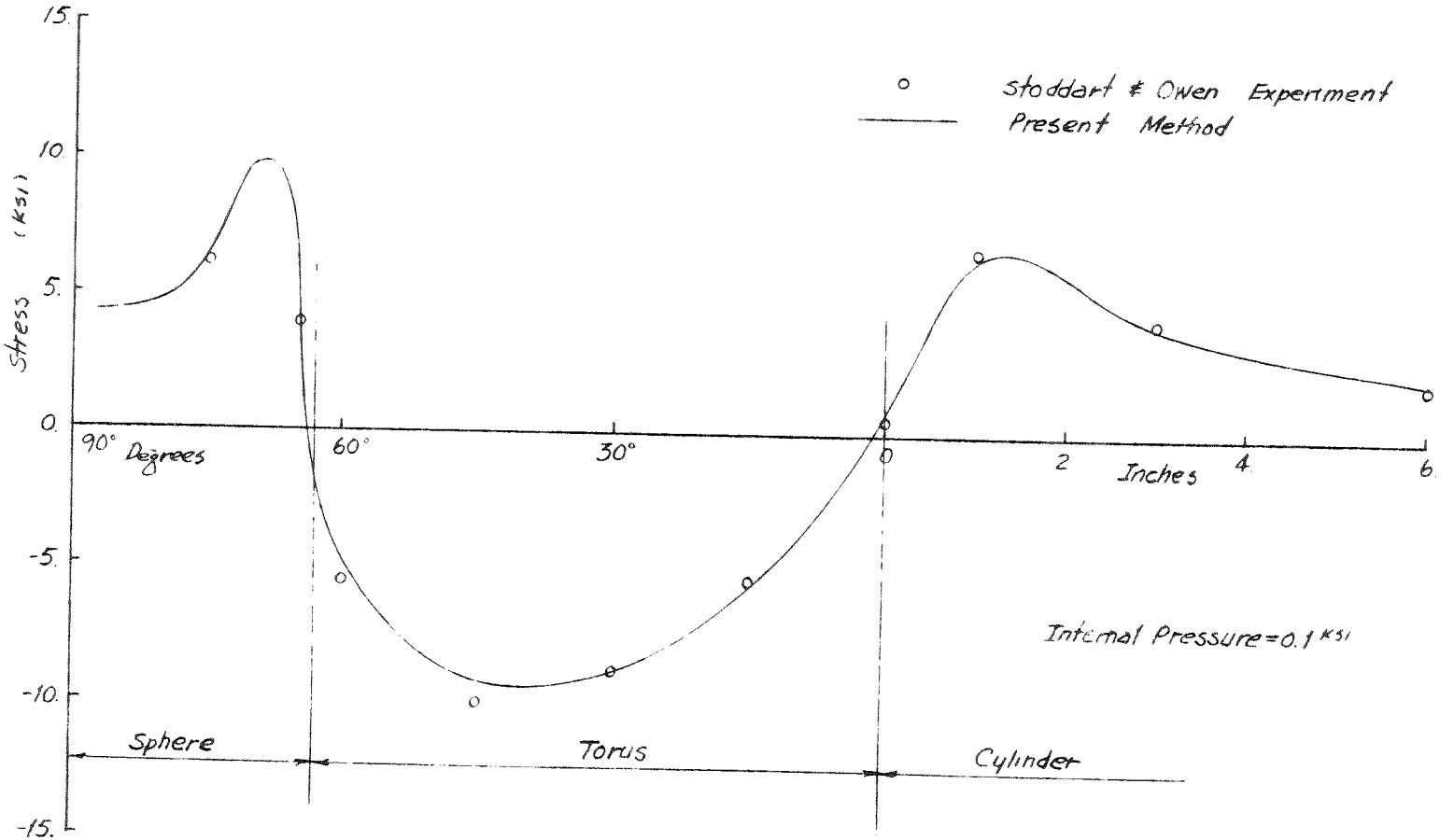

FIG 7-19 <c> TORISPHERICAL VESSEL ELASTIC ANALYSIS OUTER SURFACE MERIDIONAL STRESS

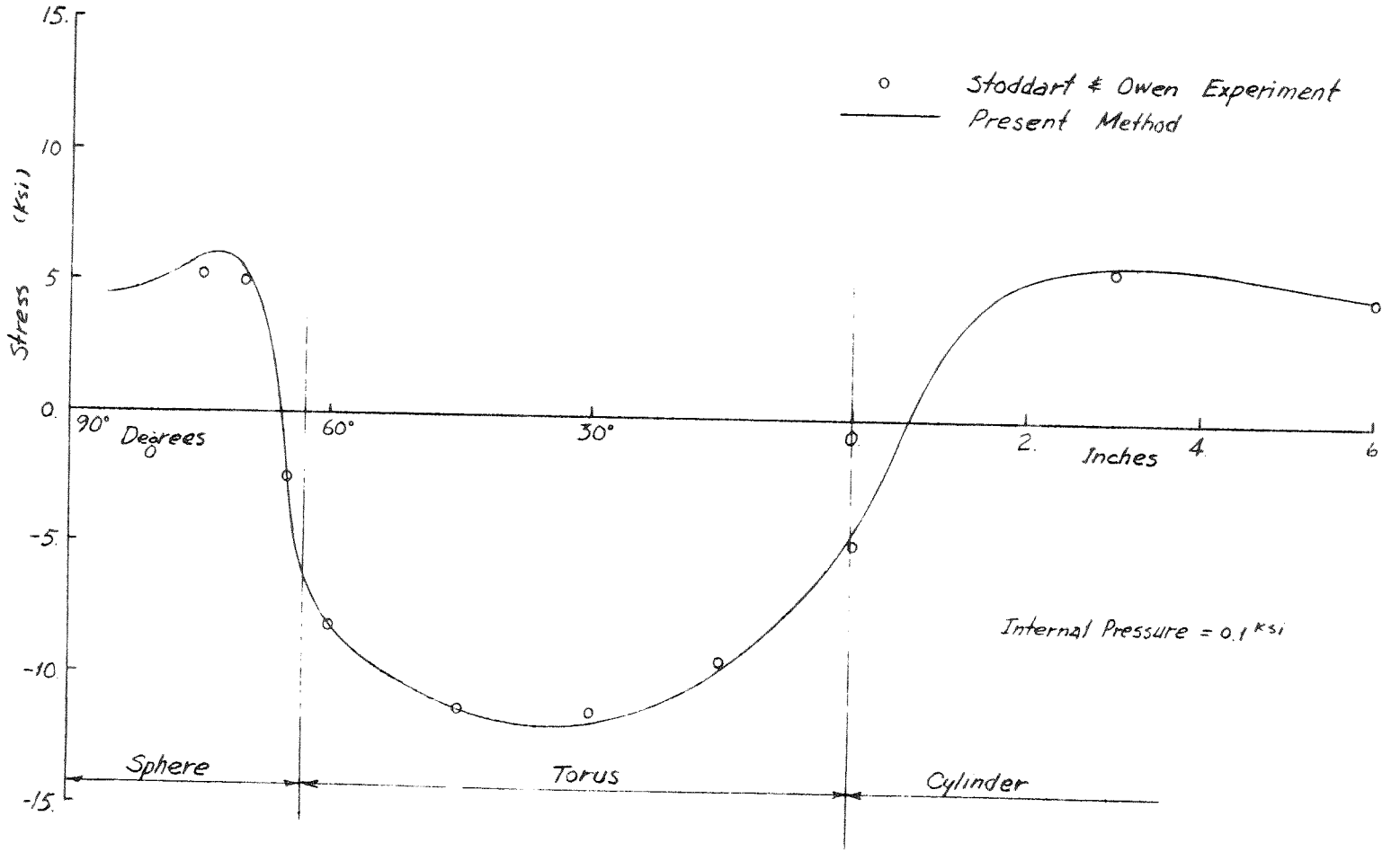

FIG 7-19 <d> TORISPHERICAL VESSEL ELASTIC ANALYSIS OUTER SURFACE CIRCUMFERENTIAL STRESS

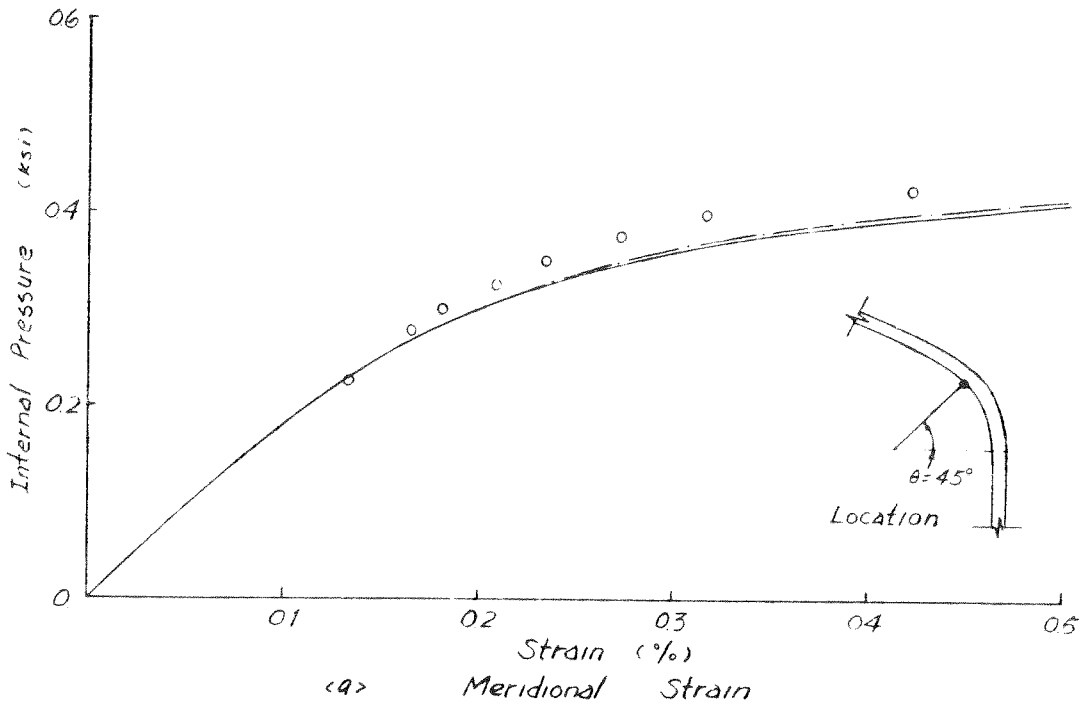

(a) Meridional Strain

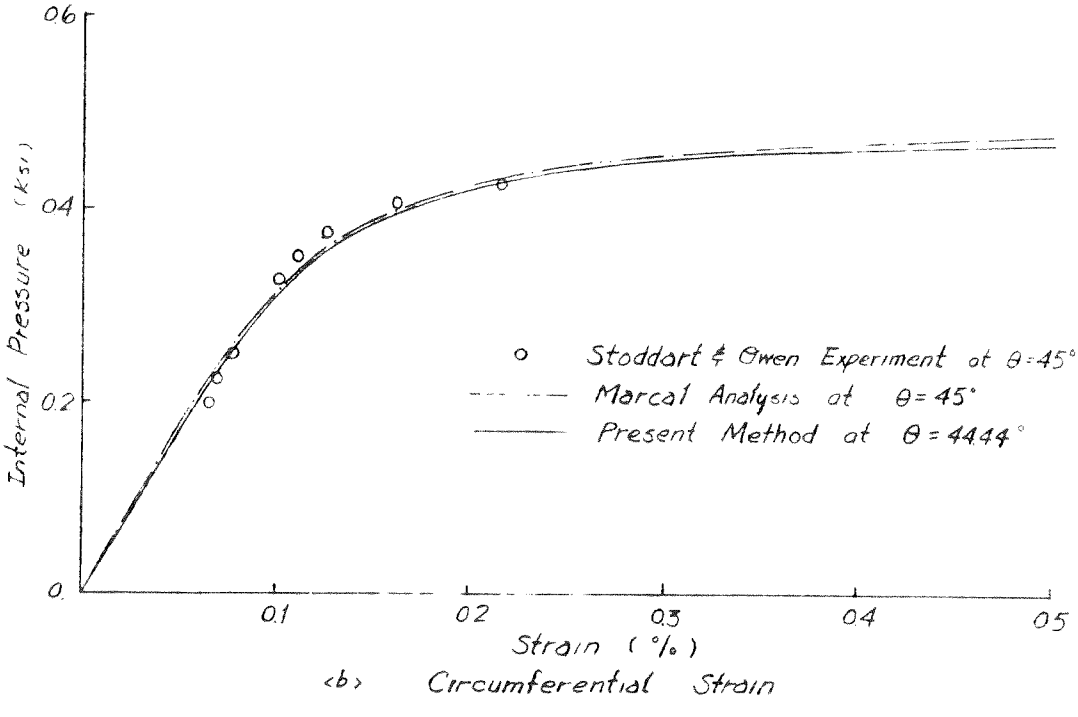

(b) Circumferential Strain

FIG 7-20 TORISPHERICAL VESSEL. VARIATION OF INNER SURFACE STRAIN WITH PRESSURE

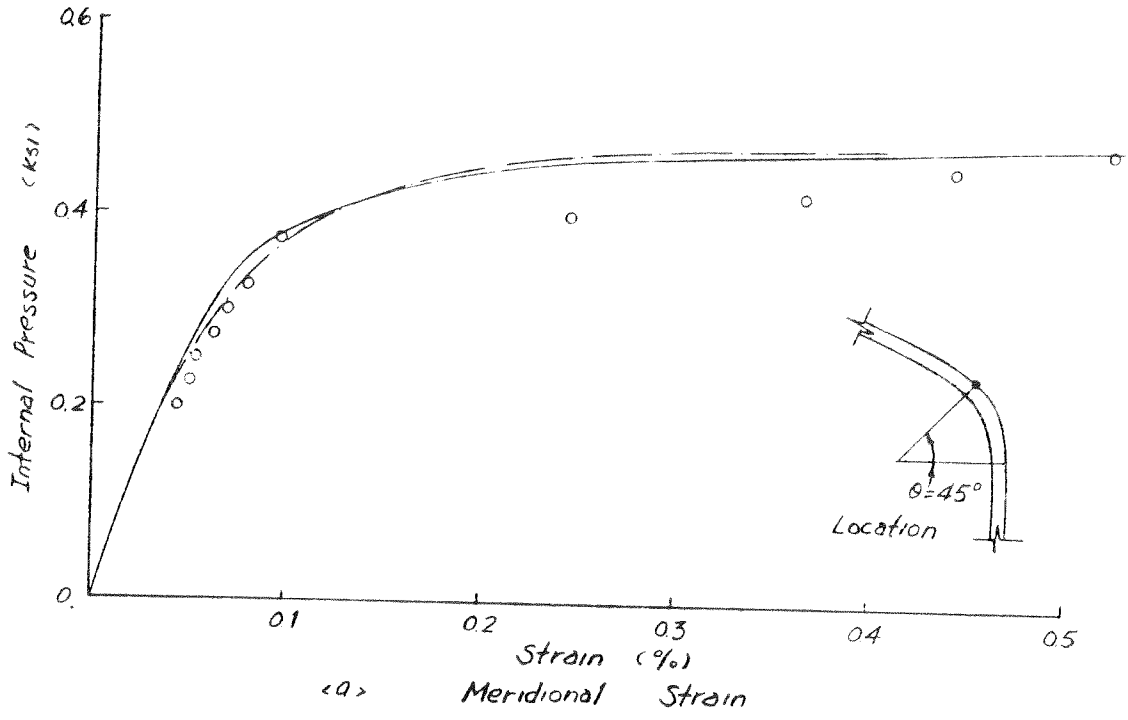

(a) Meridional Strain

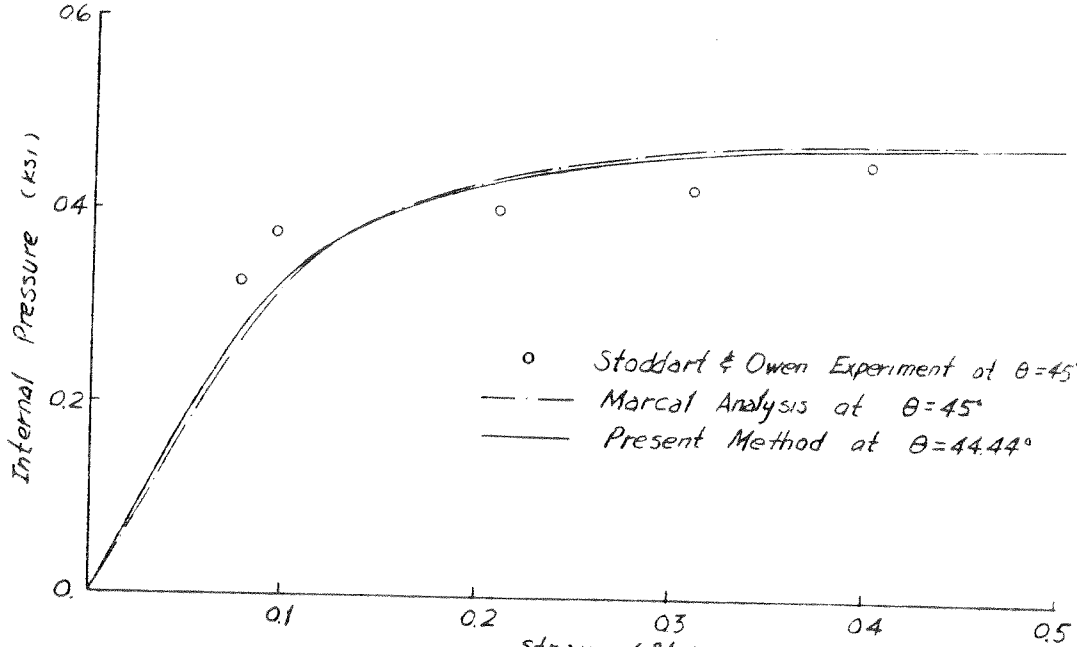

(b) Circumferential Strain

FIG T-21 TORISPHERICAL VESSEL. VARIATION OF OUTER SURFACE STRAIN WITH PRESSURE

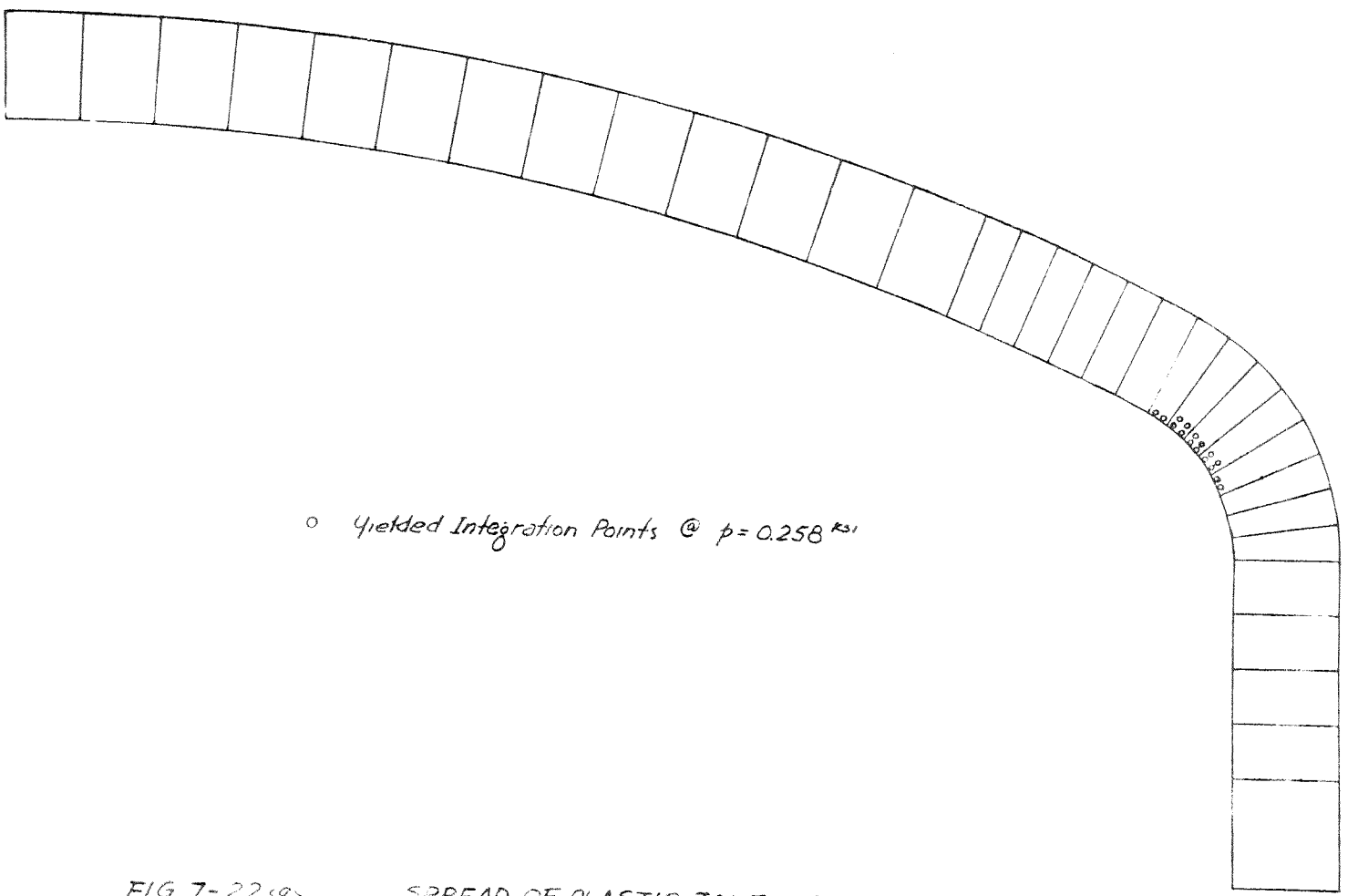

FIG 7-22(a) SPREAD OF PLASTIC ZONE IN TORISPHERICAL VESSEL

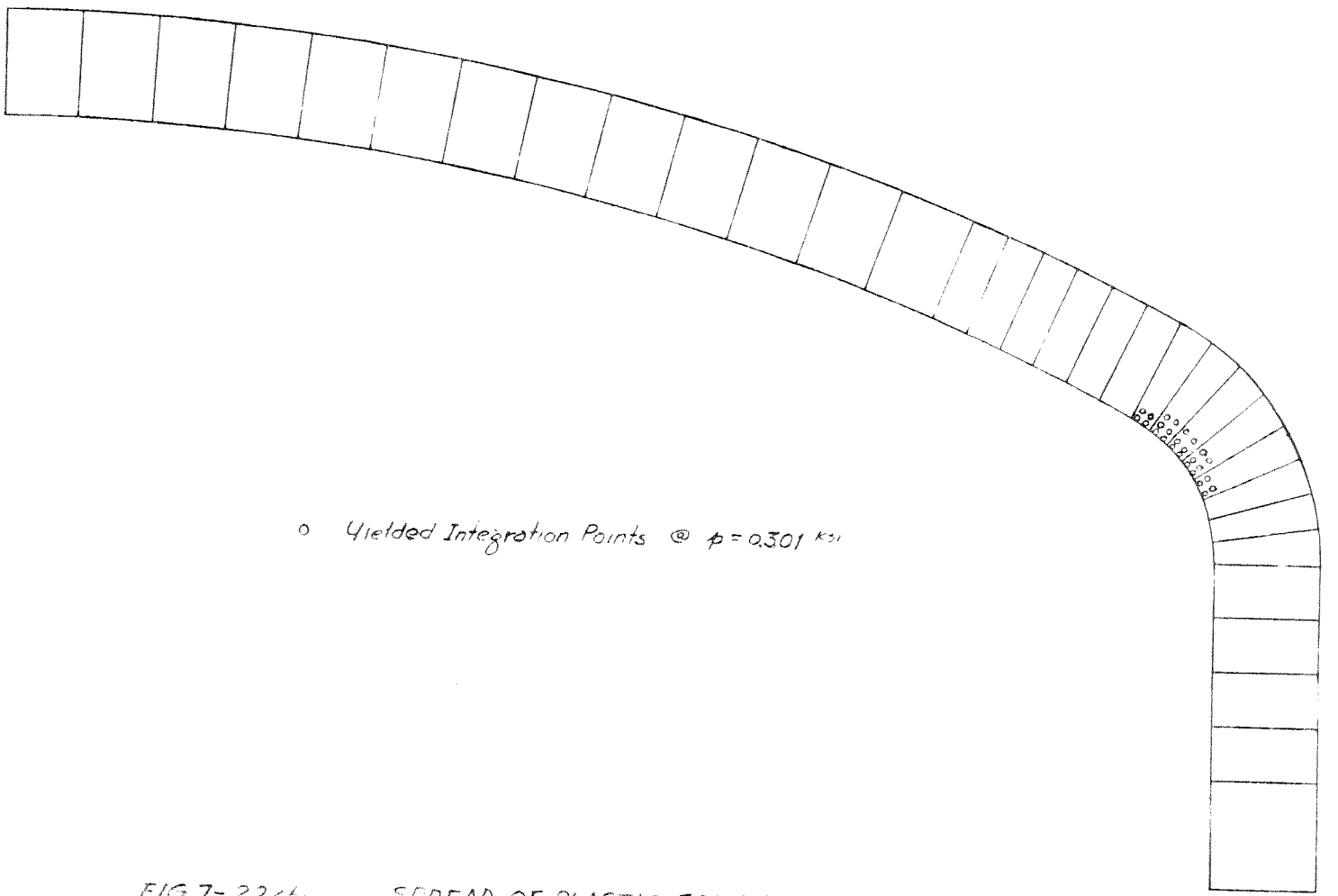

FIG 7-22(b) SPREAD OF PLASTIC ZONE IN TORISPHERICAL VESSEL

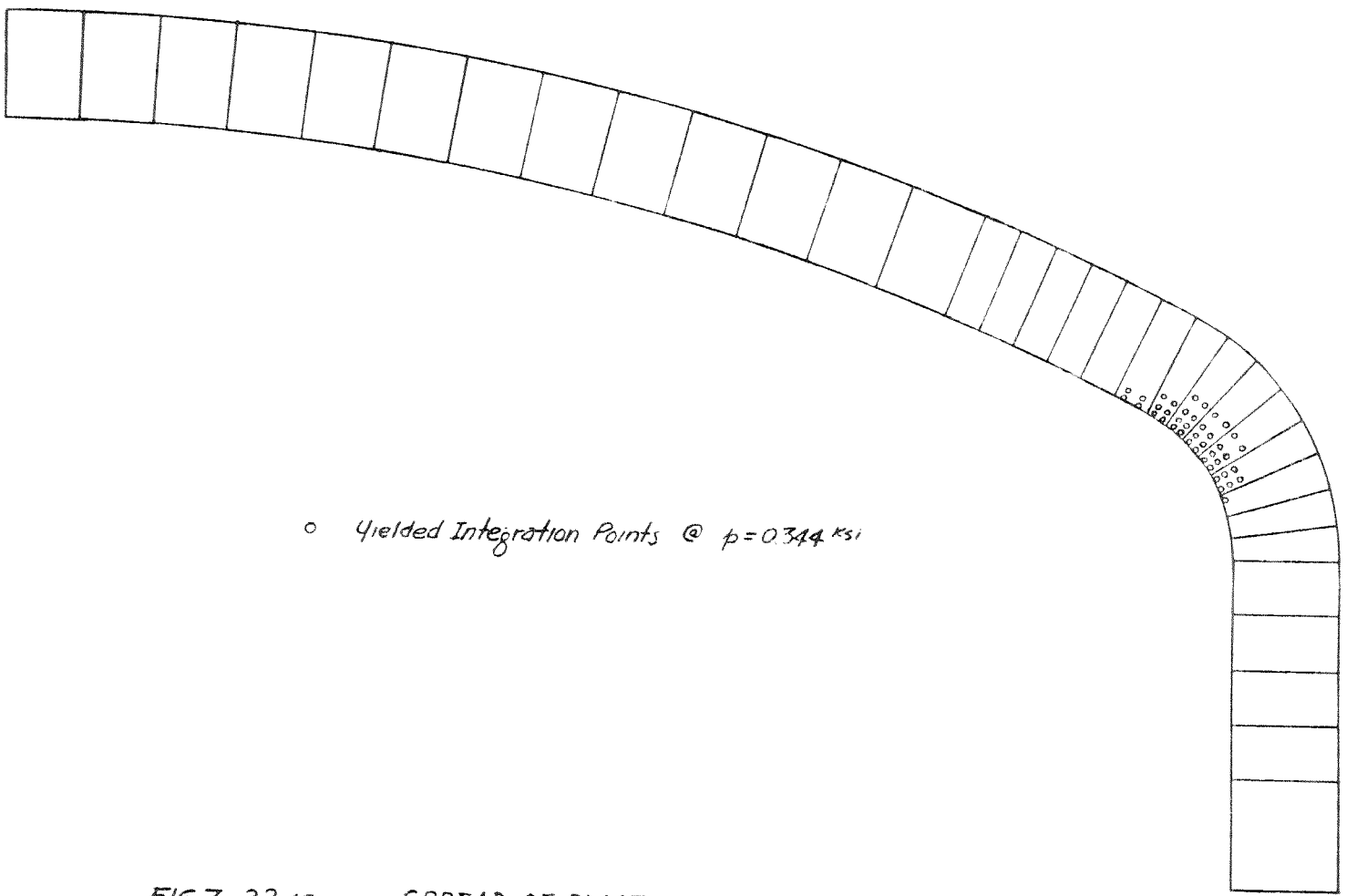

FIG 7-22 <c> SPREAD OF PLASTIC ZONE IN TORISPHERICAL VESSEL

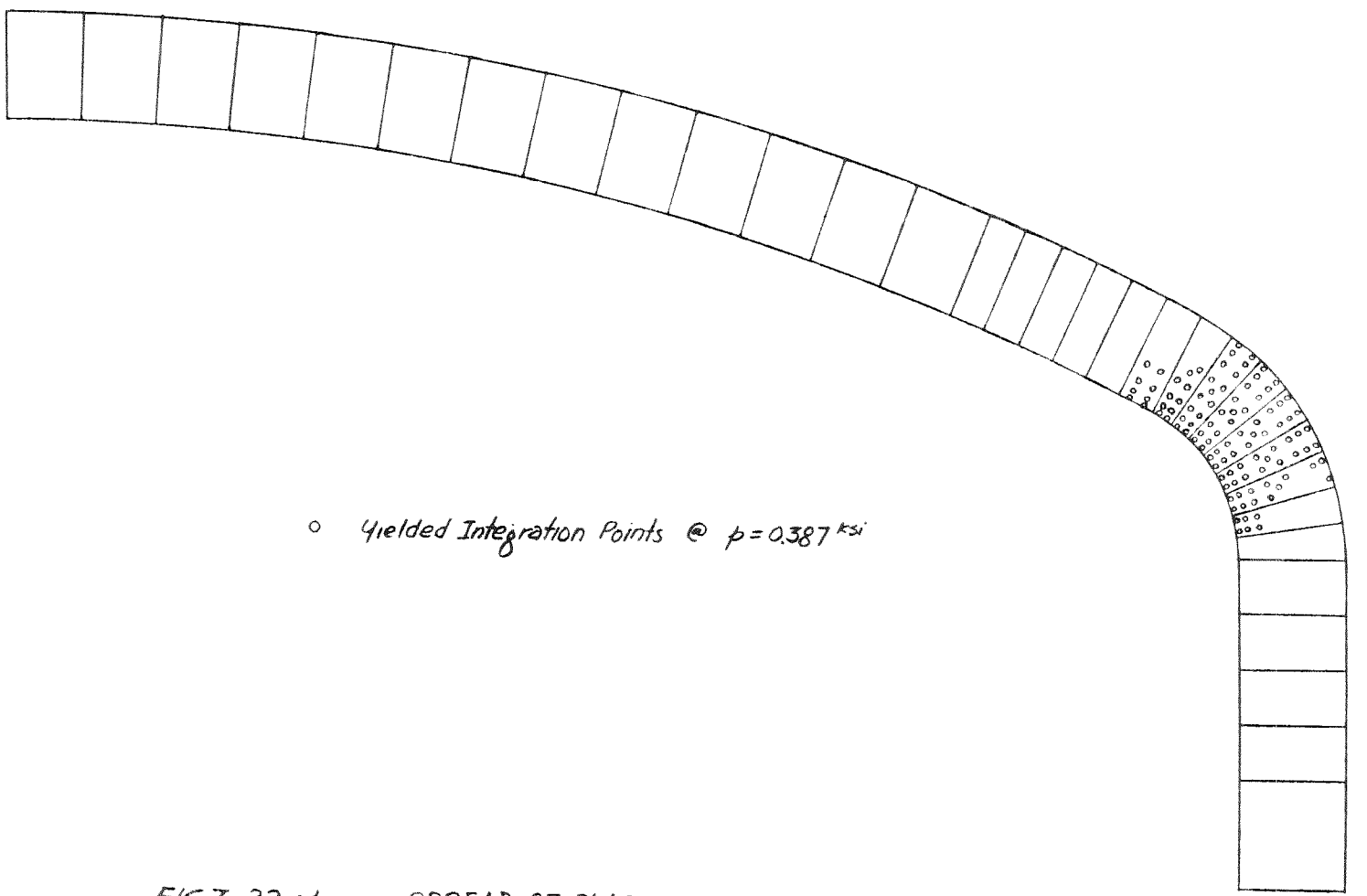

FIG 7-22 (d) SPREAD OF PLASTIC ZONE IN TORISPHERICAL VESSEL

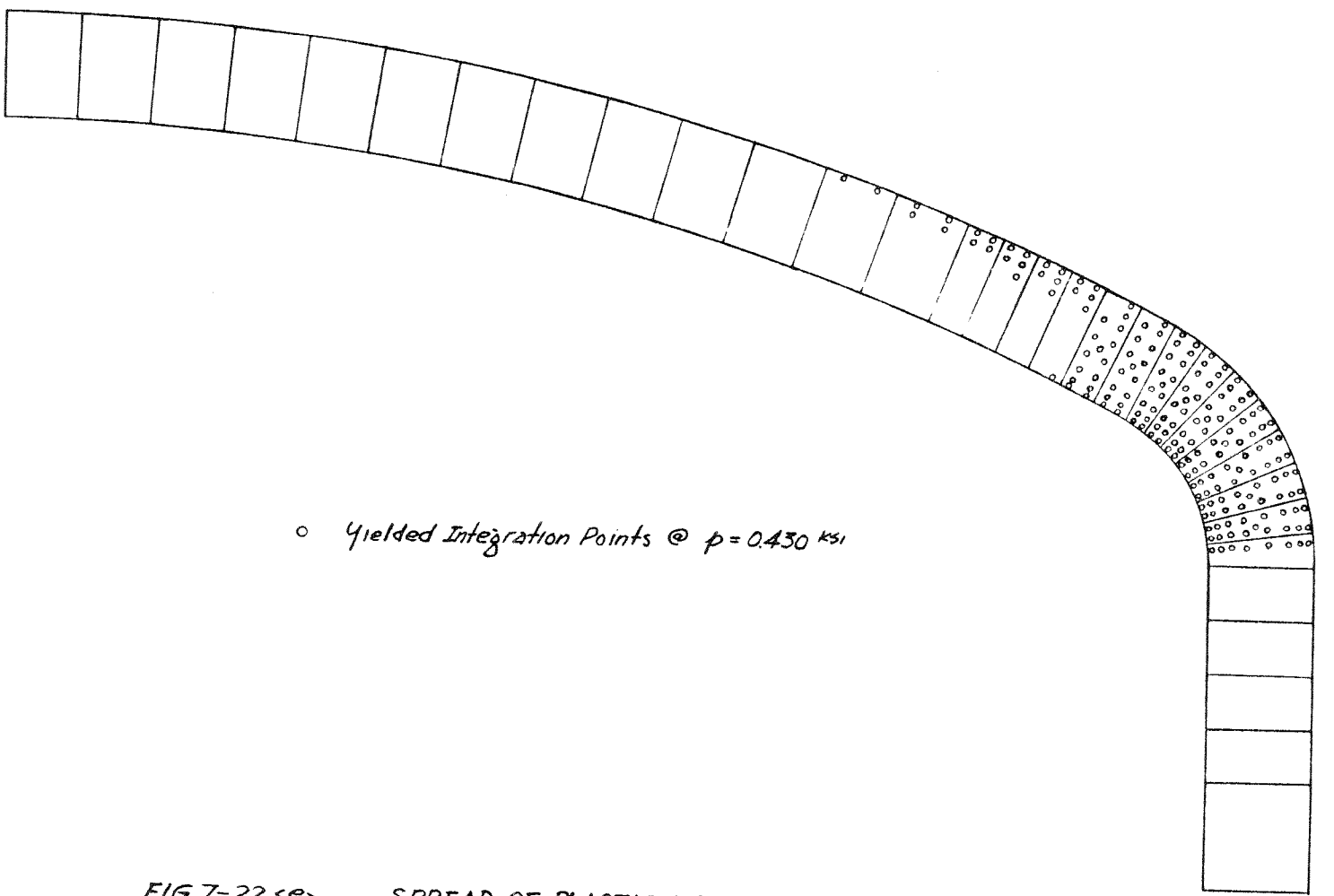

FIG 7-22 <e> SPREAD OF PLASTIC ZONE IN TORISPHERICAL VESSEL

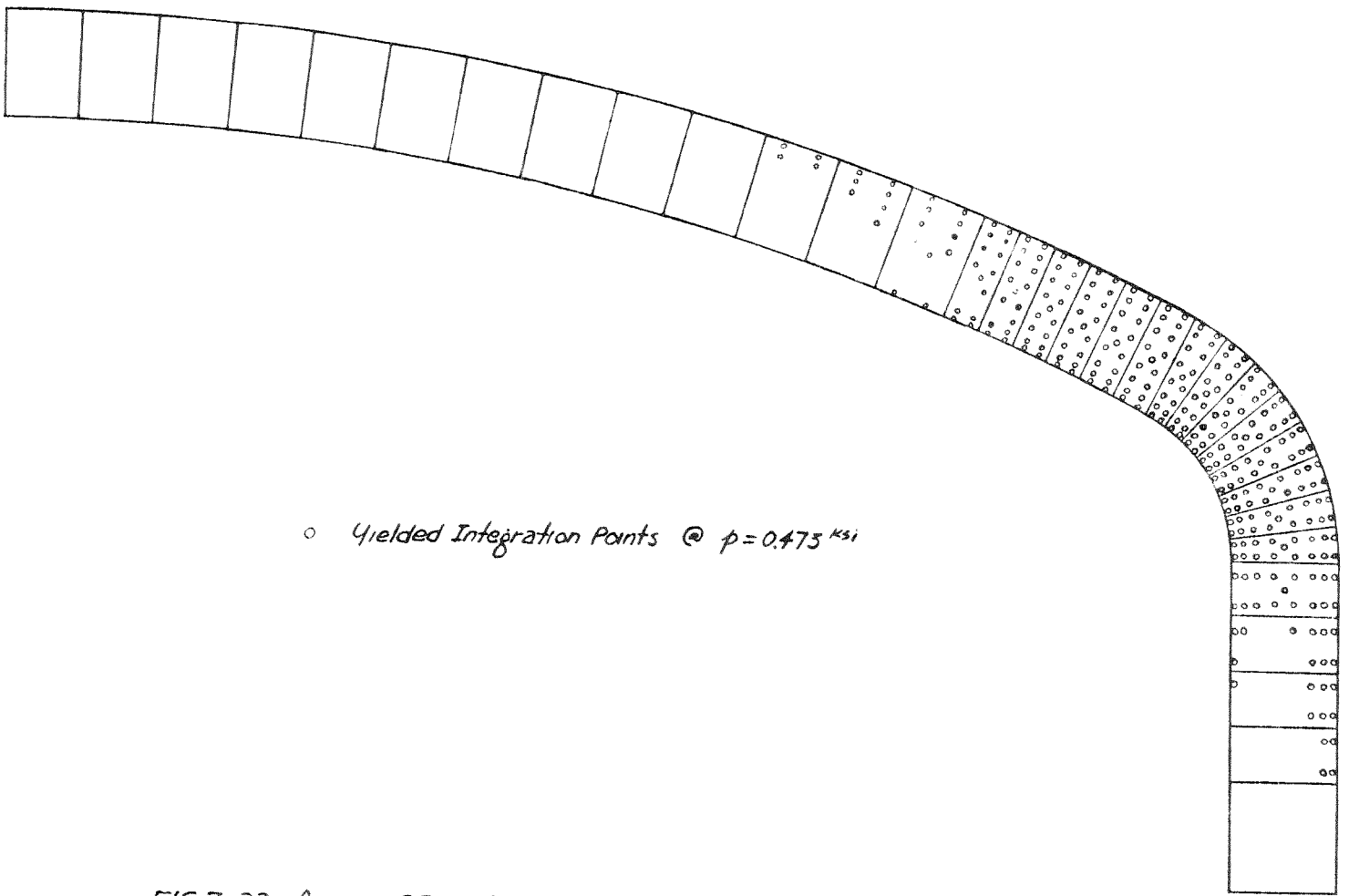

FIG 7-22 <f> SPREAD OF PLASTIC ZONE IN TORISPHERICAL VESSEL

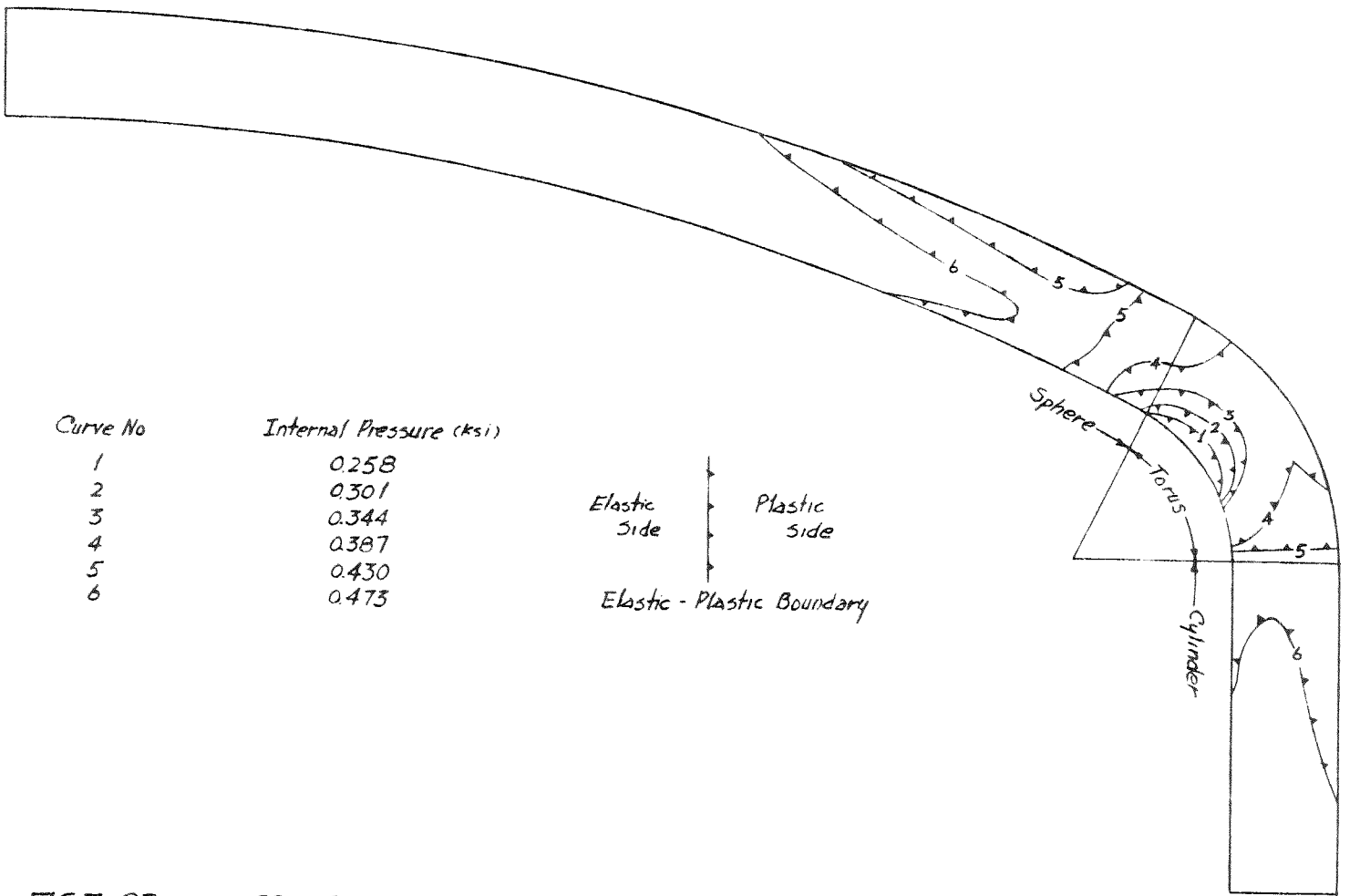

FIG 7-23 PROGRESSIVE YIELDING IN TORISPHERICAL VESSEL

<a> Structure

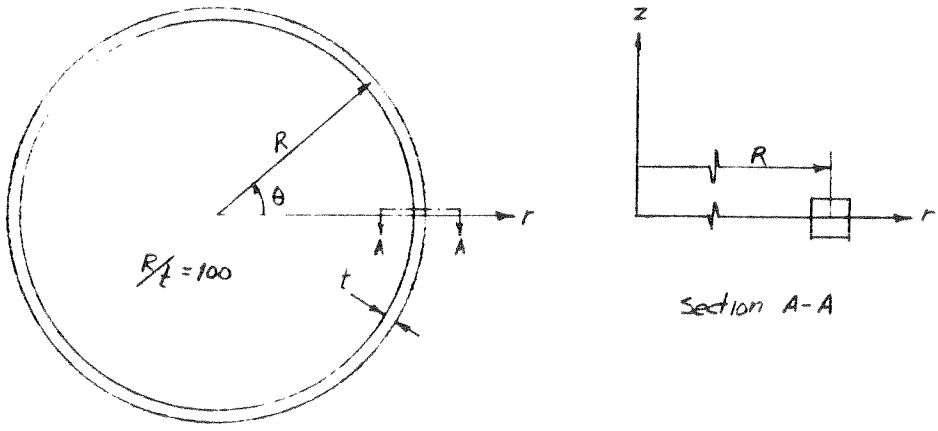

<b> Material Properties

$E = 30. \times 10^3$

$\sigma_0 = 36.$

$H/E = 0.1$

$\nu = 0.3$

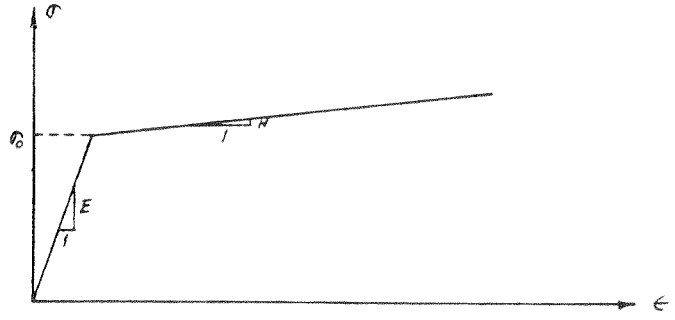

FIG 7-24 THIN CYLINDER FOR STRAIN HARDENING STUDY

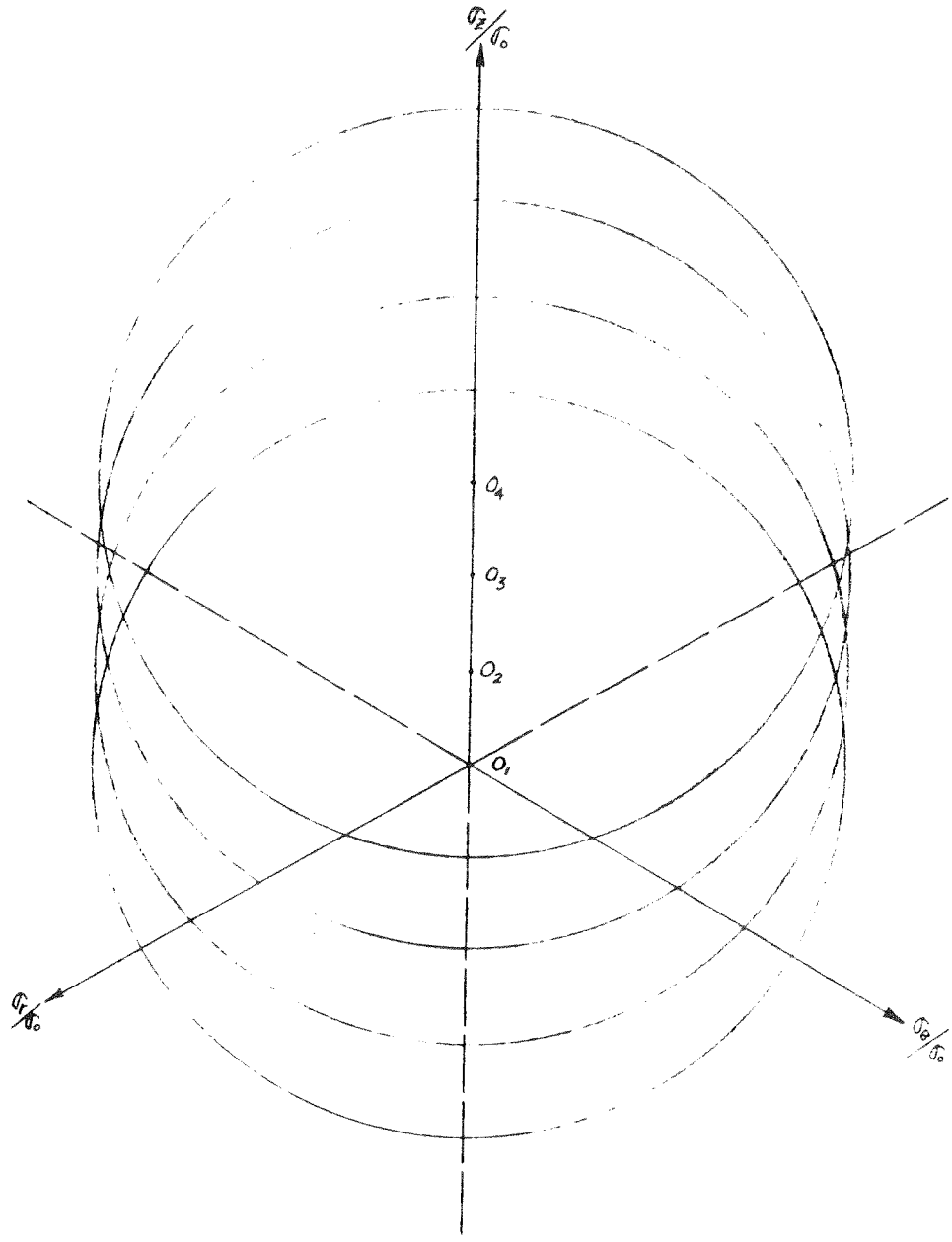

Cycle	Yield Stress $+\sigma_z/\sigma_o$	Yield Stress $+\sigma_\theta/\sigma_o$	Yield Stress $-\sigma_\theta/\sigma_o$	Center of Yield Surface	Remark
1	1.00	1.00	1.00	O_1	Initial Yield Surface
2	1.25	0.85	1.10	O_2	Subsequent Loading Surface
3	1.50	0.65	1.15	O_3	Subsequent Loading Surface
4	1.75	0.39	1.14	O_4	Subsequent Loading Surface

FIG 7-25 STRAIN HARDENING IN THIN CYLINDER YIELD SURFACE LOCATIONS FOR INCREASING AXIAL STRESS

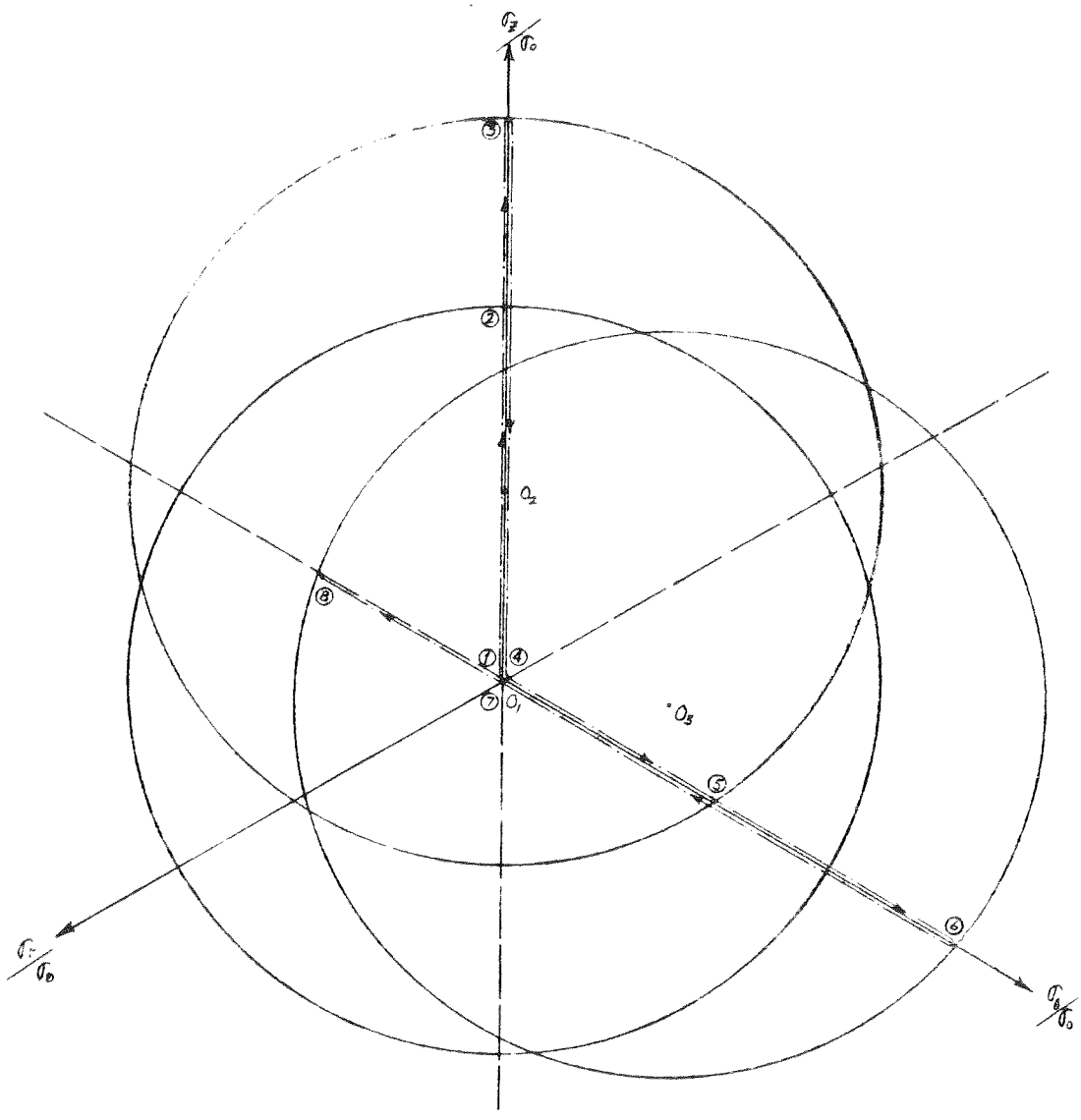

Location	σ_z/σ_0	σ_θ/σ_0	Remark
1	0.0	0.	Initial State
2	1.0	0.	Boundary of Initial Yield Surface with Center @ O_1
3	1.5	0.	Boundary of Subsequent Loading Surface with Center @ O_2
4	0	0	1st Residual State
5	0.	0.65	Boundary of Loading Surface with Center @ O_2
6	0.	1.40	Boundary of New Loading Surface with Center @ O_3
7	0.	0.	2nd Residual State
8	0.	-0.56	Boundary of Loading Surface with Center @ O_3

FIG 7-26 STRAIN HARDENING IN THIN CYLINDER
MOVEMENT OF YIELD SURFACE IN STRESS SPACE

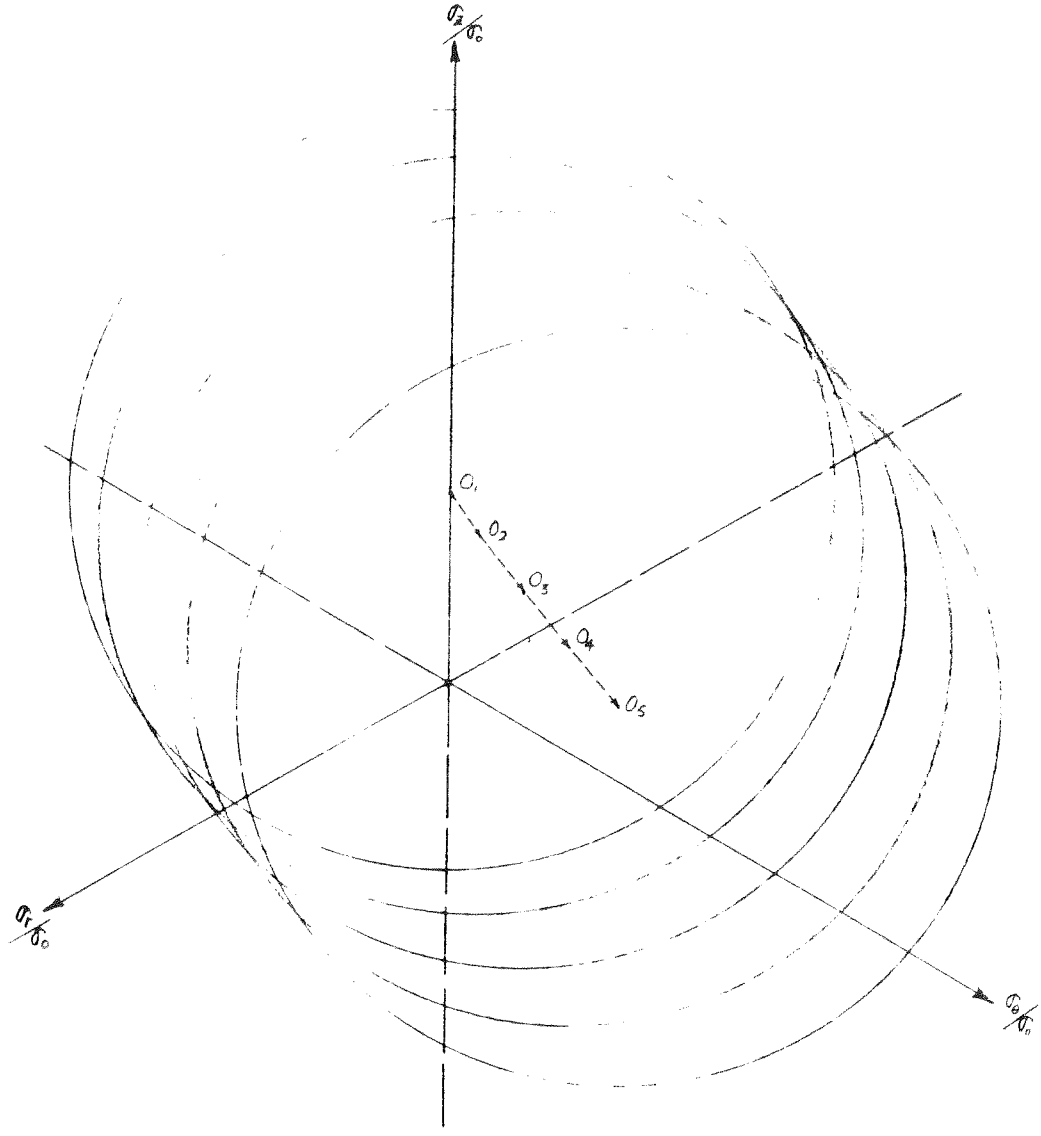

Cycle	Yield Stress in Circumferential Direction $+\sigma_\theta/\sigma_0$	$-\sigma_\theta/\sigma_0$	Center of Yield Surface	Remark
1	0.65	1.15	O_1	Correspond to O_3 of FIG. 7-25
2	0.80	1.05	O_2	
3	1.00	0.90	O_3	
4	1.20	0.74	O_4	
5	1.40	0.56	O_5	

FIG 7-27 STRAIN HARDENING IN THIN CYLINDER YIELD SURFACE LOCATIONS FOR INCREASING CIRCUMFERENTIAL STRESS FOLLOWING AXIAL STRAINING

8. CONCLUSION

8.1 SUMMARY

A general solution strategy has been presented which is applicable to a wide variety of nonlinear structural analysis problems. By simply specifying the magnitudes of three convergence tolerances, the user of a computer program may select any one of a variety of solution procedures. It is believed that with this general solution strategy, it should be possible for an experienced user to select an efficient procedure for any type of nonlinear problem, provided structural instability is not present.

A general computational procedure for inelastic finite element analysis has also been presented. This procedure appears to be quite general and to be applicable to many different types of inelastic structure. The solution strategy permits analysis by step by step methods, by iteration, and by combination of step by step and iteration procedures. Details of the computational procedure have been presented for the associated flow theory of plasticity, considering both the von Mises and Tresca yield criteria. Formulations have been presented for general isotropic strain hardening, linear kinematic hardening and a "parallel material" procedure which corresponds to a form of nonlinear kinematic hardening. Applications to both fully compatible and partially incompatible finite elements have been considered.

In the description of the procedure, the importance of the computational sequence for the solution of the "state determination" problem has been particularly emphasized. This

part of the analysis is extremely important, yet has received little attention in previous work.

A computer program for the analysis of plane and axisymmetric solids has been developed to demonstrate the validity of the computational procedure. Results for several numerical examples have shown good agreement with experimental results and with theoretical results obtained by other workers. Results for both solids and a thin shell have been presented. A comparison of alternative solution procedures for a typical case has indicated that the greatest efficiency can be expected with a Newton-Raphson type of iteration procedure. Significantly better results were obtained with partially incompatible elements than with fully compatible elements.

8.2 FURTHER STUDIES

It is believed that the procedure proposed is generally applicable to inelastic structures of essentially any type, and that by following this procedure the development of computer programs to carry out inelastic analysis can be reduced to a fairly routine task. Nevertheless, considerable additional development and testing of the procedure remain to be carried out. Required work includes:

(1) Development of techniques to include thermal loadings.

(2) More detailed investigation of strain hardening models and the corresponding computational procedures.

(3) Extension to large displacement problems. The general solution procedure should still be applicable, but that part of the state determination problem dealing with the relationship between displacement and strain is made more complex. Any attempt to extend the procedure to materials undergoing large strain will also require assumptions regarding the stress-strain relationship. The solution strategy would also need to be extended to take account of structures which become unstable.

(4) Development of more efficient data handling procedures within the computer program. The current program is fairly efficient, but is not intended to be a production tool. Major improvements in efficiency and capacity can be made.

REFERENCE

1. Taylor, G. I. and Quinney, H., "Plastic Distortion of Metals," Philosophical Transactions of the Royal Society, London, England, Series A, Vol. 230, 1931.

2. Hill, R., Lee, E. H. and Tupper, S. J., "The Theory of Combination Plastic and Elastic Deformation with Particular Reference to a Thick Tube under Internal Pressure," Proc. of the Royal Society, Series A, Vol. 191, 1947.

3. Hill, R., "The Mathematical Theory of Plasticity," Oxford, Clarendon Press, 1950.

4. Hodge, P. G. Jr. and White, G. H. Jr., "A Quantitative Comparison of Flow and Deformation Theories of Plasticity," J. of Appl. Mech., June 1950.

5. Nadai, A., "Theory of Flow and Fracture of Solids," N. Y. 1950.

6. White, G. N., "Application of the Theory of Perfectly Plastic Solids to Stress Analysis of Strain-Hardening Solids," Report A11-51, Grad. Div. Appl. Math., Brown Univ., 1950.

7. Drucker, D. C., "A More Fundamental Approach to Plastic Stress-Strain Relations," Proc. of 1st U. S. National Congress Appl. Mech., Chicago, 1951.

8. Prager, W. and Hodge, P. G. Jr., "Theory of Perfectly Plastic Solid," Dover Publication Inc., N. Y., 1968 (Edition of 1951).

9. Koiter, W. T., "Stress-Strain Relations, Uniqueness and Variational Theorems for Elastic-Plastic Materials with A Singular Yield Surface," Quart. Appl. Math. Vol. 11, No. 3, 1953.

10. Batdorf, S. B. and Budiansky, B., "Polyaxial Stress-Strain Relations of a Strain-Hardening Material," J. of Appl. Mech. Vol. 21, 1954

11. Prager, W., "Theory of Plasticity: A Survey of Recent Achievements," Proc. Institution of Mech. Eng., Vol. 169, 1955.

12. Bland, D. R., "The Associated Flow Rule of Plasticity," J. of Mech. and Phys. of Solids, Vol. 6, 1957.

13. Hodge, P. G. Jr., "A General Theory of Piecewise Linear Plasticity Based on Maximum Shear," J. of Mech. and Phys. of Solids, Vol. 5, 1957.

14. Hodge, P. G. Jr.,: Discussion of Prager's "A New Method for Analyzing Stresses and Strains in Work-Hardening Plastic Solids," J. of Appl. Mech., Vol. 24, 1957.

15. Shield, R. T. and Drucker, D. C., "Limit Strength of Thin-Walled Pressure Vessel with ASME Standard Torispherical Head," Proc. of 3rd U. S. National Congress Appl. Mech., 1958.

16. Shield, R. T. and Ziegler, H., "On Prager's Hardening Rule," Zeitschrift für angewandte Mathematik und Physik (ZAMP) 1958.

17. Drucker, D. C. and Shield, R. T., "Limit Analysis of Symmetrically Loaded Thin Shells of Revolution," J. of Appl. Mech. 1959.

18. Ziegler, H., "A Modification of Prager's Hardening Rule," Quart. Appl. Math. Vol. 17, 1959.

19. Naghdi, P. M., "Stress-Strain Relations in Plasticity and Thermoplasticity," Plasticity, Proc. of the 2nd. Symp. of Naval Structural Mechanics (edited by Lee, E. H. and Symonds, P. S.) 1960.

20. Theocaris, P. S. and Marketos, E., "Elastic-Plastic Analysis of Perforated Thin Strips of A Strain-Hardening Material" J. of Mech. and Phys. of Solids, Vol. 12, 1964.

21. Stoddart, J. S. and Owen, B. S., "Stresses in A Torispherical Pressure Vessel Head," Meeting on Stress Analysis Today, 1965 (Stress Analysis Group, Inst. Physics).

22. Drucker, D. C., "On The Continuum as An Assemblage of Homogeneous Elements or States," IUTAM Symp. on "Irreversible Aspects of Continuum Mechanics," Vienna, June 1966.

23. Ralston, A., "A First Course in Numerical Analysis," McGraw-Hill, 1965.

24. Fröberg, C. E., "Introduction to Numerical Analysis "Addison-Wesley Publishing Co. 1969.

25. Zienkiewicz, O. C., "The Finite Element Method in Engineering Science," McGraw-Hill, London, 1971.

26. Gallagher, R. H., Padlog, J. and Bijlaard, P. P., "Stress Analysis of Heated Complex Shapes," J. Am. Rocket Soc. Vol. 32, No. 5, 1962.

27. Argyris, J. H., "Elasto-Plastic Matrix Displacement Analysis of Three-Dimensional Continua," J. of the Royal Aeronautical Society, Vol. 89, 1965.

28. Argyris, J. H., "Continua and Discontinua," Proc. of 1st Conf. for Matrix Methods in Structural Mech. AFFDL-TR-66-80, Ohio, 1965.

29. Lansing, W., Jensen, W. R. and Falby, W., "Matrix Analysis Methods for Inelastic Structures," Proc. of 1st Conf. for Matrix Methods in Structural Mech. AFFDL-TR-66-80, Ohio, 1965.

30. Marcal, P. V., "A Stiffness Method for Elastic-Plastic Problems," Int'l J. Mech. Sci. Vol. 7, 1965.

31. Pope, G. G., "The Application of the Matrix Displacement Method in Plane Elasto-Plastic Problems," Proc. of 1st Conf. for Matrix Methods in Structural Mech. AFFDL-TR-66-80, Ohio, 1965.

32. Swedlow, T. L., Williams, M. L. and Yang, W. M., "Elasto-Plastic Stresses in Cracked Plates," CALCIT Report SM 65-19, Calif. Inst. of Tech. Pasadena, 1965.

33. Wissmann, J. W., "Nonlinear Structural Analysis; Tensor Formulation," Proc. of 1st Conf. for Matrix Methods in Structural Mech. AFFDL-TR-66-80, Ohio, 1965.

34. Felippa, C. A., "Refined Finite Element Analysis of Linear and Nonlinear Two-Dimensional Structures," Ph.D. Dissertation, U. C., Berkeley, SESM 66-22, 1966.

35. Marcal, P. V. and Pilgrim, W. R., "A Stiffness Method for Elastic-Plastic Shell of Revolution," J. of Strain Analysis, Vol. 1, No. 4, 1966.

36. Isakson, G. Armen, H. Jr. and Pifko, A., "Discrete-Element Methods for the Plastic Analysis of Structures," NASA Contractor Report, NASA CR-803, 1967.

37. Khojasteh-Bakht, M., "Analysis of Elastic-Plastic Shells of Revolution under Axisymmetric Loading Using the Finite Element Method," Ph.D. Dissertation, U. C., Berkeley, SESM 67-8, 1967.

38. Marcal, P. V. and King, I. P., "Elastic-Plastic Analysis of Two-Dimensional Stress Systems by the Finite Element Method," Int'l J. Mech. Sci. Vol. 9, 1967.

39. Akyuz, F. A. and Merwin, J. E., "Solution of Nonlinear Problems of Elasto-Plasticity by Finite Element Method," AIAA J. Vol. 6, No. 10, Oct. 1968.

40. Ergatoudis, J. G., Irons, B. M. and Zienkiewicz, O. C., "Curved, Isoparametric, Quadrilateral Elements for Finite Element Analysis," Int'l J. Solid Struct. 1968.

41. Witmer, E. A. and Kotanchik, J. J., "Progress Report on Discrete-Element Elastic and Elastic-Plastic Analysis of Shells of Revolution Subjected to Axisymmetric and Asymmetric Loading," Proc. of 2nd Conf. on Matrix Methods in Structural Mech. Ohio, 1968.

42. Yaghmai, S., "Incremental Analysis of Large Deformations in Mechanics of Solids with Application to Axisymmetric Shell of Revolution," Ph.D. Dissertation, U. C., Berkeley, SESM 68-17, 1968.

43. Yamada, Y., Yoshimura, N. and Sakurai, T., "Plastic Stress-Strain Matrix and Its Application for the Solution of Elastic-Plastic Problems by the Finite Element Method," Int'l J. Mech. Sci. Vol. 10, 1968.

44. Yamada, Y., Kawai, T. and Yoshimum, N., "Analysis of the Elastic-Plastic Problems by the Matrix Displacement Method," Proc. of 2nd Conf. on Matrix Method in Structural Mech. AFFDL-TR-68-150, Ohio, 1968.

45. Argyris, J. H. and Scharpf, D. W., "Methods of Elasto-Plastic Analysis," Proc. of the Symp. on Finite Element Techniques, University of Stuttgart, Germany, June 1969.

46. Marcal, P. V., "Large Deflection Analysis of Elastic-Plastic Plate and Shells," Proc. of 1st Int'l Conf. on Pressure Vessel Technology, Part I, ASME, 1969.

47. William, K., "Finite Element Analysis of Cellular Structures," Ph.D. Dissertation, U. C., Berkeley, 1969.

48. Yamada, Y., "Recent Japanese Developments in Matrix Displacement Method for Elastic-Plastic Problems," Proc. Japan-U. S. Seminar on Matrix Method of Structural Analysis and Design, Tokyo, 1969.

49. Zienkiewicz, O. C., Irons, B. M., Ergatoudis, J., Ahmad, S., and Scott, F. C., "Iso-Parametric and Associated Element Families for Two- and Three-Dimensional Analysis," Chapter 13 in, "Finite Element Methods in Stress Analysis," edit. by I. Holand and K. Bell, Tech. University of Norway, Tapir Press, Norway, Trondheim, 1969.

50. Zienkiewicz, O. C., Valliappan, S. and King, I. P., "Elastic-Plastic Solutions of Engineering Problems, Initial Stress, Finite Element Approach," Int'l J. for Num. Method in Eng. Vol. 1, 1969.

51. Bergan, P. G. "Nonlinear Analysis of Plates Considering Geometric and Material Effects," Ph.D. Dissertation, U. C., Berkeley, SESM 71-7, 1971.

52. Larsen, P. K., "Large Displacement Analysis of Shells of Revolution Including Creep, Plasticity and Viscoelasticity," Ph.D. Dissertation, U. C., Berkeley, 1971.

53. Zienkiewicz, O. C. and Nayah, G. C., "A General Approach to Problems of Large Deformation and Plasticity Using Isoparametric Elements," Proc. of 3rd Conf. on Matrix Methods in Structural Mech. Ohio, 1973.

54. Wilson, E. L., Taylor, R. L., Doherty, W. P. and Ghaboussi, J., "Incompatible Displacement Modes," Proc. of ONR Symp., University of Illinois, Urbana, Ill. 1971.

55. Wilson, E. L., "Solid SAP," Structural Eng. Lab. Report SESM 71-19, U. C., Berkeley, 1971.

56. Bogner, F. K., Mallett, R. H., Minich, M. D. and Schmit, L. A., "Development and Evaluation of Energy Search Methods of Nonlinear Structural Analysis," Tech. Report 65-113, Air Force Flight Dynamics Laboratory, Oct. 1965.

57. Mallett, R. H. and Schmit, L. A., "Nonlinear Structural Analysis by Energy Search," J. of the Structural Division, ASCE, Vol. 93, June, 1967.

58. Iwan, D. W., "The Distributed-Element Concept of Hysteretic Modeling and Its Application to Transient Response Problems," Proc. of the 4th World Conference on Earthquake Eng., Santiago, Chile, 1969.

59. Powell, G. H., "Structural Behavior of Pipelines," Consultant's report to Alyeska Pipeline Service Co. March 1971.

60. Wilson, E. L., "The Static Condensation Algorithm,"